Universidade do Minho
Escola de Engenharia

Hugo Sérgio Pitães Figueiredo

Preparation of catalysts from biosorbents supported on zeolites

Dezembro de 2011

Hugo Sérgio Pitães Figueiredo **Preparation of catalysts from biosorbents supported on zeolites**

UMinho | 2011

Universidade do Minho
Escola de Engenharia

Hugo Sérgio Pitães Figueiredo

Preparation of catalysts from biosorbents supported on zeolites

Tese de Doutoramento em Engenharia Química e Biológica

Trabalho realizado sob a orientação da
Doutora Maria Teresa Tavares
e da
Doutora Isabel Correia Neves

Dezembro de 2011

DECLARAÇÃO

Nome: Hugo Sérgio Pitães Figueiredo

Título da Tese: **Preparation of catalysts from biosorbents supported on zeolites**

Designação do Doutoramento: Doutoramento em Engenharia Química e Biológica.

Ano de conclusão: 2011

Orientadores: Dra. Maria Teresa Tavares
Dra. Isabel Correia Neves

Universidade do Minho, ___/___/_____

Assinatura: _____

ACKNOWLEDMENTS

The completion of this work would not be possible without the contribution of the following persons or institutions, to which I'm most happy to express my sincere thankfulness:

- to my supervisors, Prof. Teresa Tavares and Prof. Isabel Correia Neves, for the indispensable guidance and support throughout the execution of this work;
- to Prof. Maurício Fonseca and Dr. Iwona Kuźniarska-Biernacka from the Chemistry Department, University of Minho, for their contribution to this work;
- to all my laboratory colleagues at the Biological Engineering Deparment and Chemistry Department, University of Minho, for their assistance and collaboration throughout our academic progression;
- to Prof. Miguel Bañares from the Catalytic Spectroscopy Laboratory, *Instituto de Catálisis y Petroleoquímica*, Madrid, for welcoming me in his workgroup and for the most useful stay provided. From the same institute, special thanks to Ricardo López-Medina and Anna Lewandowska for their assistance and contribution to this work;
- to all my friends for their support;
- to my parents, without which my academic raising could not have been possible. My kindest thanks for them for the support and understanding through the good and less good times;
- to Mónica, for welcoming me as part of her life, for supporting me through the good and less good times and for her understanding during the progress of my PhD work.

This work was financially supported by the FCT – *Fundação para a Ciência e Tecnologia*, Portugal, through research grant SFRH / BD / 28201 / 2006. The author is most grateful for the concession of the research grant, without which the execution of this work would not have been possible.

ABSTRACT

Heavy metal contamination of aquifers by industrial effluents is a known environmental concern for which a recent effort for the development of treatment/remediation technologies has been conducted. Nevertheless, technologies that allow recuperation/reutilization of the metals are still of limited application.

This work presents the development of a clean technology allowing treatment and recovery of heavy metals in industrial effluents. The proposed recovered metals will be used as catalysts in liquid-phase oxidation reactions. The proposed system consists in bridging the biosorption capacity of the *Arthrobacter viscosus* bacterium with the intrinsic ion-exchange capacity of synthetic zeolites. This system was tested in the treatment of Cr(VI) solutions, in batch conditions (either in single step or sequencing reactor operation).

The system showed capacity for the treatment of Cr(VI) solutions. Although zeolites have natural limitation to exchanging Cr(VI) species, as they are anionic in solution, the bacterium is able to reduce Cr(VI) to Cr(III) and the last is cationic in solution and therefore has access to the zeolites.

Several operational parameters were evaluated in order to increase the performance of this system in the treatment of Cr(VI) solutions up to 100 mg_{Cr}/g. The pH in each reactor was allowed to vary freely in early studies. It was observed that the chemical composition of the zeolitic support had influence on the efficiency of the bioreduction of Cr(VI) to Cr(III). H^+-containing zeolites allowed higher reduction than the Na^+-containing counterparts. Despite this fact, subsequent studies demonstrated that this contribution was of minor effect when compared to the optimization of two parameters: biomass concentration and solution pH. The ensuing studies were performed with a biomass concentration of 5 g/L and controlled pH (4.0). Four zeolites were tested, HY, NaY, HMOR and NaMOR. In both single-step or sequencing reactor operation, Y zeolites demonstrated higher contribution to Cr(VI) reduction and overall chromium removal. In single-step operation, it was observed that the reduction of Cr(VI) follows a typical biosorption kinetics, being very fast during the first 24 hours, decreasing drastically thereafter. The highest uptake was achieved with the NaY support (11.7 $mg_{Cr}/g_{zeolite}$), after 27 days. This support was also tested in a long-term assay, where complete reduction of Cr(VI) was observed after 98 days. The operation in

sequencing batch reactor allowed reducing the time needed for complete Cr(VI) removal, requiring two four-day cycles with HY and NaY zeolites and three four-day cycles with HMOR and NaMOR zeolites. Maximum chromium removal was achieved with the HY support (98.2 %).

The recovery of the Cr-containing supports as catalysts was achieved. Cr-laden zeolites required that immobilization of the metal centers was performed prior to the application in liquid-phase reactions, in order to avoid leaching of chromium. The Cr-zeolites underwent immobilization of the metals through the flexible ligand method, using ligands with different nitrogen functional groups (pyridazine, pyridylazo and diphenyltriazene). All supports and catalysts were extensively characterized, confirming the successful immobilization of Cr(III) complexes in Y zeolites. It was observed that CrHY-based catalysts presented mostly Cr(III) in their structure, whereas CrNaY-based catalysts presented both Cr(VI) and Cr(III). This was found to be related to the different dynamics of both supports in the Cr(VI) biotreatment studies.

The catalytic activity of the catalysts was evaluated in two oxidation reactions, for cyclohexanol and cyclohexanone. The oxidation of cyclohexanol allowed a better understanding of the contribution of the different chromium species present. The highest conversion for this reaction was obtained with CrNaY-based catalysts (63.5 %). The presence of chromium in the reaction medium was confirmed, being of lesser extent when immobilized catalysts were employed. For the oxidation of cyclohexene, CrHY-based catalysts achieved the highest conversion of 73 %. It was found that the contribution of parent HY zeolite to the overall conversion was greater than of parent NaY zeolite, thus endowing CrHY catalysts with bi-functionality. The immobilized CrHY catalyst did not present significant decrease in activity after immobilization of chromium complexes, when compared to the parent support. For both reactions, it was possible to test the reuse of a CrNaY support and respective immobilized catalyst, confirming that the loss in activity with recycling was less pronounced when immobilized catalysts were used.

RESUMO

A contaminação de aquíferos por efluentes industriais contendo metais pesados é um problema ambiental para o qual houve um esforço recente no sentido de desenvolver tecnologias para minimizar os efeitos nos seres vivos. Apesar desses esforços, tecnologias que permitam recuperação/reutilização dos metais pesados são limitadas ou economicamente inviáveis.

Neste âmbito, este trabalho propõe uma tecnologia limpa para tratamento e recuperação de efluentes contaminados com metais pesados que permita a reutilização dos metais na forma de catalisadores para reacções de oxidação em fase líquida. O sistema proposto consiste na combinação das propriedades de biossorção de uma bactéria, *Arthrobacter viscosus*, com a capacidade intrínseca de permuta iónica de zeólitos sintéticos do tipo faujasite e mordenite. Este sistema foi testado no tratamento de soluções contendo crómio hexavalente, Cr(VI), em sistema fechado (mono-etapa ou em modo sequencial).

O sistema provou ser eficaz no tratamento das soluções de Cr(VI). Apesar dos zeólitos terem uma limitação natural à permuta de crómio hexavalente (que forma espécies aniónicas em ambiente aquoso), a bactéria é capaz de reduzir Cr(VI) a Cr(III), que existe em forma catiónica e é passível de permuta iónica no zeólito.

Vários parâmetros operacionais foram testados para melhorar o desempenho do sistema no tratamento de soluções de Cr(VI) com concentração máxima de 100 mg_{Cr}/L. Após estudos iniciais com pH livre, observou-se que a composição do suporte zeolítico interfere na eficácia da redução do Cr(VI) a Cr(III). Os zeólitos contendo iões H^+ provaram ser mais eficazes que os zeólitos contendo iões Na^+. Contudo, estudos posteriores demonstraram que a contribuição do suporte na redução do Cr(VI) é de menor efeito quando comparado com os resultados obtidos optimizando dois parâmetros: concentração de biomassa e pH da solução. Os estudos posteriores foram efectuados com uma concentração de biomassa de 5 g/L, a um pH controlado (4.0). Foram testados 4 zeólitos, HY, NaY, HMOR e NaMOR. Quer em sistema fechado de mono-etapa ou sequencial, os zeólitos Y demonstraram maior contribuição para a redução e remoção do crómio presente nas soluções. Em sistema mono-etapa, observou-se que a redução do Cr(VI) está de acordo com uma cinética típica de biossorção, sendo um processo rápido nas primeiras 24 horas de ensaio, diminuindo

drasticamente nos intervalos de tempo subsequentes. O suporte que permitiu maior *uptake* foi o NaY (11.7 $mg_{Cr}/g_{zeólito}$), ao fim de 27 dias. Este suporte foi testado num ensaio de longa duração, 98 dias, em que se observou a redução completa de uma solução de 100 mg_{Cr}/L. A operação em sistema sequencial permitiu reduzir o tempo necessário para a redução completa do Cr(VI), sendo necessários 2 ciclos de 4 dias para os suportes HY e NaY e 3 ciclos de 4 dias para os suportes HMOR e NaMOR. Neste modo, a remoção máxima de crómio foi alcançada com o suporte HY (98.2 %).

A recuperação dos suportes contendo crómio na forma de catalisadores foi conseguida. Os zeólitos com crómio necessitaram um tratamento prévio para imobilizar os centros metálicos na sua estrutura, de forma a evitar a lixiviação dos mesmos para o meio reaccional. Para o efeito, recorreu-se ao método do ligando flexível, usando ligandos contendo azoto em diferentes grupos estruturais (piridazina, piridilazo e difeniltriazeno). Todos os suportes foram extensivamente caracterizados, confirmando-se a imobilização de complexos de Cr(III) na estrutura de zeólitos Y. Observou-se que os suportes CrHY apresentam maioritariamente Cr(III) na sua estrutura e os suportes CrNaY apresentam Cr(VI) e Cr(III). Este facto foi relacionado com as dinâmicas diferentes observadas nos estudos de tratamento de soluções de Cr(VI).

A avaliação da actividade dos catalisadores foi efectuada em duas reacções de oxidação, do ciclohexeno e do ciclohexanol. A reacção do ciclohexanol permitiu um melhor entendimento das contribuições das diferentes espécies de crómio presentes. Nesta reacção, os catalisadores CrNaY obtiveram as conversões mais elevadas (63.5 %). Foi confirmada a presença de crómio no meio reaccional, sendo em menor quantidade no caso dos catalisadores que sofreram o processo de imobilização do metal. Na oxidação do ciclohexeno, os catalisadores CrHY demonstraram maior actividade, devida à maior contribuição do zeólito HY na reacção, em relação ao NaY. Neste aspecto, os catalisadores CrHY demonstraram bifuncionalidade, alcançando uma conversão máxima de 73 %. Os suportes CrHY e respectivos catalisadores não apresentaram diminuição de actividade após imobilização do crómio. Para as duas reacções, foi possível estudar a comparação da reutilização de suportes CrNaY e dos respectivos catalisadores imobilizados, sendo observada uma menor perda de actividade em cada ciclo no caso dos catalisadores imobilizados.

INDEX

CAPTION OF FIGURES

CAPTION OF TABLES

LIST OF ABREVIATIONS

(BY ALPHABETIC ORDER)

AAS	Atomic Absorbance Spectroscopy	
ChO	(compound)	cyclohexeneoxide
ChOl	(compound)	2-cyclohexen-1-ol
ChOne	(compound)	2-cyclohexene-1-one
ChTBHP	(compound)	tert-butyl-cyclohexylperoxide
DPT	(compound)	1,3-diphenyltriazene
DR-UV	Diffuse Reflectance UltraViolet-visible spectroscopy	
EPS	Extra-cellular PolySaccharides	

FAU	three letter code for a FAUjasite mineral structure
FTIR	Fourier Transform InfraRed Spectroscopy
GC	Gas Chromatography
GC-MS	Gas Chromatography coupled to Mass Spectroscopy
IE	Ion-Exchange
MeDPT	(compound) 1,3-bis(p-methylphenyl)triazene
MOR	three letter code for a MORdenite mineral structure
NODPT	(compound) 1,3-bis(p-nitrophenyl)triazene
PAN	(compound) 1-(2-pyridylazo)-2-naphthol
PyEt	(compound) 3-ethoxy-6-chloropyridazine
PyMe	(compound) 3-methoxy-6-chloropyridazine
PyP	(compound) 3-piperidino-6-chloropyridazine
SEM-EDS	Scanning Electronic Microscopy coupled to Energy Dispersive x-ray Spectroscopy
SBR	Sequencing-Batch Reactor
SBU	Secondary Building Unit
TBHP	(compound) tert-butylhydroperoxide
TGA-DTG	ThermoGravimetric Analysis coupled to Differential ThermoGravimetry
TON	Turn-Over Number
UV-Vis	UltraViolet-Visible Spectroscopy
XPS	X-ray Photoelectron Spectroscopy
XRD	X-Ray Diffraction

CHAPTER 1

INTRODUCTION

CHAPTER 1 – INTRODUCTION

Heavy metal contamination of soils and water sources is a direct consequence of human activity, mostly industrial. This particular type of pollution is hazardous to humans as heavy metals accumulate in microorganisms, progressing through the food chain [1].

Several technologies have been proposed to remediate or reduce emissions of heavy metals into the environment. However, some technologies lack the possibility of recovery and/or reuse of the metals, while processes allowing recovery may be costly to operate. Due to greater economical constraints and ever-increasing demand on metal ores, efforts have been carried out to develop recovery-reuse technologies for the treatment of heavy metal pollution [2].

One of the treatment options that has seen considerable advance in recent years is biosorption, in which inexpensive biomass or biomaterials are employed to remove heavy metal ions from aqueous media [3-5]. Recovery of the metal ions from biosorbents is possible and the generally low cost of the sorbents renders this technology of great interest.

The use of zeolites as highly valued ion-exchangers for the removal of heavy metal contamination (and other pollutants) in aqueous media has been referred as a low-cost approach by many authors [1,6,7].

The work described in this thesis presents two main objectives. The first is the development of a biotreatment system that allows recovery-reuse of chromium (Cr). This metal is present in effluents of electroplating and textile industries, which are important industrial sectors in the northern region of Portugal. The proposed system combines a biosorbent, the *Arthrobacter viscous* bacterium, with zeolitic supports (faujasite and mordenite type zeolites). The aim of joining these two constituents is to take advantage of the sorption properties of bacteria and zeolites, while the reuse of the removed metal will be performed in the catalysis field, which is the second objective of this work: the development of Cr catalysts for liquid-phase oxidation reactions, namely the oxidation of cyclohexanol and cyclohexene.

1.1 Outline

The presentation of the different aspects related to the development of this work was divided in seven chapters. Chapters 1 and 2 will be devoted to the presentation of the fundamental aspects that will enable a better understanding of the work. Chapters 3 to 6 will cover all aspects related to the development of experimental work, with presentation and discussion of the obtained results. Chapter 7 will close this thesis with a resume of the conclusions of this work.

Figure 1.1 presents the division and themes covered in the different chapters.

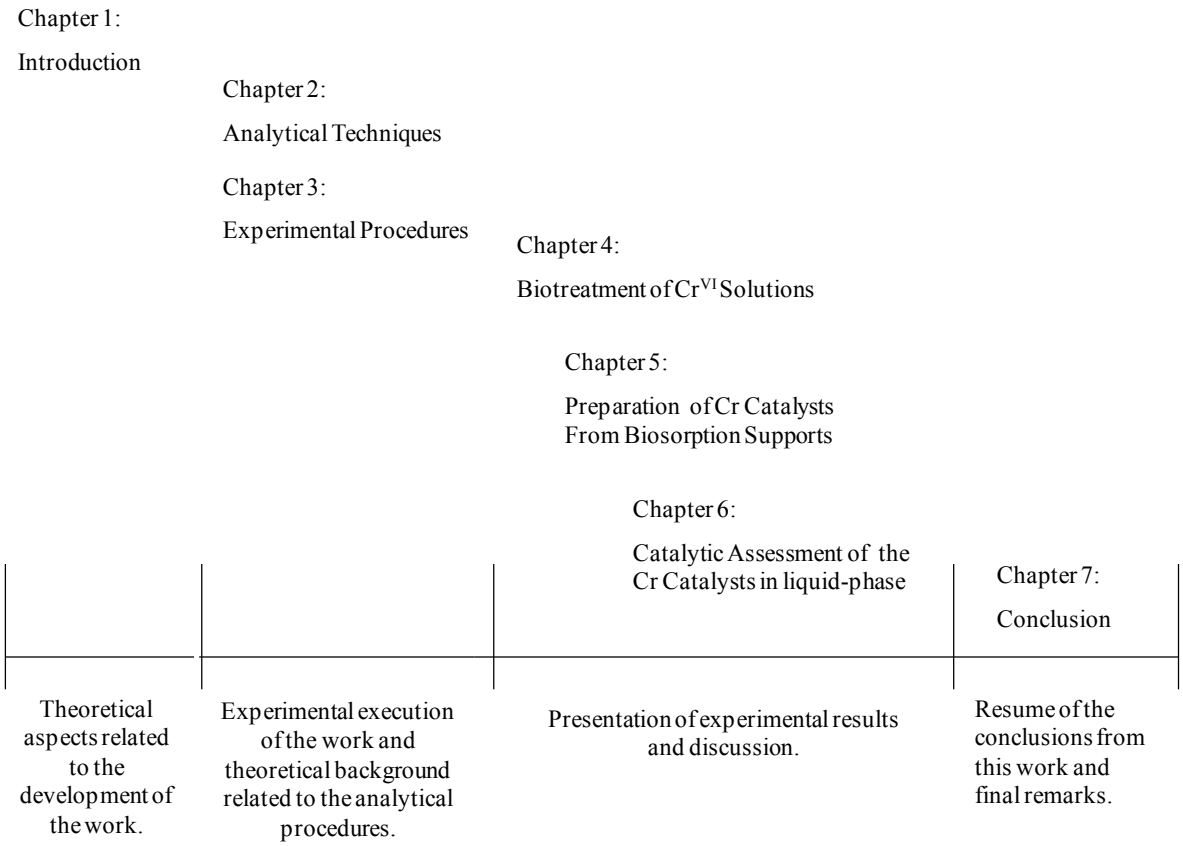

Figure 1.1: Outline of this thesis.

1.2 Theory and Fundamentals

This section presents theoretical background on the different aspects and technologies that are covered throughout this work.

The first subject presented in this section is *Chromium*, which will be followed by *Treatment of heavy metal pollution.* The following definitions are part of the proposed Cr(VI) biotreatment system: *biosorption*, which is the basis of the proposed technology (including details on the selected biosorbent, the *Arthrobacter viscosus* bacterium), and the definition of *zeolite*, which is important for the understanding of this work. *Catalysis* will be detailed following zeolites.

1.2.1 Chromium

Chromium is the element with atomic number 24. Its discovery dates back to the XVIIIth century, being reported by Louis Vauquelin, who was also responsible for the naming of this metal. Its name derives from the Greek *chroma* ("colour"), due to the different vivid colours exhibited by the different ores and compounds of this metal. Chromium is the 6th most abundant element of the Earth's crust [8] and is rarely found in the elemental form, being oxides such as chromite ($Fe_2Cr_2O_4$) the most abundant source for the metal [9].

Chromium is a transition metal, with electronic configuration [Ar] $3d^5$ $4s^1$. It can be found naturally in the II, III and VI formal oxidation states, being Cr(III) the most stable [10]. In aqueous solution, Cr(III) and Cr(VI) speciation is highly dependent on pH and Cr concentration. Compounds of the trivalent state usually form chromium hydroxides in water, being mono or polynuclear species ($CrOH^{2-}$, $Cr(OH)_2^{+}$, $Cr(OH)_3$, $Cr(OH)_4^{-}$, $Cr_2(OH)_2$ or $Cr_3(OH)_4^{5+}$), whereas the hexavalent chromium predominantly forms chromate or dichromate anions (CrO_4^{2-} and $Cr_2O_7^{2-}$, respectively) [11]. Figure 1.2 presents a speciation diagram for Cr(VI) species.

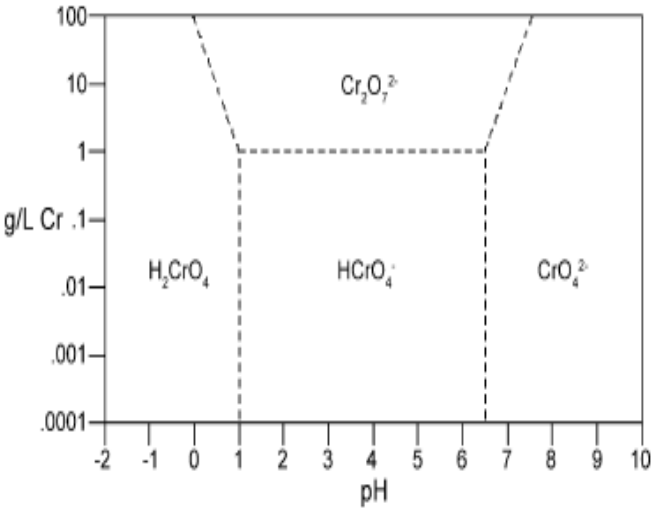

Figure 1.2: Speciation diagram for Cr(VI) (*source: Mohan and Pittman, 2006* [11]).

Hexavalent chromium species are very strong oxidizing agents. The equation for the reduction of dichromate in acid medium is given by equation 1.1.

$$Cr_2O_7^{2-} + 14H^+ + 6e^- \rightarrow 2Cr^{3+} + 7H_2O \qquad \text{(eq. 1.1)}$$

The standard reduction potential for dichromate is very high, at +1.360 V [12].

Chromium is a key element in industry. Being one of the most widespread metal in several industries [11], its main application is surface finishing on electroplating industries, being also of importance in textile industries (textile dyeing), wood preservation and production of pigments [2]. The presence of this metal in effluents from these industries is common and constitutes a potential environmental hazard if not treated properly.

Toxicological effects of chromium

Chromium in hexavalent oxidation state is very toxic. Metallic Cr does not present significant toxicity while Cr(III) is an essential trace element to living beings. In humans it assists the metabolism of glucose and cholesterol [13,14]. The mobility of Cr(III) compounds in aqueous solutions is reduced as this ion is prone to complexation with organic molecules or in the form of hydroxides [15]. In cellular structures, Cr(III) compounds are efficiently blocked by the cell wall.

Hexavalent Cr forms oxyanions compounds in aqueous media. These species are highly soluble and mobile in both aquifers and soils, which renders Cr(VI) compounds very accessible to life forms [15]. Contrarily to Cr(III) species, the Cr(VI) chromate and dichromate anions are very mobile in cellular structures, being taken by both prokaryotic and eukaryotic cells [16,17]. Owing to its high oxidation potential, as Cr(VI) reaches the cell cytoplasm and is in the presence of reducing cellular components, reduction to lower valence states may occur, leading to the formation of mainly Cr(III) species or some short-life intermediaries such as Cr(V) and Cr(IV). Once reduced, the Cr(III) species can form adducts with important biomolecules such as DNA or proteins, blocking their normal functionality, hence its mutagenic and carcinogenic effects [15-17]. Human exposure to Cr(VI) compounds leads to several health issues which may range from allergic-like reactions to more complicated respiratory tract problems [15].

Treatment of Cr-contaminated effluents

Cr is a heavy metal pollutant with high-priority for treatment [1]. According to Portuguese law (*Decreto-Lei 243/2001*, September 5th), the maximum chromium concentration in water for human consumption is 0.050 mg_{Cr}/L, while the maximum emission concentration in effluents is 2.0 mg_{Cr}/L for total Cr with a 0.1 mg_{Cr}/L limit for Cr(VI).

The common treatments for industrial Cr-containing effluents are physicochemical processes such as chemical reduction-precipitation, ion-exchange, adsorption on activated carbon, electrolysis, reverse osmosis, solvent extraction or evaporation [2,15]. The most predominantly used is chemical precipitation which requires previous reduction of Cr(VI) to Cr(III) with an adequate reductant (such as $FeSO_4$, SO_2, $BaSO_3$ or Na_2SO_3) in controlled pH conditions that would subsequently be precipitated as chromium hydroxides. This procedure has the drawbacks of consuming a considerable amount of reactants and generating Cr sludge which is normally deposited in a landfill.

Treatments which allow recovery of the metal, *recovery-reuse processes*, such as electrolysis, ion-exchange and membrane processes are currently being employed. However, the recovery of the metal is limited to local regeneration (such as electrolysis recovery in electroplating industries) or suffers from the high costs of energy consumption (reverse osmosis and membrane processes) or the cost of suitable supports (ion-exchange).

Bioremediation techniques have been recently proposed for the treatment of Cr-containing effluents. These techniques employ Cr-reducing microorganisms or simply rely on ion-exchange and adsorption phenomena on inexpensive biomass. These techniques will be further commented in sections 1.2.2 and 1.3.

1.2.2 Biosorption

The main process involved in the *Arthrobacter viscosus* – zeolite system is biosorption.

Biosorption is defined as the ability of any biomaterial to remove a given substrate from its environment. The true definition of the term "biosorption" is part of a debate where many authors offer different views on the subject. Although there is consensus on the fact that uptake during biosorption is due to physicochemical phenomena only, some authors claim that *biosorption* should only be used whenever dead biomass is involved, as it disregards any metabolism-dependent uptake processes [2,18,19]. However, other authors state that active uptake through metabolic pathways represent a negligible part of the global biosorption process in living organisms [20]. This definition is more sensitive when the removal of heavy metal ions is involved, as biomaterials cannot degrade metals [3,21]. Therefore, a distinction between *biosorption* and *bioaccumulation* is done to separate whether the removal of heavy metals is conducted by metabolic or non-metabolic processes, respectively [22].

In either way, authors agree that biosorption of heavy metals is mainly due to physicochemical process, such as adsorption on external cell wall, ion exchange, complexation, microprecipitation and oxidation/reduction [3,23]. Ion exchange is often referred as the prevalent process. The complex chemical nature of the biomolecules that constitute the external cell wall offers several functional groups such as carboxylic acids (-COOH), hydroxyl groups (-OH) and amine groups ($-NH_2$) that are able to exchange protons (H^+) with metal cations, providing the pH conditions of the medium would allow it (by influencing protonation/deprotonation of the functional groups).

While virtually any type of biomaterial can be used, such as bacteria, yeast, algae, fungi, fermentation waste or agricultural by-products such as tree bark or seed husk, microbiotic biomass is of particular interest for the application in large-scale processes. Microbes present the best compromise between surface area per volume of any living form [24],

which coupled to their low cost renders them useful materials for treatment of heavy metal contaminated effluents. Other advantages include metal recovery, possible regeneration of the biosorbents and minimal production of biological or chemical sludge [25]. Also of interest is the possibility of biosorbents to conduct selective separation of metal cations to levels as accurate as required for their further use in analytical procedures [26].

In order to be successfully applied in the removal of metals from contaminated solutions, it is often required that the biomass should be immobilized, either bound to a support or entrapped in a reactor [3,4]. Immobilization in a matrix (a polymer or an inorganic support such as silica) endows the biosorbent with mechanical resistance which is needed for continuous flow operation. Other bioreactors employ biomass immobilized through several processes, according to the specificity of the biomass itself and intended application [5]. Figure 1.3 presents some of the most used process for biomass immobilization.

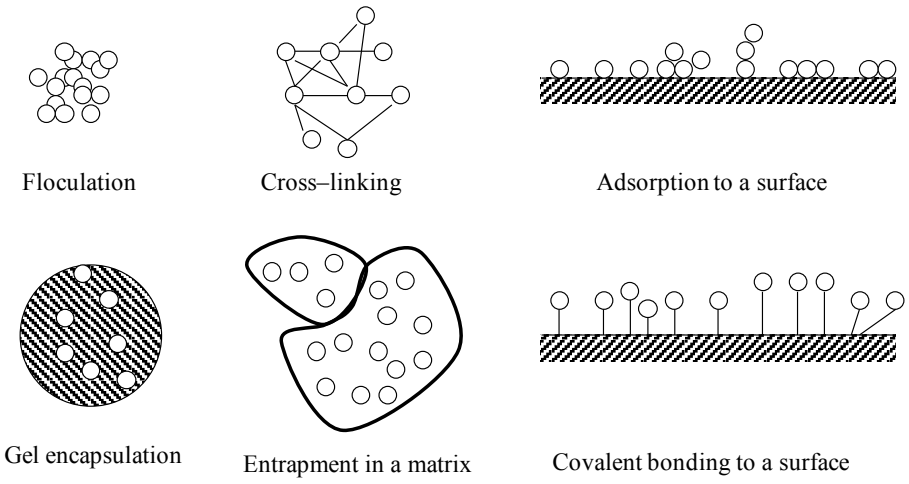

Figure 1.3: Some strategies for the immobilization of biomass.

Arthrobacter viscosus

Arthrobacter viscosus bacterium was selected as the biosorbent for the Cr(VI) biotreatment system. This bacterium presents interesting properties for the biosorption of heavy metals, such as great capacity for the production of extracellular polysaccharides (or exopolysaccharides - EPS) [27], which will increase the number of biosorption sites available for chromium ions. Also, EPS assist the fixation to a support and aggregate cellular growth, which in turn results in higher cellular concentration in biomass suspension. *Arthrobacter viscosus* bacterium is also non-pathogenic and alike most bacteria

from *Arthrobacter sp.* genus, this bacterium thrives on aquatic media such as riverbed sediments or underground.

Arthrobacter sp. bacteria present different morphology according to their growth stage. During cellular exponential growth stage the bacteria present a rod-like shape which changes to cocci in the stationary phase [28]. The Gram coloration also varies, although in the stationary phase cells are Gram-positive [29]. *Arthrobacter sp.* bacteria are also known for their high DNA C+G content, normally in excess of 70 % [28].

1.2.3 Zeolites

The selected supports for the *Arthrobacter viscosus* biosorbent were *zeolites*.

In brief, zeolites are crystalline aluminosilicates composed by alumina (Al_2O_3) and silica (SiO_2) dispersed in a well-ordered lattice.

The discovery of zeolites is attributed to the Swedish mineralogist Crønstedt (1722-1765), who reported in 1756 that a certain mineral released considerable amounts of water vapour upon heating on a flame. This mineral was later known to be stilbite and the naming zeolite originated from the combination of the Greek words *zeo* or *zein* (fusing) with *lithos* (rock), which translates the observations made by Crønstedt: "the rock that boils" [30,31].

Later research revealed that zeolites presented several framework types, some being related to other known mineral structures while others are characteristic to zeolites. However, all share the same common building block: TO_4 tetrahedra, where T is any tetrahedrally coordinated cation (Si or Al), that are bound together sharing the oxygen (O) atoms on the tetrahedra corners [32,33]. The empirical chemical formula of a zeolite is

$$M^{n+}_{x/y}[Al_xSi_yO_{2(x+y)}].pH_2O \qquad \text{(eq. 1.2)}$$

where M is the stabilizing cation (usually a metal) and *n* is the corresponding charge.

The first scientific studies with zeolites were reported in the mid-1800s. The dehydration of zeolite crystals was found to be reversible and non-damaging to the crystal transparency by Damour in 1840. Another important finding was reported by Eichorn in 1858: the

reversibility of ion-exchange in zeolites [34]. The adsorption of gases on dehydrated zeolites was reported by Friedel at the end of the XIXth century [35].

The great step in zeolite science occurred in the mid-1900s with the discovery of the synthetic pathway for the production of zeolites. Barrer and Milton are referred as the "founding fathers" of zeolite synthesis due to their discovery of the first fully synthetic zeolites of structures that were unknown to natural minerals [35,36]. Zeolites A, X and Y were amongst the first synthetic zeolites to be obtained by the hydrothermal synthesis process and soon became of great importance in industrial processes. The following trend led to the discovery of new structures and a push for high-silica zeolites was met with success with the advent of the synthesis of zeolites such as ZSM5 or Beta zeolites.

To date, more than 130 zeolitic structures are known to exist, with natural zeolites accounting for around 40 structures [32]. These structures are compiled in the *Atlas of Zeolite Framework Types*, which is responsibility of the Structure Commission of the International Zeolite Association (IZA). Each structure was given a three-letter code, such as FAU for faujasite type zeolites (Y and X zeolites), MOR for mordenite type zeolites, LTA for Linde Type-A zeolite or MFI for ZSM5 zeolite.

While the basic building block of zeolites is the TO_4 tetrahedra, several common structures of greater complexity are well known. Figure 1.4 presents an overview of the most common secondary building units (SBU).

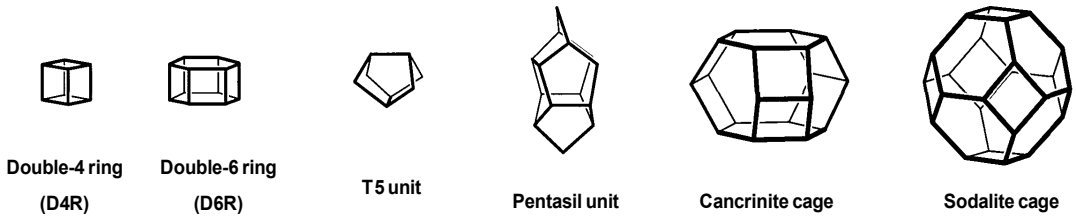

Figure 1.4: Example of some of the most common SBUs.

The zeolites used in this work belong to two distinct structures, namely, Y zeolite which is a faujasite (FAU) structure while mordenite zeolite shares the structure name with mordenite mineral (MOR). The unit cell for a FAU zeolite is cubic and comprises two SBUs: double-6 rings which bind sodalite cages, as shown in Figure 1.5. The main feature of the FAU unit cell is its central cavity, also known as supercavity or α-cavity. These are

interconnected by threedimensional channels (on all three axis directions), so that the supercavities present pore openings of 12 T or O atoms (7.4 Å in diameter). This pore size is considered a "large-pore" opening [33].

MOR zeolites are formed from five-ring SBUs [35], also named *mor* SBU. The resulting structure forms large pore openings of 12 T or O atoms, the same size as FAU. The continuous structure is strikingly different to the cavity-laden FAU zeolites, with one-dimensional large pore channels along the [001] axis and 8-ring pores are present in the [010] axis, although these are inaccessible to most molecules [37].

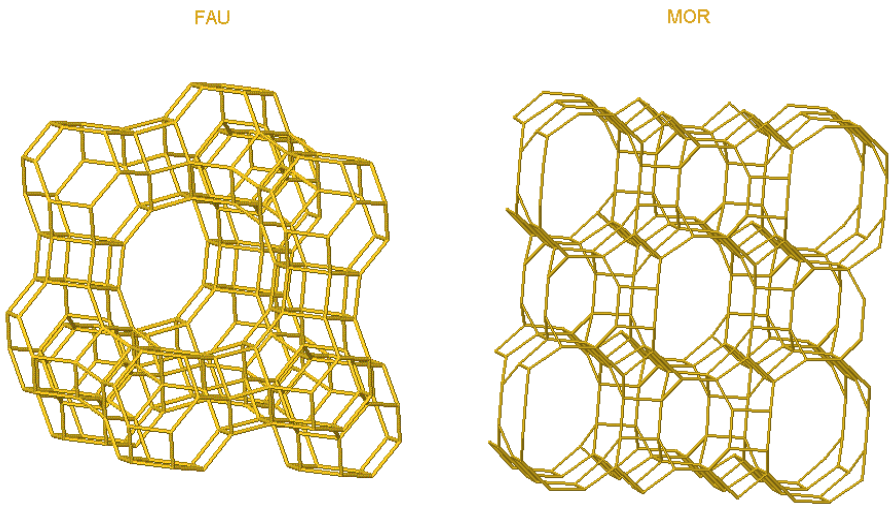

Figure 1.5: FAU and MOR framework types. Corner atoms represent either Si or Al atoms, while lines represent O bridges.

The zeolite properties are related to their particular chemical composition as well as their structure. One of the most important factors in zeolite chemistry is the presence of aluminium (Al) atoms in the structure. Silicon atoms are tetravalent, which renders the SiO_4 units neutral in electric charge, whereas the trivalent Al atoms are not able to fully compensate the charges of the four neighbouring oxygen atoms, meaning that the AlO_4 tetrahedra are negatively charged. This charge is balanced by the presence of extraframework cations, mostly of alkali- or earth-metal elements. These cations are kept in the zeolite framework by electrostatic forces that can easily be countered by other cationic species and this gives rise to the ion-exchange ability of zeolites. Ion exchange capacity of

a zeolite is related to the amount of Al atoms present in the framework, so that Al-rich zeolites are widely used in ion-exchange processes, such as detergent softening.

Another important feature of the zeolitic structure is the microporosity of the well-defined structure. Most zeolites present two types of porosity, primary and secondary. Primary porosity is related to the framework structure itself while secondary porosity originates from eventual macropores on the structure, resulting from the interspaces between small sized zeolite crystallites or structural defects [38,39]. The microporosity leads to high surface areas which can exceed 700 m^2/g [40]. For this reason, zeolites present great adsorption properties, which render them useful in industrial applications such as gas drying or purification.

Another aspect of the well-defined and rigid structures of zeolites is their ability to separate molecules, as their pores and channels dimensions are in the range of molecular sizes [41,42]. Molecular sieving using zeolites is another important industrial application and shape selectivity is a key factor for the successful implementation of zeolites in industrial catalysis.

1.2.4 Catalysis

Catalysis is a cumulative term for the physicochemical processes which lead a certain material to act on the course of a chemical reaction without being consumed in the same reaction. A material with these properties is named *catalyst* which, according to the IUPAC definition is a component which is strange to the reaction, yet changes the rate of reaction while not being consumed in the process [43].

A catalyst decreases the activation energy of a reaction, offering favourable energetic pathways to the reaction, according to the diagram in Figure 1.6. A reaction is considered a *catalytic reaction* if a one of more turn-over number of events (TON) occurs at the catalyst or catalytic sites [44].

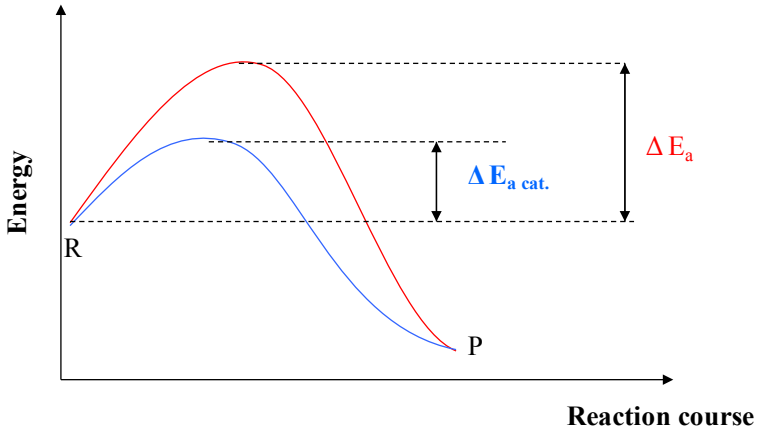

Figure 1.6: Energy diagram for a non-catalyzed reaction (red) and the equivalent catalyzed reaction (blue).

Although catalysts may alter the rate of the reaction, either increasing or decreasing (these are named *inhibitors*), the equilibrium position of the reaction is not altered. The effect on the reaction rate is related to the *activity* of the catalyst. Despite the equilibrium position being kept, the distribution of reaction products can be changed by the presence of catalysts - this is named *catalyst selectivity* and is another important feature of catalysis. The different energetic pathways that catalysts offer may induce preferable formation of a given product in multi-product reactions, which also includes the formation of new products that would not be obtained under normal reaction conditions.

Since the physicochemical phenomena behind catalytic activity are diverse, it is possible to divide catalysts under several categories. Catalysts are divided in heterogeneous or homogeneous, according to their physical state being different of the same as the substrate. A third distinction is used by some authors to place biocatalysts (enzymes) outside purely heterogeneous or homogeneous catalysts [44]. From the chemical point of view, catalysts can be of acid or alkaline type, redox type or a combination of more than one of these types (named a bifunctional catalyst).

Homogeneous catalysts are generally more active, since the limitation of mass transfer by diffusion is favourable if catalysts and reactants are dispersed on the same phase. Homogeneous catalysts are still highly valued in organic synthesis [45]. Heterogeneous catalysts are susceptible to diffusion limitations between bulk reactants and the catalytic active sites on the catalyst surface, requiring efficient mass transfer in order to be

comparatively active as the homogeneous counterparts. However, the greater ease in recovery from reaction as well as greater stability and resistance are key features for industrial-scale use, to the point that efforts leading to the preparation of heterogeneous catalysts from homogeneous equivalents are still conducted.

Catalysis by metals

Metallic compounds are some of the oldest heterogeneous catalysts to be used industrially. One of the earliest industrial applications was the Haber process for the production of ammonia with an iron catalyst in the early 1900s. It was based on studies of this catalyst that Emmett and Brunauer reported one of the earliest advances in understanding the surface phenomena on metals that led to catalytic activity. For the given reaction, the authors found that the chemiosorption of nitrogen in the catalyst was the rate-determining step of the reaction [46]. Up to this day, studies on the full understanding of chemical reactivity of metal surfaces due to chemiosorption phenomena are still conducted [47].

Metals in the form of homogenous complexes were also known to be catalysts since the XIXth century and are still widely used in redox catalysis [48]. These compounds can form coordination species with the transient intermediaries or stabilizing otherwise less likely reaction compounds. Oxidation with peroxides can also be catalysed by metal particles, through electron-transfer processes that lead to free radical formation of alkylperoxy or hydroperoxy radicals [49]. In this particular case second-row transition metals offer more stable radical intermediaries, as the catalytic activity of first-row transition metals may be so high that decomposition of the peroxides to unreactive compounds (such as H_2 and H_2O from H_2O_2) may occur, hindering the conversion of the substrate [50].

Zeolites as catalysts

Zeolites are used in many reactions as catalysts: acid, basic, acid-basic, redox and bifunctionual. However, their great application is in the field of acid catalysis for hydrocarbon transformations [39,41].

The catalytic activity of zeolites is related to framework structure and composition. Framework AlO_4 tetrahedra create a negative charge which can be compensated by

positively charged ions. The zeolitic acidic sites can be generated by the introduction of protons in the structure, that will create the Brønsted acid sites, as shown in Figure 1.7.

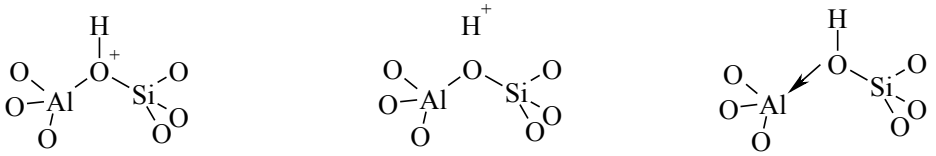

Figure 1.7: Possible representations of the Brønsted acid sites present in zeolites.

The global activity of Brønsted acid sites depends on several factors, such as their density in the framework, the zeolite Si/Al ratio (which will interfere in the acid strength of the sites) and local strain on bond angles. It was found that high-silica zeolites present much stronger Brønsted acid sites, despite their lesser availability of Al T atoms, which led to the development of high-silica zeolites such as the ZSM5, which are of great importance for the petrochemical industry.

Zeolites may also present Lewis acidity by loss of water of the Brønsted acid sites upon heating, according to Figure 1.8.

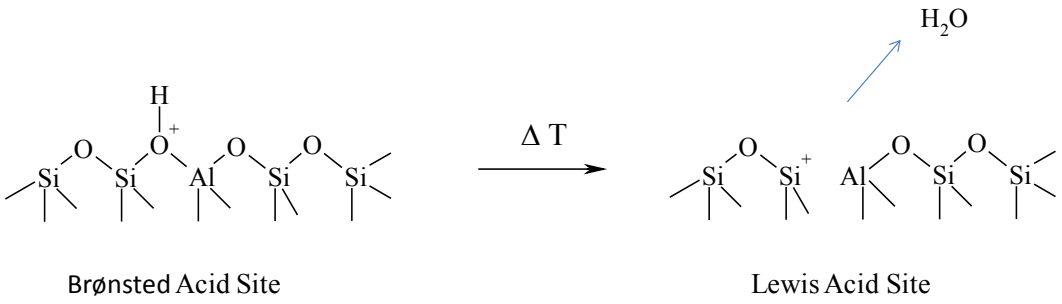

Figure 1.8: Generation of Lewis Acid sites in zeolites.

Zeolites can also be modified or synthesised for use in catalysis by inclusion of metal species in their structure. This can be achieved by two ways: a synthetic way, where isomorphic substitution of T atoms with selected metals is performed and a post-synthetic way, consisting of a simple ion-exchange with a salt of the desired metal or inclusion of the metal active centre by grafting/tethering onto the zeolite surface (Figure 1.9) [49].

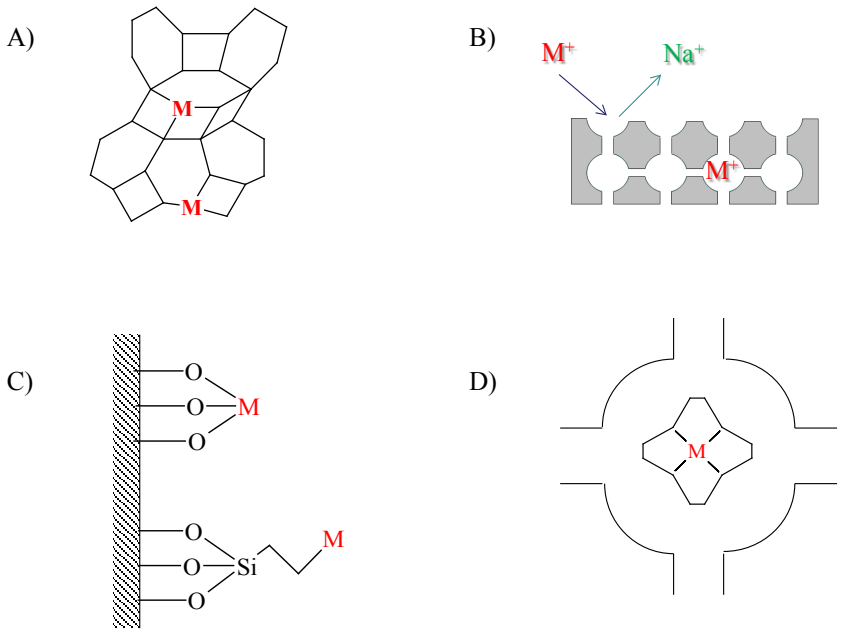

Figure 1.9: Examples of insertion of metal species into zeolites: A) isomorphic substitution, B) ion-exchange, C) grafting (top) and tethering (bottom) and D) encapsulation of metal complexes in supercavities.

The insertion of catalytically active metal species offers the possibility of operating bifunctional catalysts. The earliest example of success in the synthesis of isomorphic-substituted zeolites was the synthesis of TS1 by Enichem, where Ti(IV) was used to substitute Al atoms in the structure of a MFI zeolite (also called a titanosilicate) [39,49]. Ion-exchange with transition metal cations or complexes is also a possible way of forming stable heterogenous catalysts, while grafting or tethering (covalent bonding of the metal to the zeolite) are some of the most used techniques for the preparation of stable asymmetric catalysts [51].

Encapsulated metal complexes are somewhat different from other metal-zeolite catalysts, as in this case there is no physical interaction between the metal complex and host, which will eliminate possible interferences in the electronic environment of the central metal ion [51]. The encapsulation of metal complexes can be achieved by *in-situ* assembly of the complex or by synthesizing the zeolite around the previously formed complex [33]. Both approaches have specific requirements to be successfully implemented.

The *in-situ* synthesis requires that the size of ligand molecules used for the coordination with the central metal is such that it allows them to diffuse through the zeolite pores and,

upon coordination, the bulk volume of the complex becomes larger than the pores accessing the cavity, blocking the exit of the metal. This process is called the *flexible ligand method*, also known as *ship-in-a-bottle* synthesis. A schematic view is presented in figure 1.10.

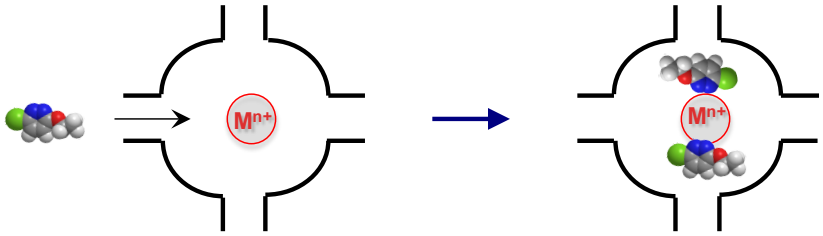

Figure 1.10: Immobilization of a metal ion in a zeolitic cavity by the flexible ligand method.

The target zeolite structures for this approach are three-dimensional structures with cavities interconnected by well-defined pores. In this case, FAU zeolites are amongst the most used ones while BEA zeolites can also be used [33].

In alternative, the encapsulation process may be performed by building the "bottle" around the "ship", also known as *zeolite synthesis* [52]. Once having a formed complex, it is possible to synthesize the zeolite so that the cavities will be occupied by the coordination structures. However, it is an absolute requirement that the metal complex may be able to tolerate the hydrothermal synthesis conditions, namely, pH and temperature, and that crystallization of the zeolite synthesis gel may occur around the metal complex. Although these requirements are somewhat limiting to prepare catalysts, Fe and Cu phtalocyanines complexes have been successfully encapsulated in X and Y zeolites [52]. The resulting complex immobilization in zeolites is very attractive for catalysis in redox reactions.

1.3 Recent Developments

This section presents an overview of the achievements on the several areas of knowledge used in this study, with focus on the particular nature of chromium.

1.3.1 Biosorption of hexavalent chromium

The recent interest on the biosorption of heavy metals as a potential clean and low-cost technology resulted in a great effort from researchers worldwide and publications on this field have increased steadily over the past 30 years. In their recent review, Park *et al.* referred that while the first studies on metal ions uptake by microbial biomass date back to 1902, publications on the biosorption field (as a whole) are currently in excess of 3000 [25].

One of the most particular aspects on the biosorption of hexavalent chromium is that the global mechanism is somewhat different to other metals. This is due to the combination of two facts: Cr(VI) species are anionic in solution, which differ from most other heavy metals which tend to form cationic species; secondly, Cr(VI) species present a high reduction potential and are known to be strong oxidants.

The global mechanism of hexavalent chromium biosorption has been subject of intense research and some doubts remained until recent studies. According to Saha and Orvig, four different processes were proposed, combining the possibilities of adsorption in anionic or cationic surfaces with possibility or absence or Cr(VI) reduction [53]:

- *anionic adsorption*, based on the data from adsorption of anionic Cr(VI) species on protonated surfaces (at low pH), whereas at high pH, where the number of protonated sites decreases, adsorption of hexavalent chromium is limited due to charge repulsion between the chromic anions and the predominantly negative charge of the biomass surface;
- *adsoption-coupled reduction*, strongly defended by Park *et al.*, based on data from several analytical methods that confirm the formation of Cr(III) species during biosorption in the presence of acid [54-56]. These data are supported by other authors who used electromagnetic spectroscopy to determine the formation of Cr(V) intermediaries on the biosorption of Cr(VI) by *Arthrobacter sp*.

bacteria. The reduced Cr(III) species were not accumulated by the bacteria [28,57];

- *anionic and cationic adsorption*, where hexavalent chromium is adsorbed in the surface as well as the reduced trivalent chromium species;
- *reduction and anionic adsorption*, similar to the previous, without retention of the reduced trivalent species that remain in solution.

The question that many authors raise on whether biosorption of heavy metals should use live or dead biomass also remains for the particular case of Cr(VI) biosorption, especially as both live and dead biomass are able to perform the reduction to Cr(III), being either bacteria, fungi or algae [21,58,59]. An interesting review from Sen and Dastidar covered the aspects of performing the biosorption of Cr(VI) with live or dead biomass [60]. According to the authors the usage of dead biomass has the advantage of eliminating dependency on the operating temperature, pH conditions and resistance to the toxicological effects to suit the biomass requirements. This is the approach mostly defended by Volesky, Tsezos and Park [4,19,25]. However, enzymatic side-processes which could assist Cr(VI) reduction only occur when live biomass is used, and this is one of the advantages of using live cells. Although most authors agree that there is a degree of bioaccumulation by living cells, some enzymatic process take place externally to the cell [15,61]. Moreover, living cells can trigger defence mechanisms when exposed to Cr(VI) (or other metals), namely cell wall modification in thickness or composition, which allows increased retention of the metal outside the cell wall [23,62]. A third alternative is also considered by other authors, which is the use of growing cells instead of fully grown suspensions. This approach counters the need for cultivation, harvesting and treatment, but requires the cells to be Cr-tolerant during this stage.

The usage of *Arthrobacter sp.* bacteria in the biotreatment of Cr(VI) solutions has been reported by several authors. Tsibakhashvili *et al*. have based their studies on the mechanism of Cr(VI) bioreduction with *Arthrobacter oxydans* [28,57,63-65] on the detection of Cr(V) intermediaries by ESR spectroscopy. Isolation of *Arthrobacter crystallopoietes* from Cr(VI) contaminated sites was reported by Camargo *et al.*, who also used molecular biology to understand the biological processes that related to Cr(VI) reduction and bioaccumulation [66]. Horton *et al.* identified *Arthrobacter aurescens* as an indigenous Cr-reducing bacterium consortium from a Cr-contaminated aquifer [67]. In recent studies, Mishra and Mukesh reported the identification of *Arthrobacter sp.* on isolates collected from an

effluent from an electroplating facility that contained chromium [68]. Patra *et al*. also isolated *Arthrobacter sp*. bacteria from Cr(VI) contaminated sites and found them to be Cr(VI)-reducing bacteria [69].

The use of a suspension of *Arthrobacter viscosus* to treat a Cr(VI) solution was reported by Silva *et al.* [70]. The suspended bacteria (5 g/L) were able to completely reduce a 100 mg_{Cr}/L solution within a pH range of 1-4, whereas maximum chromium uptake was 12.6 $mg_{Cr}/g_{biomass}$. While lower pH values were found to favour the rate of Cr(VI) reduction, higher pH allowed greater metal retention by the biomass. This was attributed to the surface protonation degree. High surface protonation at pH 1 offered more positively-chargerd adsorption sites for chromate or dichromate ions, while reduced Cr^{3+} ions were not retained by the surface due to electrostatic repulsion. These findings are in agreement to the studies of Park *et al*.

1.3.2 Usage of zeolites for the treatment of Cr(VI) solutions

Due to their great affinity for ion-exchange with heavy metal cations, zeolites are often reported as interesting supports for the treatment of heavy metal pollution, in cost-efficiency terms [1,6,7]. However, direct use of zeolites on the treatment of Cr(VI) solution is not possible as the electrostatic repulsion forces between anionic chromate or dichromate ions and the net negative charge of the framework hinders ion-exchange of these species. Moreover, even the ion-exchange of other cationic metal ions may suffer obstruction when Cr(VI) species are present in solution, as it was reported by Mier *et al*. [71].

Despite their lack of affinity for anionic species, the versatility of zeolites compensated for this natural limitation and this property was responsible for the dedication of several researchers in improving the ability of zeolites for Cr(VI) retention. This improvement was met with success through different methodologies, which resulted in supports for the direct adsorption of chromate and dichromate ions or *via* indirect processes that involve previous reduction of Cr(VI). These methodologies can be separated into three categories: *surfactant-modified zeolites*, *surface functionalization* and *metal modification*. None of these processes requires changes promoted during synthesis or crystallization of zeolites, meaning they are applicable to natural zeolites as well.

Surfactant modified zeolites (SMZs)

The modification of zeolites with surfactant molecules induces changes in the polarity of the surface, *i.e.*, inverting the zeta potential of the zeolite surface. This strategy consists on the deposition of quaternary amine salts with long alkyl chains on the zeolitic surface. If the solution concentration of the surfactant is below the critical micelle concentration (CMC), an ordered monolayer of molecules is deposited on the surface (named hemimicelle), with the positive charge of the amine centre directed towards the surface and the long hydrophobic alkyl chains pointing outwards. However, if the surfactant concentration exceeds its CMC, a double layer will form (known as admicelle), with the top layer inversed; with the positive centre pointing outwards (Figure 1.11)

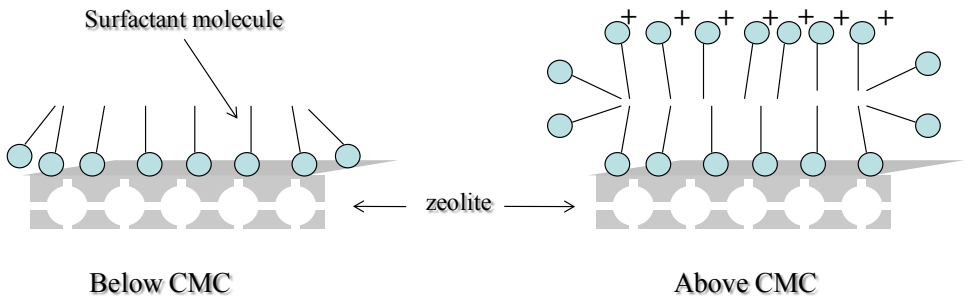

Figure 1.11: Formation of a hemimicelle and admicelle, at different surfactant concentrations.

Once the admicelle is formed on the zeolite surface, the positive charges of the quaternary amine salts allow the retention of the negatively charged chromate or dichromate species, as illustrated in Figure 1.12:

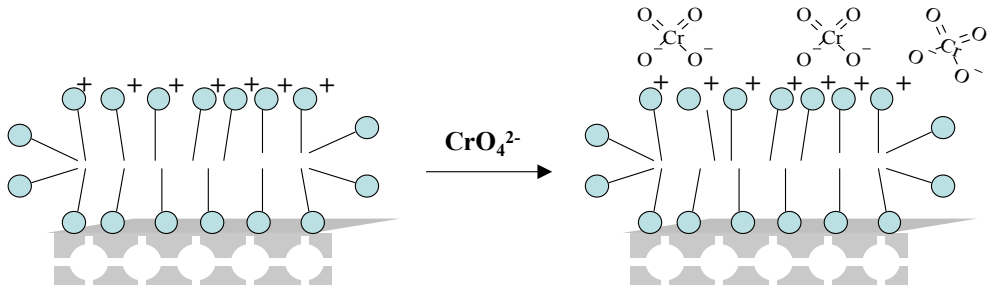

Figure 1.12: Retention of chromate ions by SMZs.

This process not only allows retention of chromate, as it promotes the capture of other metal oxyanions (such as molybdenate and arsenate). Nevertheless, it was confirmed by Bowman that the retention of these oxyanions occurs without reduction of the metal [72]. According to the same author, the characteristic ion-exchange of zeolites remains unaltered, which allows the simultaneous retention of anionic and cationic species [73]. Also, SMZs are tolerant to extreme pH and ionic strength conditions and to organic solvents, allowing their application in the same conditions as unmodified zeolites [74].

One of the earliest attempts to tailor an inorganic support was reported by Boyd *et al*. in 1988. The authors reported the application of the hexadecyltrimethylammonium (HDTMA) surfactant to modify soil samples in a bid to increase the retention of organic compounds [75]. Later, Santiago *et al*. reported the use of ethylhexadecyldimethylammonium (EHDDMA) and cetylpyridinium (CPD) surfactants to modify zeolites, achieving uptakes of Cr(VI) below 1 $mg_{Cr}/g_{support}$ [1]. The evaluation of the mechanism of chromate removal was also conducted, and several authors reported that the Langmuir adsorption model provided good fitting for both the retention of surfactant molecules on the zeolite and further Cr(VI) removal by different SMZs [76]. Another interesting feature of SMZs is the potential reusability of the sorbent, as demonstrated by Zeng *et al.* The authors reported the preparation of HDTMA-surfacted clinoptilolite and chabazite SMZs that were rinsed with HCl (0.1 M) after a first cycle of Cr(VI) removal, achieving 90 % of the original uptake on a second cycle of Cr(VI) removal [77].

In terms of uptake capacities of SMZs, the highest figures were reported by Zeng *et al.*, using modified natural chabazite zeolite to remove Cr(VI) up to 14.0 mg_{Cr}/g_{SMZ} [77,78].

Surface functionalization of zeolites

A different approach to provide zeolites with species having affinity for Cr(VI). This is achieved *via* surface functionalization, by grafting these species to the zeolite framework. There are differences towards SMZs, mainly the fact that covalent bonding is involved between the zeolite and the functional group that is inserted. The most common grafting agents are hybrid organic-inorganic compounds, such as alkyl silanes. These are able to react with surface silanol groups (SiOH), which offer good reactivity towards the grafting

agent [79]. An example of grafting minopropyl-triethoxy-silane (APTES) into a silica-like surface is presented in Figure 1.13.

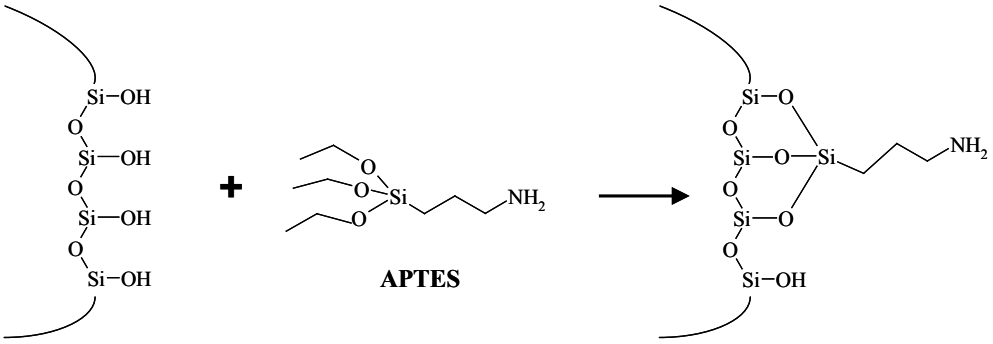

Figure 1.13: Grafting of APTES to a silica-like surface.

Although this process is more suited for silicates or silica-based supports, zeolites can also be used provided they offer a low Si/Al ratio or present a Si-rich external surface, since surface-laid Al centres do not present the hydroxyl groups as the surface SiOH counterparts. However, the internal area of zeolites, which is much greater than the external area, lacks silanol groups that are replaced by the hydroxyl groups available as the Si-(OH)-Al acid Brønsted sites [80]. Therefore, Si-rich zeolites with nano-crystallinity are better suited for surface functionalization, according to Song *et al*. [81].

In the example shown in Figure 1.13, APTES is of great interest to the removal of Cr(VI) oxyanions as the terminal amino group ($-NH_2$) is easily protonated at acidic pH, resulting in a positively charge that is responsible for the attraction of the chromate/dichromate anions (in a process similar to the observed in SMZs). Figure 1.14 presents a schematic view of the retention of Cr(VI) by APTES-functionalized silica-rich surfaces.

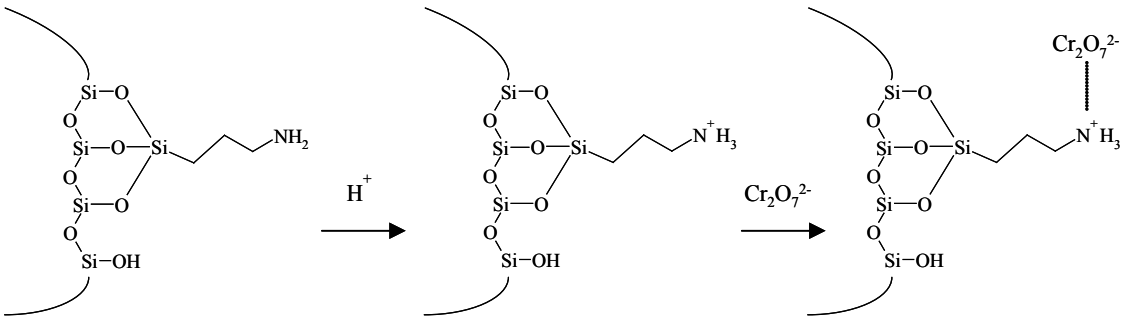

Figure 1.14: Retention of dichromate anion by previously protonated amino-functionalized silica.

Other terminal groups may include metal species that are used to coordinate with specific targets. Fryxell *et al*. reported the use of silica functionalized with Cu-(ethylenediamine) complexes that were found to coordinate to aqueous As(V) and Cr(VI) species, even on the presence of competing anions, such as sulphate [82]. The authors reported a maxium uptake of 54 $mg_{Cr}/g_{Support}$, tested on initial concentrations up to 1000 mg_{Cr}/L. Yukoi *et al.* reported that a MCM-41 zeolite functionalized with coordinated Fe(III) was able to remove the oxyanions of Cr(VI), As(V), Mo(VI) and Se(VI), achieving a maximum uptake of 95 $mg_{Cr}/g_{support}$ from initial concentrations of 230 mg_{Cr}/L [83]. Another work on separation of Cr(VI) was reported by Lam *et al.*, using NH_2 and Na^+COO^- functionalized MCM-41 supports. The latest was found to be useful on the separation of Cr(VI) from Cu(II) ions at pH 2 while the support achieved an uptake of 23 $mg_{Cr}/g_{support}$ from diluted solutions (7 mg_{Cr}/L) [84].

Similar SMZs, functionalized zeolites also retain their natural ion-exchange capacities, which is useful in the preparation of multi-functional supports. One type of bifunctional support for the removal of Cr(VI) was proposed by Barquist and Larsen, using magnetic NaY zeolite functionalized with APTES. The magnetization of NaY was achieved by ion-exchanging Fe(III) and Fe(II) in order to form magnetic iron oxides after mild alkaline treatment. This modification was chosen to allow easy recovery of the APTES-treated supports, which present hydrophobicity and tend to form colloidal suspension in water media. The reported uptake was to 44 $mg_{Cr}/g_{support}$ from 100 mg_{Cr}/L solutions [85].

Modified zeolites with chromium-reducing metals

Unlike the two previous processes for zeolite modification that were detailed in this section, modification of zeolites with Cr(VI)-reducing metals and subsequent ion-exchange of the reduced Cr(III) species by the zeolite is an indirect process for the removal of hexavalent chromium with zeolites. This process is similar in operation to the proposed *Arthrobacter viscosus*-zeolite system, although the Cr(VI) reducing species are inserted in the zeolite framework prior to use in solution.

Some metals or metal ions are able to contribute as electron donors for the reduction of hexavalent chromium. Iron (Fe) is a long-time studied metal for this process [86], although aluminium (Al) and barium (Ba) have also been successfully used [87,88]. Fe(II)-modified

FAU zeolites have been used by Kiser and Manning to treat Cr(VI)-containing solutions and the overall mechanism was studied in detail [89]. According to the authors, the reversibility of ion-exchange of Fe(II) by the zeolites provides an effective mean for delivering this reactant for subsequent reduction of Cr(VI) to Cr(III), which is favorable under environmentally relevant conditions. Since the formed Cr(III) readily displaces the Fe(II) ions from the zeolite exchange sites, a cooperative mechanism between these two favorable reactions occurs. Furthermore, the presence of the Al–O–Si or SiO_2 surfaces in the zeolite structure may assist the reduction of Cr(VI) with Fe(II) by providing a catalytic effect. The observed uptake was of the same magnitude as SMZs, with a maximum of 15.6 $mg_{Cr}/g_{support}$ being achieved by the Fe(II)-FAU support. Comparable results were obtained by Bolortamir and Egashira using natural Mongolian clinoptilolite modified with Ba^{2+} ions to achieve a maximum uptake of 14.0 $mg_{Cr}/g_{zeolite}$, while the unmodified zeolite samples only achieved residual chromate removal [88].

1.3.3 Use of chromium as catalyst for oxidation reactions

The oxidation of organic compounds has long been considered of great importance in chemistry and in industrial processes, mainly for organic synthesis [90]. As an example, the oxidation of C-H or C-C bonds into more reactive C-OH or C=O allows the formation of precursors which can be subsequently selectively transformed into other added-value products [91]. However, oxidation of organic compounds is an inefficient process which is greatly assisted by the use of adequate catalytic processes [92]. Furthermore, catalysts are now required to allow the use of environmental-friendly oxidants such as O_2, H_2O_2 or RO_2H to replace undesirable inorganic oxidants like $K_2Cr_2O_7$ or $KMnO_4$ [93].

According to Muzart, chromium has been used in this field since the dawn of organic synthesis. This author presented a comprehensive view of the uses of homogeneous Cr catalysts in several types of organic oxidation reactions, distinguishing between the different formal oxidation states while keeping larger focus on Cr(III)- and Cr(VI)-catalysed reactions [94,95]. Despite the known problems associated to the toxicity of this metal, coupled to the possible difficulties in end-of-reaction recovery or disposal of the catalyst, the author pointed out the great activity and versatility of chromium catalysts. Reckoned homogenous Cr-based catalysts are the Jones reagent (CrO_3, H_2SO_4 and

acetone), the Collins reagent (CrO_3 and pyridine) and the PCC reagent (CrO_3, pyridine and HCl) [96].

Weckhuysen *et al*. have commented on the application of supported Cr catalysts in several reactions, from olefin oxidation to polymerization and hydrogenation-dehydrogenation of alkanes [97]. Concerning the authors' comments on olefin oxidation, Cr catalysts are very active in the oxidation of alcohols, although Cr(VI) oxide proved to be a much more active catalyst than Cr(III) oxide in the oxidation of methanol. Cr-aluminophosphate molecular sieves (Cr-APO) were referred as excellent catalysts for the oxidation of secondary alcohols with *tert*-butylhydroperoxide (*t*-BuOOH). The authors also commented on the activity of heterogeneous Cr catalysts on amorphous supports on the oxidation of hydrocarbons.

Athough the usefulness of Cr heterogeneous catalysts is acknowledged, the actual degree of heterogeneity in these catalysts is still subject of some debate. Arends and Sheldon have reported several works on the subject of Cr leaching from heterogeneous catalysts [49,98]. According to the authors, even framework-substituted catalysts such as Cr-APOs molecular sieves present loss of Cr ions in the solution when in contact with alkylhydroperoxide oxidants (RO_2H), which led to the breakdown of Al-O-Cr and Si-O-Cr bonds. Lounis *et al.* have used a Cr(III) ion-exchanged ZSM5 zeolite as catalyst for the oxidation of several alcohols with *t*-BuOOH and reported the leaching of Cr species during heating of the reaction mixture [90]. The authors indicated the complexation of Cr with the alkyl peroxide to be responsible for the leaching of the metal species, as it led to the formation of a soluble complex. However, the authors also observed the re-adsorption of part of the leached species during the cooling down of the reaction mixture. Schuchardt *et al.* reported the preparation and test of Cr(III)-silicate catalyst and the authors also observed homogenous character due to leached Cr ions in the liquid-phase oxidation of cyclohexane with *t*-BuOOH or in the oxidation of cyclohexane with hydrogen peroxide [99,100]. The authors concluded that the loss of Cr was due to solvolysis of the Cr-O bonds from the support with polar compounds, such as water or peroxides.

Despite the constant debate on the stability of heterogeneous Cr catalysts, this subject is not commonly covered in publications reporting the use of zeolite-encapsulated Cr complexes. This can be due to the specific nature of these catalysts, being the closest heterogeneous equivalents to the stable homogenous Cr complexes which are widely used in organic oxidation. One of the earliest successful applications of encapsulated Cr complexes was

reported by Maurya *et al*., on the wet peroxide oxidation of phenol using Cr(III)-*salen* complexes encapsulated in Y zeolite [101,102]. The authors compared the activity of this catalyst to Fe(III) and Bi(III) equivalents and concluded that the Cr(III)-based catalysts achieved higher phenol conversion.

1.3.4 Oxidation reactions of cyclohexene and cyclohexanol

The two model reactions chosen to test the recovered Cr-biosorption supports as catalysts are the oxidation of cyclohexene and cyclohexanol. These reactions are somewhat different in nature, as cyclohexene is an olefin while the oxidation of cyclohexanol takes the common pathway for the oxidation of a secondary alcohol, with the formation of the ketone derivative, as illustrated in Figure 1.15.

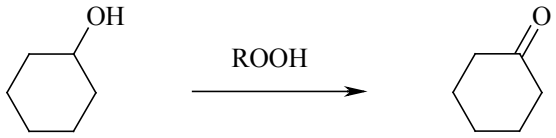

Figure 1.15: Peroxide oxidation of cyclohexanol into cyclohexanone.

The production of cyclohexanone has particular industrial interest since this compound is a precursor to the production of nylon-6 and nylon-6,6 [93].

Catalysts containing hexavalent Cr derivatives are very active on the oxidation of cyclohexanol [103,104]. The associated problems of toxicity and catalyst recovery have led to developments of heterogeneous catalysts. Since Cr(VI) is an active catalyst for this reaction, some authors reported the preparation of heterogeneous catalysts which employed this metal ion. An interesting work was reported by Parentis *et al.* who studied the oxidation of cyclohexanol with *tert*-butylhydroperoxide in the presence and in the absence of molecular oxygen, using a Cr(III) silica-supported catalyst [105]. The authors concluded that the presence of O_2 increases overall conversion of cyclohexanol, although the reaction can take place in its absence, although with a slightly lower conversion. Moreover, O_2 was considered a co-oxidant, since when in absence of *tert*-butylhidroperoxide, molecular oxygen was not able to induce any oxidation of cyclohexanol, hence the alkyl peroxide was the initiator of the reaction. The authors also proposed the following reaction mechanism:

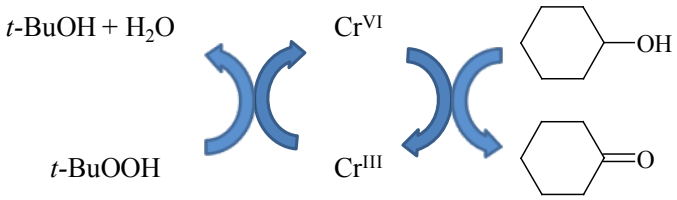

Figure 1.16: Proposed mechanism of cyclohexanol oxidation with *tert*-butylhydroperoxide using Cr catalysts.

The research into developing heterogeneous Cr catalysts for this reaction led to different approaches. A report on the use of Cr oxides was given by Nakamura and Matsuhashi, who employed Cr(VI) oxides supported in zirconia (CrO_3/ZrO_2) as an efficient heterogeneous catalyst [96]. Isomorphic Cr-substituted molecular sieves have also been tested for the oxidation of cyclohexanol, as it was reported by Laha and Gläser [106]. The authors reported the synthesis of Cr(III)-containing MCM and APO molecular sieves, named CrMCM-41, CrMCM-48 and CrAPO-5. The catalytic tests showed activity for the reaction. However, leaching of Cr species into the reaction medium was found to occur, with higher incidence on the mesoporous MCM-based catalyst than in the microporous APO counterpart.

The second oxidation reaction covered in this work is the oxidation of cyclohexene. Compared to the previous reaction, cyclohexene has a more intricate oxidation behaviour, with the competition of C-H and C=C bonds for the active oxidant [92]. This will have an effect on the mechanism being due to epoxidation or allylic oxidation. This reaction may yield a significant number of products, being the most common presented in Figure 1.17.

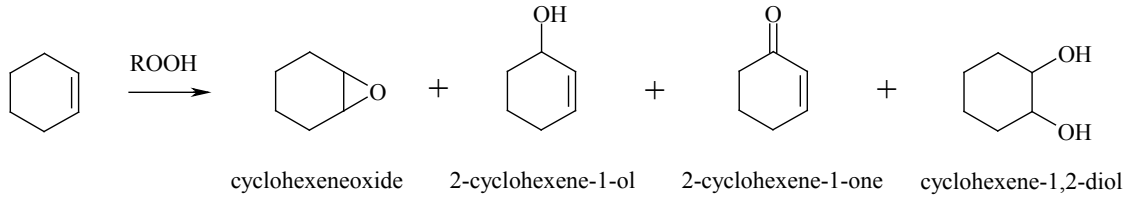

Figure 1.17: Main reaction products of the peroxide oxidation of cyclohexene.

The activity of Cr catalysts for this reaction is not as widely recognized as in the case of the oxidation of cyclohexanol. However, some authors presented the successful use of Cr

catalysts. As early as 1994, Bautista *et al.* reported the use of mixed $CrPO_4$-$AlPO_4$ for the oxidation of cyclohexene [107]. Sakthivel *et al.* published a report on the use of CrMCM molecular sieves as interesting catalysts for the oxidation of olefins, which were subsequently tested for the oxidation of cyclohexene with *tert*-butylhydroperoxide [108,109]. The authors proposed a free radical mechanism to be responsible for the reaction, with Cr radical centres being generated by the peroxide action. Cr supported on silica was also tested by Adam *et al.*, using silica from rice husk and a Cr(III) solution in the synthesis gel. The catalysts were tested with H_2O_2 on the oxidation of cyclohexane and cyclohexene, being comparatively as active as other high-surface area heterogeneous catalysts [110].

Works on the use of Cr complexes encapsulated in zeolites have been recently reported. Masoud Salavati-Niasari has devoted his work to the preparation of this type of catalysts for reactions such as cyclohexene oxidation, studying different metals and supports, although recurrently using Y zeolite for the encapsulation of the metal complexes [111-113]. In a recent paper, Abbo and Titinchi reported the *in-situ* synthesis of thio-Schiff base complexes of Cr(III), Zn(II) and Ni(II) in Y zeolite [114]. The authors conducted the oxidation of cyclohexene with H_2O_2 at 80 ºC and observed that both Ni and Cr encapsulated complexes present good activity for the reaction, achieving more than 70 % conversion, whereas the Zn counterpart was not active.

1.4 References

[1] S.E. Bailey, T.J. Olin, R.M. Bricka, D.D. Adrian, A Review of Potentially Low-cost Sorbents for Heavy Metals, Water Research. 33 (1999) 2469-2479.

[2] A. Agrawal, V. Kumar, B.D. Pandey, Remediation Options for the Treatment of Electroplating and Leather Tanning Effluent Containing Chromium—a Review, Mineral Processing and Extractive Metallurgy Review. 27 (2006) 99-130.

[3] M. Gavrilescu, Removal of Heavy Metals from the Environment by Biosorption, Engineering in Life Sciences. 4 (2004) 219-232.

[4] D. Kratochvil, B. Volesky, Advances in the Biosorption of Heavy Metals, Trends in Biotechnology. 16 (1998) 291-300.

[5] P. Le Cloirec, Y. Andrè, C. Faur-Brasquet, C. Gérente, Engineered Biofilms for Metal Ion Removal, Reviews in Environmental Science and Bio/Technology. 2 (2003) 177-192.

[6] S. Babel, T.A. Kurniawan, Low-cost Adsorbents for Heavy Metals Uptake from Contaminated Water: a review, Journal of Hazardous Materials. 97 (2003) 219-243.

[7] O. Hernandez-Ramirez, S.M. Holmes, Novel and Modified Materials for Wastewater Treatment Applications, Journal of Materials Chemistry. 18 (2008) 2751-2761.

[8] A. Demirci, A.L. Pometto, Enhanced Organically Bound Chromium Yeast Production, Journal of Agricultural and Food Chemistry. 48 (2000) 531-536.

[9] R. Saha, R. Nandi, B. Saha, Sources and Toxicity of Hexavalent Chromium, Journal of Coordination Chemistry. 64 (2011) 1782-1806.

[10] A.J. Bard, R. Parsons, J. Jordan, Standard Potentials in Aqueous Solution, 1st ed., New York, 1985.

[11] D. Mohan, C.U. Pittman, Activated Carbons and Low Cost Adsorbents for Remediation of Tri- and Hexavalent Chromium from Water, Journal of Hazardous Materials. 137 (2006) 762-811.

[12] D.A. Skoog, D.M. West, F.J. Holler, Fundamentals of Analytical Chemistry, 7th ed., Saunders College Publishing, 1996.

[13] H. Bağ, A.R. Türker, M. Lale, A. Tunçeli, Separation and Speciation of Cr(III) and Cr(VI) with *Saccharomyces cerevisiae* Immobilized on Sepiolite and Determination of Both Species in Water by FAAS., Talanta. 51 (2000) 895-902.

[14] H.C. Lukaski, Chromium as a Supplement, Annual Review of Nutrition. 19 (1999) 279-302.

[15] K. Cheung, J. Gu, Mechanism of Hexavalent Chromium Detoxification by Microorganisms and Bioremediation Application Potential: a Review, International Biodeterioration & Biodegradation. 59 (2007) 8-15.

[16] G.J. Puzon, A.G. Roberts, D.M. Kramer, L. Xun, Formation of Soluble Organo-chromium(III) Complexes After Chromate Reduction in the Presence of Cellular Organics, Environmental Science and Technology. 39 (2005) 2811-2817.

[17] G.J. Puzon, R.K. Tokala, H. Zhang, D. Yonge, B.M. Peyton, L. Xun, Mobility and Recalcitrance of Organo-chromium(III) Complexes, Chemosphere. 70 (2008) 2054-2059.

[18] T.A. Davis, B. Volesky, A. Mucci, A Review of the Biochemistry of Heavy Metal Biosorption by Brown Algae, Water Research. 37 (2003) 4311-4330.

[19] M. Tsezos, E. Remoudaki, V. Angelatou, Biosorption Sites of Selected Metals Using Electron Microscopy, Comparative Biochemistry and Physiology Part A: Physiology. 118 (1997) 481–487.

[20] N. Ahalya, R.D. Kanamadi, T.V. Ramachandra, Biosorption of Chromium (VI) From Aqueous Solutions by the Husk of Bengal Gram (*Cicer arientinum*), Electronic Journal of Biotechnology. 8 (2005) 258-264.

[21] L. Velásquez, J. Dussan, Biosorption and Bioaccumulation of Heavy Metals on Dead and Living Biomass of *Bacillus sphaericus*, Journal of Hazardous Materials. 167 (2009) 713-6.

[22] A.I. Zouboulis, M.X. Loukidou, K.A. Matis, Biosorption of Toxic Metals From Aqueous Solutions by Bacteria Strains Isolated From Metal-polluted Soils, Process Biochemistry. 39 (2004) 909-916.

[23] F. Veglió, F. Beolchini, A. Gasbarro, Biosorption of Toxic Metals: an Equilibrium Study Using Free Cells of *Arthrobacter sp.*, Process Biochemistry. 32 (1997) 99–105.

[24] E. Kulczycki, F.G. Ferris, D. Fortin, Impact of Cell Wall Structure on the Behavior of Bacterial Cells as Sorbents of Cadmium and Lead, Geomicrobiology Journal. 19 (2002) 553-565.

[25] D. Park, Y.-S. Yun, J.M. Park, The Past, Present, and Future Trends of Biosorption, Biotechnology and Bioprocess Engineering. 15 (2010) 86-102.

[26] B. Godlewska-Żyłkiewicz, Microorganisms in Inorganic Chemical Analysis, Analytical and Bioanalytical Chemistry. 384 (2006) 114-123.

[27] E. López, I. Ramos, M.A. Sanromán, Extracellular Polysaccharides Production by *Arthrobacter viscosus*, Journal of Food Engineering. 60 (2003) 463-467.

[28] N.Y. Tsibakhashvili, L.M. Mosulishvili, T.L. Kalabegishvili, E.I. Kirkesali, M.V. Frontasyeva, E.V. Pomyakushina, S.S. Pavlov, H.-Y.N. Holman, ENAA Studies of Chromium Uptake by *Arthrobacter oxydans*, Journal of Radioanalytical and Nuclear Chemistry. 259 (2004) 527-531.

[29] D. Paris, R. Blondeau, Isolation and Characterization of *Arthrobacter sp.* From Activated Sludge of a Pulp and Paper Mill, Water Research. 33 (1999) 947–950.

[30] P.P. Pescarmona, An Exploration of Silsesquioxanes and Zeolites using High-Speed Experimentation, T.U. Delft, 2003.

[31] C. Colella, A.F. Gualtieri, Cronstedt's Zeolite, Microporous and Mesoporous Materials. 105 (2007) 213-221.

[32] P. Payra, P.K. Dutta, Zeolites: A Primer, in: S.M. Auerbach, K.A. Carrado, P.K. Dutta (Eds.), Handbook of Zeolite Science and Technology, New York, Basel, Marcel Dekker, Inc., 2003.

[33] A. Corma, H. Garcia, Supramolecular Host-Guest Systems in Zeolites Prepared by Ship-in-a-Bottle Synthesis, European Journal of Inorganic Chemistry. 2004 (2004) 1143-1164.

[34] H. van Bekkum, E.M. Flanigen, J.C. Jansen, Introduction to Zeolite Science and Practice, Amsterdam, Elsevier, 1991.

[35] J. Čejka, H. van Bekkum, Zeolites and Ordered Mesoporous Materials: Progress and Prospects, Amsterdam, Elsevier, 2005.

[36] C.S. Cundy, P.A. Cox, The Hydrothermal Synthesis of Zeolites: History and Development from the Earliest Days to the Present Time, Chemical Reviews. 103 (2003) 663-702.

[37] R.F. Lobo, Introduction to the Structural Chemistry of Zeolites, in: S.M. Auerbach, K.A. Carrado, P.K. Dutta (Eds.), Handbook of Zeolite Science and Technology, New York, Basel, Marcel Dekker, Inc., 2003.

[38] G.V. Tsitsishvili, T.G. Andronikashvili, G.N. Kirov, L.D. Filizova, Natural Zeolites, Chichester, Ellis Horwood, 1992.

[39] M. Guisnet, F.R. Ribeiro, Zeólitos - Um Nanomundo ao Serviço da Catálise, Lisboa, Fundação Calouste Gulbenkian, 2004.

[40] H. Figueiredo, B. Silva, C. Quintelas, M.F.R. Pereira, I.C. Neves, T. Tavares, Biosorption of Hexavalent Chromium Based on Modified Y Zeolites Obtained by Alkaline Treatment, Environmental Engineering and Management Journal. 9 (2010) 305-311.

[41] M. Stocker, Gas Phase Catalysis by Zeolites, Microporous and Mesoporous Materials. 82 (2005) 257-292.

[42] M.R. Maurya, S.J.J. Titinchi, S. Chand, Spectroscopic and Catalytic Activity Study of N,N'-bis (salicylidene)propane-1,3-diamine copper(II) Encapsulated in Zeolite-Y, Applied Catalysis A: General. 228 (2002) 177-187.

[43] J.L. Figueiredo, F.R. Ribeiro, Catálise Heterogénea, Lisboa, Fundação Calouste Gulbenkian, 1989.

[44] G. Smith, F. Notheisz, Heterogeneous Catalysis in Organic Chemistry, Amsterdam, Elsevier, 1999.

[45] G.J. Hutchings, Heterogeneous Asymmetric Catalysts: Strategies for Achieving High Enantioselection, Annual Review of Materials Research. 35 (2005) 143-166.

[46] J.H. Sinfelt, Some Recent Developments in Catalysis by Metals, The Journal of Physical Chemistry. 90 (1986) 4711-4723.

[47] J. Greeley, J.K. Nørskov, M. Mavrikakis, Electronic Structure and Catalysis on Metal Surfaces., Annual Review of Physical Chemistry. 53 (2002) 319-48.

[48] I.I. Moiseev, Catalysis: 2000 AD, Kinetics and Catalysis. 42 (2001) 1-22.

[49] I.W.C.E. Arends, R.A. Sheldon, Activities and Stabilities of Heterogeneous Catalysts in Selective Liquid Phase Oxidations: Recent Developments, Applied Catalysis A: General. 212 (2001) 175-187.

[50] D.E. De Vos, M. Dams, B.F. Sels, P.A. Jacobs, Ordered Mesoporous and Microporous Molecular Sieves Functionalized with Transition Metal Complexes as Catalysts for Selective Organic Transformations, Chemical Reviews. 102 (2002) 3615-3640.

[51] P. McMorn, G.J. Hutchings, Heterogeneous Enantioselective Catalysts: Strategies for the Immobilisation of Homogeneous Catalysts, Chemical Society Reviews. 33 (2004) 108-22.

[52] C.R. Jacob, S.P. Varkey, P. Ratnasamy, Selective Oxidation Over Copper and Manganese Salens Encapsultaed in Zeolites, Microporous and Mesoporous Materials. 22 (1998) 465-474.

[53] B. Saha, C. Orvig, Biosorbents for Hexavalent Chromium Elimination From Industrial and Municipal Effluents, Coordination Chemistry Reviews. 254 (2010) 2959-2972.

[54] D. Park, Y.-S. Yun, J.M. Park, XAS and XPS Studies on Chromium-binding Groups of Biomaterial During Cr(VI) Biosorption., Journal of Colloid and Interface Science. 317 (2008) 54-61.

[55] D. Park, Y.-S. Yun, J.Y. Kim, J.M. Park, How to Study Cr(VI) Biosorption: Use of Fermentation Waste for Detoxifying Cr(VI) in Aqueous Solution, Chemical Engineering Journal. 136 (2008) 173-179.

[56] D. Park, S.-R. Lim, Y.-S. Yun, J.M. Park, Reliable Evidences That the Removal Mechanism of Hexavalent Chromium by Natural Biomaterials is Adsorption-coupled Reduction., Chemosphere. 70 (2007) 298-305.

[57] T.L. Kalabegishvili, N.Y. Tsibakhashvili, H.-Y.N. Holman, Electron Spin Resonance Study of Chromium(V) Formation and Decomposition by Basalt-inhabiting Bacteria, Environmental Science and Technology. 37 (2003) 4678-4684.

[58] Z. Noreen, A. Hameed, R. Faryal, Comparative Analysis of Biosorption Potential for Chromium Removal by Live and Dead Biomass of *Aspergillus niger* ZH2, International Journal of Chemical Reactor Engineering. 8 (2010) A143.

[59] H. Doshi, A. Ray, I.L. Kothari, Bioremediation Potential of Live and Dead *Spirulina*: Spectroscopic, Kinetics and SEM Studies., Biotechnology and Bioengineering. 96 (2007) 1051-63.

[60] M. Sen, M.G. Dastidar, Chromium Removal Using Various Biosorbents, Iranian Journal of Environmental Health Science & Engineering. 7 (2010) 182-190.

[61] B. Poljsak, I. Pócsi, P. Raspor, M. Pesti, Interference of Chromium with Biological Systems in Yeasts and Fungi: a Review., Journal of Basic Microbiology. 50 (2010) 21-36.

[62] Z. Lin, Y. Zhu, T.L. Kalabegishvili, N.Y. Tsibakhashvili, H.-Y. Holman, Effect of Chromate Action on Morphology of Basalt-inhabiting Bacteria, Materials Science and Engineering: C. 26 (2006) 610-612.

[63] N. Tsibakhashvili, T. Kalabegishvili, L. Mosulishvili, E. Kirkesali, S. Kerkenjia, I. Murusidze, H.-Y. Holman, M.V. Frontasyeva, S.F. Gundorina, Biotechnology of Cr(VI) Transformation into Cr(III) Complexes, Journal of Radioanalytical and Nuclear Chemistry. 278 (2008) 565-569.

[64] N.Y. Tsibakhashvili, T.L. Kalabegishvili, A.N. Rcheulishvili, I.G. Murusidze, O.A. Rcheulishvili, S.M. Kerkenjia, H.-Y.N. Holman, Decomposition of Cr(V)-diols to Cr(III) Complexes by *Arthrobacter oxydans*, Microbial Ecology. 57 (2009) 360-6.

[65] R. Codd, P.A. Lay, N.Y. Tsibakhashvili, T.L. Kalabegishvili, I.G. Murusidze, H.-Y.N. Holman, Chromium(V) Complexes Generated in *Arthrobacter oxydans* by Simulation Analysis of EPR Spectra, Journal of Inorganic Biochemistry. 100 (2006) 1827-1833.

[66] F.A.O. Camargo, F.M. Bento, B.C. Okeke, W.T. Frankenberger, Hexavalent Chromium Reduction by an Actinomycete, *Arthrobacter crystallopoietes* ES 32., Biological Trace Element Research. 97 (2004) 183-94.

[67] R.N. Horton, W.A. Apel, V.S. Thompson, P.P. Sheridan, Low Temperature Reduction of Hexavalent Chromium by a Microbial Enrichment Consortium and a Novel Strain of *Arthrobacter aurescens*, BMC Microbiology. 6 (2006) 5.

[68] S. Mishra, M. Doble, Novel Chromium Tolerant Microorganisms: Isolation, Characterization and their Biosorption Capacity, Ecotoxicology and Environmental Safety. 71 (2008) 874-879.

[69] R.C. Patra, S. Malik, M. Beer, M. Megharaj, R. Naidu, Molecular Characterization of Chromium (VI) Reducing Potential in Gram Positive Bacteria Isolated from Contaminated Sites, Soil Biology and Biochemistry. 42 (2010) 1857-1863.

[70] B. Silva, H. Figueiredo, I.C. Neves, T. Tavares, The role of pH on Cr (VI) Reduction and Removal by *Arthrobacter viscosus*, International Journal of Chemical and Biomolecular Engineering. 43 (2009) 59-62.

[71] M. Vaca Mier, R. López Callejas, R. Gehr, B.E. Jiménez Cisneros, P.J.J. Alvarez, Heavy Metal Removal with Mexican Clinoptilolite: Multi-Component Ionic Exchange, Water Research. 35 (2001) 373-378.

[72] R.S. Bowman, Applications of Surfactant-modified Zeolites to Environmental Remediation, Microporous and Mesoporous Materials. 61 (2003) 43-56.

[73] G.M. Haggerty, R.S. Bowman, Sorption of Chromate and Other Inorganic Anions by Organo-zeolite, Environmental Science & Technology. 28 (1994) 452–458.

[74] I. García-Sosa, M. Solache-Ríos, M. Olguín, J. Jiménez-Becerril, Preparation and Characterization of a Mexican Organo Clinoptilolite-heulandite Mineral and its Evaluation for the Sorption of Cadmium and Cobalt, Journal of Radioanalytical and Nuclear Chemistry. 256 (2003) 273-277.

[75] S.A. Boyd, J.-F. Lee, M.M. Mortland, Attenuating Organic Contaminant Mobility by Soil Modification, Nature. 333 (1988) 345-347.

[76] M. Ghiaci, R. Kia, A. Abbaspur, F. Seyedeyn-Azad, Adsorption of Chromate by Surfactant-modified Zeolites and MCM-41 Molecular Sieve, Separation and Purification Technology. 40 (2004) 285–295.

[77] Y. Zeng, H. Woo, G. Lee, J. Park, Removal of Chromate From Water Using Surfactant Modified Pohang Clinoptilolite and Haruna Chabazite, Desalination. 257 (2010) 102-109.

[78] Y. Zeng, H. Woo, G. Lee, J. Park, Adsorption of Cr(VI) on Hexadecylpyridinium Bromide (HDPB) Modified Natural Zeolites, Microporous and Mesoporous Materials. 130 (2010) 83-91.

[79] T. Kawai, K. Tsutsumi, Reactivity of Silanol Groups on Zeolite Surfaces, Colloid & Polymer Science. 276 (1998) 992-998.

[80] D. Bruhwiler, G. Calzaferri, Selective Functionalization of the External Surface of Zeolite L, Comptes Rendus Chimie. 8 (2005) 391-398.

[81] W. Song, J.F. Woodworth, V.H. Grassian, S.C. Larsen, Microscopic and Macroscopic Characterization of Organosilane-functionalized Nanocrystalline NaZSM-5., Langmuir. 21 (2005) 7009-7014.

[82] G.E. Fryxell, J. Liu, T.A. Hauser, Z. Nie, K.F. Ferris, S. Mattigod, M. Gong, R.T. Hallen, Design and Synthesis of Selective Mesoporous Anion Traps, Chem. Mater. 11 (1999) 2148–2154.

[83] T. Yokoi, T. Tatsumi, H. Yoshitake, Fe($^{3+}$) Coordinated to Amino-functionalized MCM-41: an Adsorbent for the Toxic Oxyanions with High Capacity, Resistibility to Inhibiting Anions, and Reusability After a Simple Treatment., Journal of Colloid and Interface Science. 274 (2004) 451-457.

[84] K.F. Lam, K.L. Yeung, G. Mckay, Selective Mesoporous Adsorbents for $Cr_2O_7^{2-}$ and Cu^{2+} Separation, Microporous and Mesoporous Materials. 100 (2007) 191-201.

[85] K. Barquist, S.C. Larsen, Chromate Adsorption on Bifunctional, Magnetic Zeolite Composites, Microporous and Mesoporous Materials. 130 (2010) 197-202.

[86] J.P. Gould, The Kinetics of Hexavalent Chromium Reduction by Metallic Iron, Water Research. 16 (1982) 871-877.

[87] C.J. Lin, S.L. Wang, P.M. Huang, Y.M. Tzou, J.C. Liu, C.C. Chen, J.H. Chen, C. Lin, Chromate Reduction by Zero-Valent Al Metal as Catalyzed by Polyoxometalate, Water Research. 43 (2009) 5015-5022.

[88] T. Bolortamir, R. Egashira, Removal of Hexavalent Chromium from Model Tannery Wastewater by Adsorption Using Mongolian Natural Zeolite, Journal of Chemical Engineering of Japan. 41 (2008) 1003-1009.

[89] J.R. Kiser, B.A. Manning, Reduction and Immobilization of Chromium(VI) by Iron(II)-treated Faujasite, Journal of Hazardous Materials. 174 (2010) 167-174.

[90] Z. Lounis, a Riahi, F. Djafri, J. Muzart, Chromium-exchanged Zeolite (CrE-ZSM-5) as Catalyst for Alcohol Oxidation and Benzylic Oxidation with t-BuOOH, Applied Catalysis A: General. 309 (2006) 270-272.

[91] C. Jin, W. Fan, Y. Jia, B. Fan, J. Ma, R. Li, Encapsulation of Transition Metal Tetrahydro-Schiff Base Complexes in Zeolite Y and Their Catalytic Properties for the Oxidation of Cycloalkanes, Journal of Molecular Catalysis A: Chemical. 249 (2006) 23-30.

[92] I. Kuźniarska-Biernacka, K. Biernacki, A.L. Magalhães, A.M. Fonseca, I.C. Neves, Catalytic Behavior of 1-(2-pyridylazo)-2-naphthol Transition Metal Complexes Encapsulated in Y Zeolite, Journal of Catalysis. 278 (2011) 102-110.

[93] J.D. Chen, H.E.B. Lempers, R.A. Sheldon, Ti_Al-β and CrAPO-5 as Heterogeneous Catalysts for Selective Oxidations in the Liquid Phase, Colloids and Surfaces A: Physicochemical and Engineering Aspects. 101 (1995) 137-146.

[94] J. Muzart, Chromium-catalyzed Oxidations in Organic Synthesis, Chemical Reviews. 92 (1992) 113-140.

[95] J. Muzart, Homogeneous Cr(VI)-Catalyzed Benzylic, Allylic and Propargylic Oxidations by tert-Butyl Hydroperoxide, Mini-Reviews in Organic Chemistry. 6 (2009) 9-20.

[96] H. Nakamura, H. Matsuhashi, Heterogeneous Liquid-Phase Oxidation of Alcohols with Solid Oxidizing Reagents of Vanadium (V) Oxide and Chromium (VI) Oxide Supported on Zirconium (IV) Oxide, Bulletin of the Chemical Society of Japan. 68 (1995) 997–1000.

[97] I.E. Wachs, Recent Conceptual Advances in the Catalysis Science of Mixed Metal Oxide Catalytic Materials, Catalysis Today. 100 (2005) 79-94.

[98] R.A. Sheldon, M. Wallau, I.W.C.E. Arends, U. Schuchardt, Heterogeneous Catalysts for Liquid-Phase Oxidations: Philosophers' Stones or Trojan Horses?, Accounts of Chemical Research. 31 (1998) 485-493.

[99] R. Serpa da Cruz, J. Martins de Souza e Silva, U. Arnold, U. Schuchardt, Catalytic Activity and Stability of a Chromium Containing Silicate in Liquid Phase

Cyclohexane Oxidation, Journal of Molecular Catalysis A: Chemical. 171 (2001) 251-257.

[100] E.V. Spinacé, U. Schuchardt, D. Cardoso, Oxidation of Hydrocarbons with Peroxides Catalyzed by Chromium(III) and Iron(III) Incorporated in SAPO-37 Framework, Applied Catalysis A: General. 185 (1999) L193-L197.

[101] M.R. Maurya, S.J.J. Titinchi, S. Chand, Oxidation of Phenol with H_2O_2 Catalysed by Cr(III), Fe(III) or Bi(III) N,N'-bis (salicylidene) Diethylenetriamine (H_2saldien) Complexes Encapsulated in Zeolite-Y, Journal of Molecular Catalysis A: Chemical. 193 (2003) 165–176.

[102] L.F. Liotta, M. Gruttadauria, G. Di Carlo, G. Perrini, V. Librando, Heterogeneous Catalytic Degradation of Phhenolic Substrates: Catalysts Activity., Journal of Hazardous Materials. 162 (2009) 588-606.

[103] J.-D. Lou, L.-H. Zhu, L.-L. Pan, L. Li, F. Li, C.-L. Gao, Solvent-Free Oxidation of Secondary Alcohols with Chromium Trioxide, Synthesis and Reactivity in Inorganic, Metal-Organic, and Nano-Metal Chemistry. 36 (2006) 585-587.

[104] M. Salavati-Niasari, E. Zamani, M.R. Ganjali, P. Norouzi, Synthesis, Characterization and Liquid Phase Oxidation of Cyclohexanol Using tert-butylhydroperoxide over Host (zeolite-Y)/guest (copper(II) complexes of 12- and 13-Membered Diaza Dioxa Schiff-base Macrocyclic ligand) Nanocomposite Materials (HGNM), Journal of Molecular Catalysis A: Chemical. 261 (2007) 196-201.

[105] M.L. Parentis, N.A. Bonini, E.E. Gonzo, Catalytic Reactivity of Cr/SiO_2 in the Liquid Phase Oxidation of Cyclohexanol by tert-butyl Hydroperoxide, Reaction Kinetics and Catalysis. 76 (2002) 243-248.

[106] S. Laha, R. Glaser, Characterization and Catalytic Performance of [Cr]MCM-41 and [Cr]MCM-48 Prepared by Either Classical or Microwave Heating, Microporous and Mesoporous Materials. 99 (2007) 159-166.

[107] F.M. Bautista, J.M. Campelo, A. Garcia, D. Luna, J.M. Marinas, A.A. Romero, M.R. Urbano, Chromium-aluminium Orthophosphates, III. Acidity and Catalytic Performance in Cyclohexene and Cumene Conversions on CrPO4−AlPO4 (20–50 wt.% AlPO4) Catalysts Obtained in Aqueous Ammonia, Reaction Kinetics & Catalysis Letters. 53 (1994) 55-63.

[108] A. Sakthivel, S.E. Dapurkar, P. Selvam, Allylic Oxidation of Cyclohexene Over Chromium Containing Mesoporous Molecular Sieves, Applied Catalysis A: General. 246 (2003) 283-293.

[109] A. Sakthivel, S.E. Dapurkar, P. Selvam, Mesoporous (Cr)MCM-41 and (Cr)MCM-48 Molecular Sieves: Promising Heterogeneous Catalysts for Liquid Phase Oxidation Reactions, Catalysis Letters. 77 (2001) 155–158.

[110] F. Adam, C.L. Fook, Chromium Modified Silica From Rice Husk as an Oxidative Catalyst, Journal of Porous Materials. 16 (2008) 291-298.

[111] M. Salavati-Niasari, Host (nanopores of zeolite-Y)/guest [manganese(II) with 12-membered tetradentate N_2O_2, N_2S_2 and N_4 donor macrocyclic ligands] Nanocatalysts: Flexible Ligand Synthesis, Characterization and Catalytic Activity, Transition Metal Chemistry. 33 (2008) 443-452.

[112] M. Salavati-Niasari, M. Shaterian, M.R. Ganjali, P. Norouzi, Oxidation of Cyclohexene with tert-butylhydroperoxide Catalysted by Host (Nanocavity of zeolite-Y)/guest (Mn(II), Co(II), Ni(II) and Cu(II) Complexes of N,N′-bis(salicylidene)phenylene-1,3-diamine) Nanocomposite Materials (HGNM), Journal of Molecular Catalysis A: Chemical. 261 (2007) 147-155.

[113] M. Salavati-Niasari, S. Abdolmohammadi, Host (Nanocavity of zeolite-Y)/guest (12- and 14-membered azamacrocyclic Ni(II) complexes) Nanocatalyst: Synthesis, Characterization and Catalytic Oxidation of Cyclohexene with Molecular Oxygen, Journal of Inclusion Phenomena and Macrocyclic Chemistry. 60 (2007) 145-152.

[114] H.S. Abbo, S.J.J. Titinchi, Metallo Salicylidenetriazol Complexes Encapsulated in Zeolite-Y: Synthesis, Physicochemical Properties and Catalytic Studies, Topics in Catalysis. 53 (2010) 1401-1410.

CHAPTER 2

ANALYTICAL TECHNIQUES

CHAPTER 2 – ANALYTICAL TECHIQUES

This chapter presents theory and background information on the different analytical techniques employed throughout this work. Also, additional details concerning the application of these techniques to the specific nature of the samples produced in this work are included.

The different techniques employed in this work can be separated into five main groups, namely *spectral techniques*, *X-ray techniques*, *microscopy techniques, thermal analysis techniques* and *chromatographic methods.*

2.1 Spectral techniques

These techniques are based on the interaction phenomena between matter and electromagnetic radiation from specific spectrum regions.

2.1.1 Fourier Transform Infrared Spectroscopy (FTIR)

Fourier Transform Infrared Spectroscopy (FTIR) is widely used in molecular characterization or identification of compounds. Although mostly used as a qualitative technique, it is also possible to operate FTIR spectrometers in quantitative analysis.

Infrared spectroscopy is based on the absorption of radiation on the infrared spectral region by any material. This technique has seen intense development during the XX^{th} century and is now one of the most widespread and straightforward methods for the determination of molecular structure.

When infrared radiation is absorbed by a material, excitation of the molecular vibration levels occurs. Since electromagnetic radiation interacts with matter through electric or magnetic fields, molecular vibrations can only be excited if they are capable of changes in dipole moment [1]. Hence, a non-polar diatomic molecule such as O_2 presents no absorption of infrared radiation. Molecular vibration also depends directly on the chemical

nature of the bond; therefore, the frequency of the absorbed radiation by a chemical group is specific [2]. The vibrational frequency of a chemical bond is given by

$$\nu = 130.3\sqrt{\left(f\left[\frac{1}{m_1}+\frac{1}{m_2}\right]\right)} \quad \text{(eq. 2.1)}$$

where ν is the absorbance frequency (in cm^{-1}), f is the force constant of the bond (in $N.m^{-1}$) and m_1 and m_2 are the atomic masses of the atoms (in atomic units) [3]. Although the absorption frequency of a given chemical group is specific, influence from the chemical environment on the molecule may cause interactions that change the frequency value, therefore increasing the individuality of the infrared fingerprint of a molecule.

Chemical groups often allow several vibration modes to take place. When variation in chemical bond length occurs, the vibrational mode is called *stretch*. For a simple three atom group, if there is variation on the angle formed by the group, then it is called *bending*. Other possible vibrational modes are *rotation* and *twisting* of the molecule. Figure 2.1 presents a schematic view of the possible stretching and bending modes on a molecule.

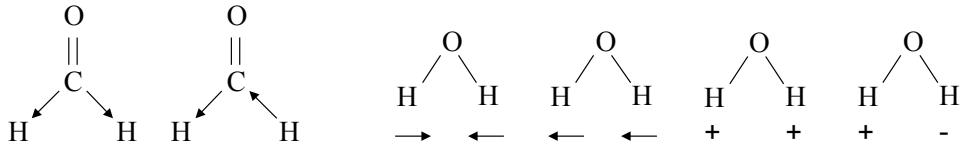

Figure 2.1: Symmetric and asymmetric stretch modes of the C-H bond of the formaldehyde molecule and bending modes for the water molecule. "+" and "-" refer the movement to the front or to the back on the perpendicular view to the plane.

An early typical infrared spectrometer would consist of an infrared radiation source, a monochromator (either optical prisms or slit grids) and a detector. Its operation mode is based on dispersive methods. Further evolution in electronics and informatics led to the implementation of interferometry methods. For this, the development of the Michelson interferometer was a key step, which was coupled to the use of Fourier transform to achieve what is known as Fourier Transform Infrared spectroscopy (FTIR). The advantages of interferometry spectrometer are greater spectrum acquisition speed, higher sensitivity and, in most cases, the elimination of a double-beam process (simultaneous reading of reference and sample spectra).

FTIR analysis is a powerful and popular technique used in the materials characterization field.

Zeolite characterization by FTIR analysis provides useful structural information. According to Jentys and Lercher [4], the crystalline lattice of zeolites presents well defined absorption regions between 500–4000 cm^{-1}, namely double ring vibrations (500–600 cm^{-1}), T-O-T symmetric and asymmetric stretch (750–1150 cm^{-1}) and T-OH vibrational modes (3000–4000 cm^{-1}). These are indicated in Figure 2.2. Moreover, the absorbance of structural water molecules is identified by the band at 1600 cm^{-1} [5].

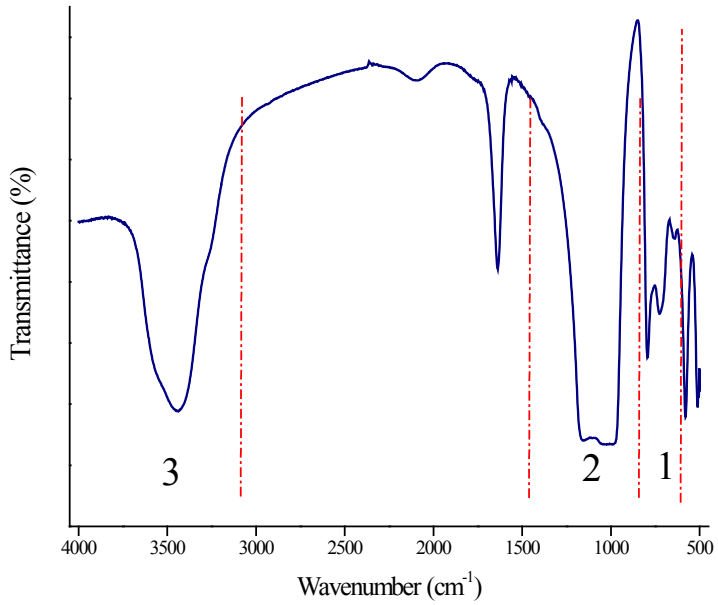

Figure 2.2: Double-ring vibration region (1), T-O-T stretching region (2) and T-OH vibration region (3).

FTIR spectroscopy has allowed the characterization of zeolites in almost every detail, such as framework structure, location of sites and cations and also adsorption and catalytic properties of zeolites [6]. In a recent study, Ghesti *et al.* have used FTIR spectroscopy to determine framework Si/Al ratios [7]. Moreover, this technique can be employed for the identification of compounds that are introduced or react inside the framework.

Application of FTIR spectroscopy to microorganism analysis has also been successfully achieved. Maquelin *et al.* have reported the usage of combined microscopy-FTIR analysis to the identification of microorganisms by vibrational techniques [8]. FTIR spectroscopy has also been employed by Omoike and Chorover for the characterization of extracellular

substances produced by *Bacillus subtilis*, as well as the adsorption properties of the same to solid surfaces [9,10].

2.1.2 Raman Spectroscopy

Vibrational Raman Spectroscopy is related to Infrared Spectroscopy, since it originates from vibrational and rotational transitions. However, the processes that occur are quite different. Raman spectroscopy is based on the light scattering effects that take place when a material absorbs monochromatic radiation from the visible to infrared region.

When a sample is hit by visible to infrared radiation, most of the scattered radiation is due to elastic Rayleigh scattering. However, a small fraction of the scattered radiation was observed to have a different frequency compared to the incident radiation – this is known as the *Raman effect*, discovered in 1928 [11]. The inelastic scattered radiation is very weak in intensity, when compared to the elastic counterpart, in which only one between 10^6 and 10^7 photons are inelastically scattered by a Raman process. This inelastic scattering is obtained when a sample allows polarization modulation by electronic, vibrational and rotational motion [6].

A photon scattered from a molecular transition to a higher energy state has a lower frequency than the incident photons – this is originated from a Stokes process. Conversely, if the molecular transition is towards a lower energy state, the scattered photon has a higher frequency and the process is called anti-Stokes. A Stokes process generates a photon with frequency described by equation 2.2:

$$v_{scat} = v_{in} - \Delta E/h \qquad \text{(eq. 2.2)}$$

where ΔE is the energy transition on the molecular vibrational state and h is the Planck's constant. For an anti-Stokes processes, equation 2.2 turns into

$$v_{scat} = v_{in} + \Delta E/h \qquad \text{(eq. 2.3)}$$

Therefore, an equal ΔE generates two different scattered photon frequencies, of the same shift when compared to the excitation radiation frequency. For this fact, Raman spectroscopy spectra are compared in terms of frequency shifts – called *Raman shift* – rather than specific absorption frequencies, as it is the case for FTIR spectroscopy. Despite Stokes and anti-Stokes processes generate the same Raman shift, they occur with different proportion and Stokes processes are predominant. This is mainly due to the fact that

molecules on the ground energy state, which originate Stokes lines, are more abundant than molecules on an excited energy level that return to the lower energy levels, which are responsible for the anti-Stokes lines [6].

Since the amount of photons scattered by Raman effect is very small, an intense excitation light is required to generate a significant Raman signal. Modern Raman spectrometers employ lasers as light source, which comply with the requirements for a monochromatic and highly energetic excitation source. Moreover, lasers can be applied to samples in any state (liquid, gas or solid) or even suspensions or solutions [11].

Although Raman spectroscopy is vibrational in nature, it arises from the changes in polarizability of a molecule during vibration, rather than variation of the dipole moment that occurs in infrared spectroscopy [3]. Hence, Raman and FTIR spectroscopy are complementary in terms of the information that is retrieved from a sample. While FTIR spectroscopy is well established in organic chemistry as a useful characterization technique, Raman spectroscopy is more adequate for the identification of inorganic or coordination compounds.

The study of zeolitic structures using Raman spectroscopy has been achieved. Initial studies on this field met technical difficulties, arising from the strong background noise which masked Raman signals. Early attempts to solve this issue concluded that the strong fluorescence was mainly due to the presence of organic fluorescent molecules that could be formed inside the framework or the presence of iron (Fe) impurities [12]. For most cases, oxidation of samples at high temperatures removed the organic fluorescent species, whereas changing the excitation wavelength resulted in a decrease of fluorescence. The latest was possible with the advent of near infrared excitation sources and Fourier Transform Raman (FT-Raman) spectroscopy [6]. Although Raman signal intensities can be lower in FT-Raman, application to zeolite study was achieved [13].

Raman spectroscopy is able to offer data from zeolite framework and from charge-balancing cations present in the structure or framework-substituted heteroatoms. The strongest zeolite structure-sensitive bands arise from the motion of T-O-T bonds and normally appear in the Raman shift region between 300–600 cm^{-1} [12]. The most intense band in this region often correlates with T-O-T angles from diverse building units, as well as with the Si/Al ratio of the matrix [6]. Bands in this region can be influenced by the charge-balancing cations present. Adsorbed molecules are also possible to be detected by

Raman spectroscopy, especially when compared to FTIR spectroscopy, where the strong T-O-T absorbance around 1200 cm^{-1} may mask the presence of other species.

2.1.3 Ultraviolet-visible (UV-Vis) spectroscopy

Ultraviolet-visible (UV-Vis) spectroscopy refers to absorption spectroscopy or reflectance spectroscopy in the ultraviolet-visible spectral region. UV-Vis spectroscopy belongs to the electronic spectroscopy techniques and is widely used in quantitative analysis, although it may also provide molecular qualitative information.

UV-Vis radiation is sufficiently energetic to promote electronic transitions from lower energy to higher orbitals. When an electron receives the exact energy difference between two orbitals from a photon with the corresponding *hv* energy, the transition from the lower energy orbital to the higher energy orbital takes place. Since *h* is a constant, the photon frequency *v* is determinant for the electronic transition to take place.

At an atomic level, absorption of radiation by valence electrons occurs at discrete lines of the exact wavelength required for the electronic orbital transition. However, in a molecular environment, several energy levels can be found for the bonding electrons, and UV-Vis absorption spectra will consist of a multitude of closely packed absorption lines, which will translate to absorption bands as a whole [14].

Bonding electrons are able to transit from the corresponding highest occupied molecular orbit (HOMO) to the corresponding lowest unoccupied molecular orbit (LUMO). For a sigma bond (σ), electrons can move to the corresponding anti-bonding σ^* orbital. Double and triple π electrons move to the anti-bonding π^* orbit, whereas non-bonding *n* electrons can transit to both σ^* and π^* orbitals. These transitions are schematically illustrated in Figure 2.3:

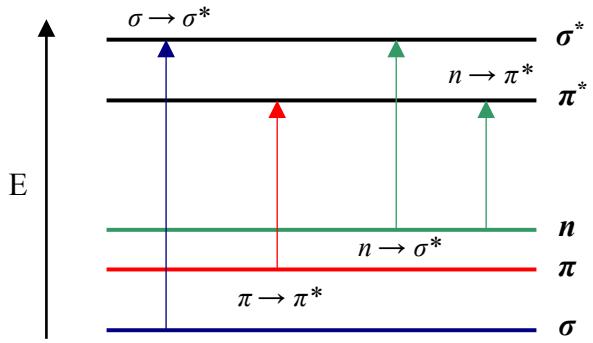

Figure 2.3: Comparative view of the possible orbital transitions and the respective energy gaps.

As it can be seen from Figure 2.3, σ electrons require the highest energy for the transition to occur. This is due to the fact that σ bonds are the most stable of chemical bonds and the energy required to excite an electron in this orbital often requires radiation with wavelength below 180 nm [14]. Conversely, π electrons from double or triple bonds are more loosely held by the attraction of the nuclei, thus requiring lesser excitation energy and correspondingly, higher wavelengths, situated in the ultraviolet or visible region of the spectrum. Functional groups possessing this kind of electrons are named *chromophores*. Identification of chromophores in a molecule by UV-Vis spectroscopy is somewhat possible – precise determination of maximum absorption wavelengths is influenced by other molecular interaction phenomena, such as conjugation with other chromophores, solvent interaction or other vibrational effects. Still, some data on maximum absorbance wavelengths of specific chromophores can be found. Nevertheless, UV-Vis spectroscopy can be used as a screening tool for the detection of unsaturated groups in an unknown sample.

The most common application of UV-Vis spectroscopy is in quantitative analysis. Most compounds absorb in the UV-Vis region (organic species, transition metal ions, biological samples, etc.), and even non-absorbing species can be previously treated with chromophoric reagents to be UV-Vis active (provided that the reaction is complete and with known stoichiometry). Whenever its application is possible, the latest process is preferable as it presents increased analytical specificity and higher sensitivity.

The absorbance of a sample, at a given wavelength, is given by equation 2.4

$$Abs = \log \frac{P_0}{P} \qquad \text{(eq. 2.4)}$$

where *Abs* stands for absorbance, P_0 is the beam power submitted to the sample and P is the power of the transmitted beam. Provided that absorbance is kept between 0 to 1 at a given wavelength, a linear relationship between concentration of chromophores and sample absorbance exists, which is translate by *Beer's law* (equation 2.5).

$$Abs = \varepsilon lC \qquad \text{or} \qquad Abs = l.\Sigma\varepsilon_i C_i \qquad \text{(eq. 2.5)}$$

where ε is the molar extinction coefficient, l is the overall optical path and C is the concentration of the absorbing species.

Another key element for the widespread use of UV-Vis spectroscopy is the simplicity of UV-Vis spectrometers. These equipments usually consist of a light source (normally coupled tungsten filament/D_2 lamps), a monochromator responsible for selecting the exact wavelength which will be used for analysis, a sample compartment and a detector. Several sample compartments are available for analysing samples in all physical states or allowing detection of either transmitted light, reflected light (diffuse-reflectance UV-Vis spectroscopy) or fluorescent light (fluorescent spectroscopy).

2.1.4 Atomic Absorbance Spectroscopy (AAS)

Atomic absorbance spectroscopy (AAS) is based on the ability of several elements to absorb electromagnetic radiation in specific wavelengths (spectral lines). Other atomic spectroscopy techniques are atomic emission and/or atomic fluorescence spectroscopy, which are based on emission of radiation of excited elements [15].

In atomic absorbance spectroscopy techniques, samples are atomized into their elemental components. Once the elements are in the gas phase, the freedom from all molecular or ionic interaction allows each of the elements to absorb radiation from a monochromatic source. By transmitting radiation from a source with the exact wavelength in which a given element absorbs, the transmitted beam will suffer a decrease in intensity that is dependent on the quantity of absorbing species in the atomized sample vapour.

A basic atomic absorbance spectrometer consists on an atom cell unit, responsible for the atomization of the sample, a monochromatic light source, an atomic chamber and a transmitted light detector. The most common atom cell resorts to a flame atomizer, normally a laminar-flow burner, which first nebulises the sample and carries it into a flame, where the fuel/oxidant mixture promotes the atomization. It is also in the flame that the

sample travels through the light beam, which is usually provided by a hollow cathode lamp, normally specific to the element being analysed. The light beam travels through the flame, where the absorbing atomic species decrease the intensity of the beam, which is then determined by the detector. Figure 2.4 presents the schematic view of a single beam atomic absorbance spectrometer with a laminar-flow burner.

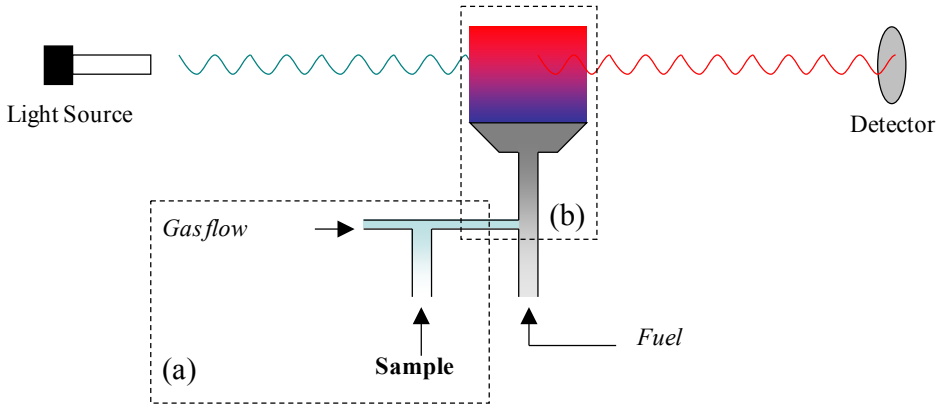

Figure 2.4: Schematic view of an atomic absorbance spectrometer, depicting in (a) the sample nebulizer, and in (b) the laminar-flow burner.

Provided that dependence in sample concentration and signal response can be met, AAS is a powerful analytical technique. The main analytical field for this technique is the determination of the concentration of metals and metalloids, given the good sensitivity and little interference for these elements [16].

2.2 X-Ray Techniques

These techniques employ radiation on the X-ray region to obtain information on the chemical and structural composition of solid materials.

2.2.1 X-ray Photoelectron Spectroscopy (XPS)

X-ray Photoelectron Spectroscopy (XPS) is a technique where a monochromatic X-ray radiation source is used to eject electrons from atoms of a sample.

When radiation in the X-ray region is absorbed by an atom in ultra high vacuum conditions, the excitation of electrons from the inner layers may occur. Since X-ray radiation is highly energetic, the ejection of electrons from the innermost atomic layers occurs and this is the primary source of detectable electrons. Additionally, relaxation through displacement of electrons from a higher energy orbital to fill the vacancy left after ejection results in emission of X-ray fluorescence. Also, ejection of additional electrons from outer orbital may arise from relaxation, which is known as the Auger effect [4].

The binding energy of an ejected electron is given by equation 2.6:

$$E = h\upsilon - E_b - \Phi \qquad \text{(eq. 2.6)}$$

where E is the kinetic energy of the electron, hv is the energy of the X-ray beam, E_b is the electron binding energy and Φ is the work function.

Since the energy levels of electrons from atomic inner layers depend on the environment of the atom and on its chemical state, this results that ejected electrons possess energy levels that are specific to the elements from which they were removed. Also, the binding energy of an electron also contains information on the charge of the same elements, as the charge of an atom affects the electronic energy levels.

Although this technique is spectroscopic in its nature, the fact that the probing depth of the X-ray beam is limited, ultimately restricts the application of this technique to the characterization of the qualitative and quantitative composition of the sample surface or near-surface layers (usually up to 10 nm depth).

This technique provides useful information on the chemical composition of the top layers on a zeolite surface. Moreover, it is capable of identifying between different oxidation states of the atoms present on the zeolite surface.

2.2.2 X-Ray Diffraction (XRD)

X-ray diffraction (XRD) is a powerful technique for determining crystal structure of crystalline materials and use for the characterization of crystalline materials such as zeolites.

X-ray diffraction occurs when a crystal solid is hit with X-ray radiation that is directed at specific angles (or continuous arcs). The diffraction is due to interference phenomena between the X-ray photons with wavelength comparable to inter-atomic planes on a crystal lattice, and the electrons from the atoms in the crystal lattice.

Since a crystalline material presents well-defined planes with a high density of atoms, electronic density will be therefore high. This increases the chance of a merely elastic collision between the X-ray photons and electrons, giving rise to a high density of diffracted photons. If the geometry of the atomic planes and the X-ray beam sets diffracted photons in the same phase, they will interfere constructively (Figure 2.5).

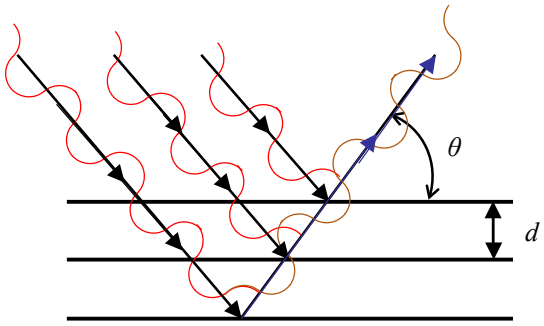

Figure 2.5: Illustration of X-ray diffraction from constructive interference of diffracted photons.

The angle θ at which the diffraction occurs is predicted by Bragg's law,

$$n\lambda = 2d\sin\theta \qquad \text{(eq. 2.7)}$$

where d is the inter-planar distance of the diffracting lattice planes and λ is the wavelength of the X-ray beam. This law is the basic principle of XRD analysis, as the different crystalline materials present specific inter-planar distances and geometries which will yield specific line diffraction profiles [17].

XRD analysis is a very useful tool in zeolite science, mainly used for determination of long-range order and phase purity, as well as for the characterization of unit cell geometry [4]. Also, it can be used for the determination of the chemical composition of zeolites, namely Si/Al ratios. This is due to the fact that a Si-O bond has a different length than Al-O bond and this will cause the unit cell dimensions to vary according to the Si/Al ratio.

The unit cell dimensions of a given zeolite are determined from the Miller index *h, k* and *l* of the diffracting plane, according to equation 2.8, which is a representation of Bragg's law:

$$n\lambda = 2d_{hkl}\sin\theta \qquad \text{(eq. 2.8)}$$

In the case of cubic geometry, such as in FAU type zeolites, the unit cell parameter (a_0) will have a single value, given by

$$a_0 = \frac{\sqrt{(h^2+k^2+l^2)}}{2\sin\theta} \quad \text{(eq. 2.9)}$$

According to ASTM D3942-80, the unit cell parameter of a FAU zeolite is calculated from the average of the a_0 values for the peak positions for the Miller index 533, 642 and 555. This parameter is also used for the determination of Si/Al ratios by the Breck and Flanigen equation [18]:

$$\frac{\text{Si}}{\text{Al}} = \frac{192-[115.2(a_0-24.191)]}{115.2(a_0-24.191)} \qquad \text{(eq. 2.10)}$$

where the relation 115.2(a_0-24.191) indicates the number of Al atoms per unit cell.

2.3 Microscopy Techniques

2.3.1 Scanning Electron Microscopy (SEM)

Scanning Electron Microscopy (SEM) is a widespread surface characterization tool in materials science. This technique allows a magnified view of a sample surface and, since electrons are used as the light source, allows much greater resolution than common optical microscopes.

The SEM technique consists of directing a beam of high-energy electrons into a sample, ensuing detection of the electrons that are reflected by the surface. The sample is required to be electrically conductive, although non-conductive samples can be covered by a thin metallic film in order to comply with this requirement. When the electron beam hits the sample, three distinct phenomena originate the different types of reflected radiation:

- *primary electrons* are reflected when inelastic collisions take place, such as collision of electrons and atomic nuclei. These electrons possess energy levels similar to the incising beam;
- *secondary electrons* result from inelastic collisions with the electrons which are present in electron clouds of sample atoms. This results in electrons from outer orbitals being removed from the atoms and scattered at lower energies than primary electrons. This is the main source of detectable electrons in SEM;
- *X-rays emission* takes place if the electron beam removes electrons from the inner orbitals, where the relaxation of the atom occurs with emission of radiation in the X-ray region. The photon wavelength is specific to the element from which the electron is removed, and this is useful for qualitative analysis of a sample.

A SEM microscope possesses a detector for each type of reflected emission, being the image formed from the combined input of the different detectors. Primary electrons detectors are usually placed very distant to the sample, since these electrons are very energetic and can travel longer distances. Secondary electrons, being less energetic, are detected in the sample surroundings, the same for X-rays. Figure 2.6 presents a schematic view of a SEM microscope.

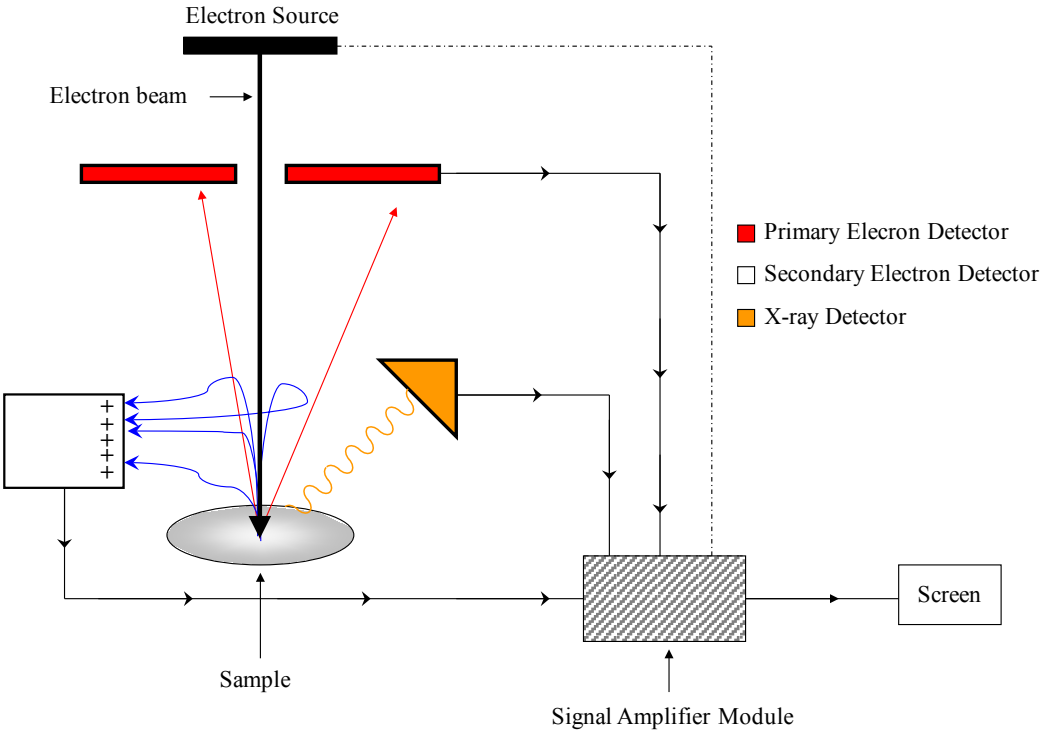

Figure 2.6: Schematic view of a SEM microscope.

Although less useful for SEM imaging, detection of X-ray signals allows elemental analysis of a sample, both qualitative and quantitative. This technique is known as Energy Dispersive X-Ray Spectroscopy (EDS or EDX) and although it is possible to use separately, this technique is most commonly found associated to SEM and TEM (Transmission Electron Microscopy). This confers the ability of SEM-EDS microscopes to characterize a sample in visual and elemental terms.

2.4 Thermal Analysis Techniques

2.4.1 Thermogravimetric Analysis (TGA)

Thermogravimetric analysis (TGA) is a thermal technique which allows the evaluation of changes in sample mass with respect to temperature.

This technique can be applied to materials with temperature-dependant physico-chemical properties that may promote variations in mass. However, some physico-chemical processes do not promote mass changes, such as crystallization, glass transition or fusion. Nevertheless, some important processes can be monitored by TGA, and these include evaporation/sublimation, decomposition (partial or total), oxidation and adsorption/desorption.

A TGA study can be run with temperature scan (dynamic study) or at a constant temperature (isothermal study). In a dynamic study, the plotting of temperature *vs.* sample mass results on a thermogravimetric curve. Figure 2.7 illustrates the appearance of a thermogravimetric curve and the processes taking place:

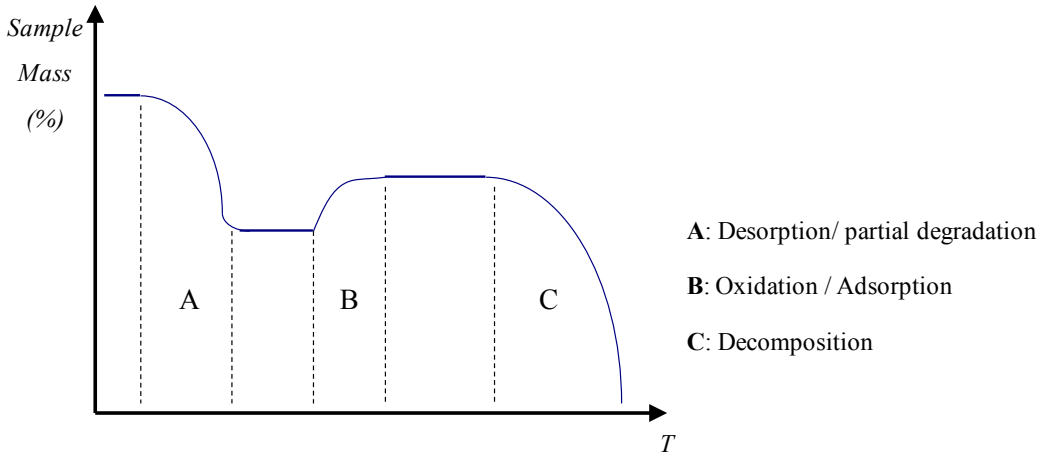

Figure 2.7: Example of a thermogravimetric curve and the attribution of the corresponding processes.

A thermogravimetric curve is dependent of several experimental factors, being heating rate one of the most important. Due to the thermal inertia of the sample, at low heating rates, the temperature at which a process begins is shifted to a lower temperature range, whereas for higher heating rates the same processes will start at higher temperatures. Therefore, in order to correctly compare the thermogravimetric behaviour of different samples, it is required that all samples have been subject to the same heating rate.

An auxiliary tool for the thermogravimetric characterization of a material is the Differential Thermogravimetry (DTG), which is simply the derivative of sample mass variation against temperature. Figure 2.8 presents the aspect of a combined TGA-DTG analysis:

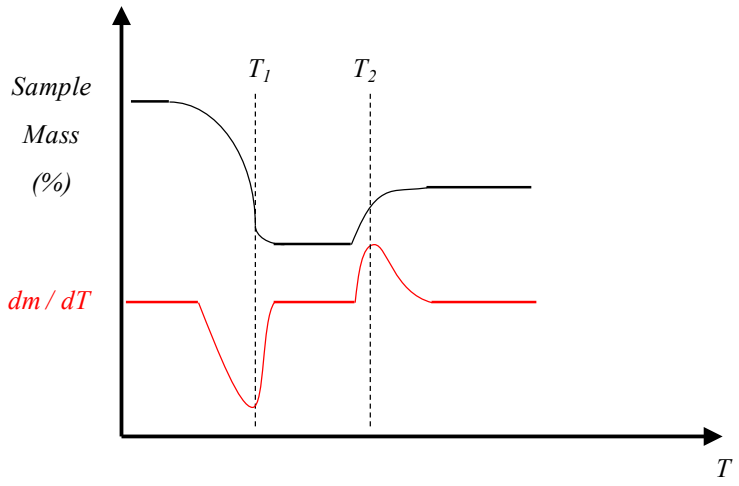

Figure 2.8: Examples of TGA (black line) and DTG (red line) curves of a sample.

DTG is useful for the exact determination of the temperatures at which the maximum rate of mass variation takes place. DTG may also be used to identify the presence of certain compounds on a mixture or complex samples, as the DTG peak position of a compound is constant under the same heating rate. For the precise determination of mass variation, TGA is more helpful.

A simple thermogravimetric analyser consists of two main components: a microbalance connected to a sample holder placed on an oven. Most TGA analysers also allow the selection of the oven atmosphere, which can be inert (He, N_2) or oxidizing/reducing (air, O_2 or CO). A schematic view of a TGA analyser is shown in Figure 2.9:

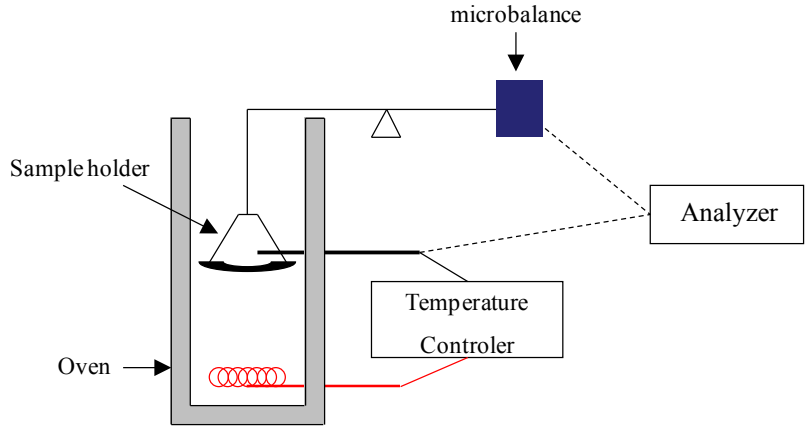

Figure 2.9: Schematic view of a simple thermogravimetric analyser.

The application of TGA-DTG to zeolite samples allows a straightforward determination of the amount of adsorbed species. Water is the most common and its desorption usually occurs on a temperature range below 150 ºC [19]. For higher temperatures, zeolites are inert up to 600 ºC and the inclusion of other compounds can be detected in this range, namely immobilized metal complexes [19-21]. Advanced applications of TGA to the study of zeolite samples includes coupling with Differential Scan Calorimetry to determine the heat of adsorption of adsorbates, as well as the use of basic molecules to determine overall acidity [4].

2.5 Chromatographic Methods

2.5.1 Gas-phase Chromatography (GC)

Gas-phase chromatography (GC) is based on the partition between a mobile gaseous phase carrying the analyte and a stationary phase, either consisting of a solid (*gas-solid chromatography*) or immobilized liquid (*gas-liquid chromatography*). Gas-solid chromatography is based on the physical adsorption of the vaporized sample whereas in gas-liquid chromatography, the separation is based on the partition between the sample components and a liquid-phase that is immobilized on an inert solid. Due to the limited application of gas-solid chromatography (as adsorption is non-linear), gas-liquid chromatography is the most widespread use for GC [14].

Alike the other chromatographic methods, the basic principle in GC is the separation of the components of a sample by their different affinity as they elute through a stationary phase. However, GC adds the possibility to control the temperature of elution, which will affect the affinity between analyte and stationary-phase, allowing the separation and determination of closely related molecules.

In GC, the sample (mobile phase) is vaporized and injected into the stationary phase (a chromatographic column). The column is kept inside an oven with temperature control (either isothermal or dynamic). The effluent of the column is then passed through a detector which is able to measure the amount of analyte that is exiting the column. A simple diagram of a GC apparatus is presented in Figure 2.10:

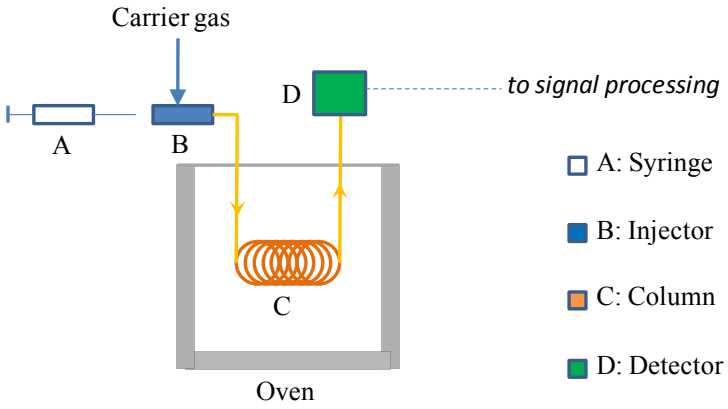

Figure 2.10: Schematic diagram of a gas chromatograph.

The injector is responsible for evaporating the sample and feeding an appropriate amount of the latest into the column. GC columns can be *packed* or *capillary*, with variable length, diameter and composition of stationary phase. The internal coating of the liquid phase must be thermally stable, chemically inert and present a solvent-like behaviour to the sample. A typical coating for non-polar capillary columns consists of polydimethyl siloxane or phenyl.polydimethyl siloxane. Progressive substitution with polar functional groups (such as polyethylene glycol) will shift the affinity of the columns towards polar compounds.

The ultimate section of a GC chromatograph is the detector. The two most commonly employed detectors in GC analysis are the *flame ionization detector* (FID) and *thermal conductivity detector* (TCD). The FID consists of a H_2/air burner fitted with a collector electrode over the flame, which measures the conductivity of the sample. When organic compounds are pyrolized by the flame, ions are produced, which decreases electrical resistance, allowing electric current to flow through the plasma. This current is detected by the electrode and the amount of ionized species (which in turn is related to their concentration) promotes a linear response. A drawback of this detector is the impossibility of measuring non-combustible compounds (such as H_2O). The TCD measures changes in the thermal conductivity of an electrically heated element. The flowing of gas molecules will draw heat from the detector and increase its electrical resistance and this is the measured signal. The TCD can be used with most organic and inorganic species and is non-destructive, allowing further analysis of the sample (for example, on a mass spectrometer). However it possesses low sensitivity and limits the choice of carrier gas.

The signals acquired by the detector are presented as a *chromatogram*, which can be depicted as detector signal *vs.* elution time or as detector signal *vs.* temperature. Signals appear as peaks and are useful in both qualitative and quantitative analysis of the sample. The elution time of a component is constant; however, it is only applicable to the identification of compounds on samples of known composition (since the retention time depends on experimental variables and is not unique to a certain compound). In quantitative analysis, peak area is related to the analyte concentration on the sample by

$$A_{analyte} = f.C_{analyte} \qquad \text{(eq. 2.11)}$$

where f is the response factor of the detector to the specific analyte and varies according to the nature of the analyte and the detector type.

2.6 References

[1] D. Steele, IR Spectroscopy, Theory, in: John C Lindon (Ed.), Encyclopedia of Spectroscopy and Spectrometry, Oxford, Elsevier, 1999: pp. 1066-1071.

[2] B.H. Stuart, Biological Applications of Infrared Spectroscopy, Chichester, John Wiley & Sons, Ltd., 1997.

[3] A.S. Gilbert, IR Spectral Group Frequencies of Organic Compounds, in: J.C. Lindon (Ed.), Encyclopedia of Spectroscopy and Spectrometry, Oxford, Elsevier, 1999: pp. 1035-1048.

[4] A. Jentys, J.A. Lercher, Techniques of Zeolite Characterization, in: H. van Bekkum, P.A. Jacobs, E.M. Flanigen, J.C. Jansen (Eds.), Introduction to Zeolite Science and Practice, Amsterdam, Elsevier, 2001: pp. 345-386.

[5] W. Mozgawa, The Influence of Some Heavy Metals Cations on the FTIR Spectra of Zeolites, Journal of Molecular Structure. 555 (2000) 299-304.

[6] C. Li, Z. Wu, Microporous Materials Characterized by Vibrational Spectroscopies, in: S.M. Auerbach, K.A. Carrado, P.K. Dutta (Eds.), Handbook of Zeolite Science and Technology, New York, Basel, Marcel Dekker, Inc., 2004: pp. 8858-8859.

[7] G.F. Ghesti, J.L. Macedo, V.C.I. Parente, J. Dias, S.C.L. Dias,, Investigation of Pyridine Sorption in USY and Ce/USY Zeolites by Liquid Phase Microcalorimetry and Thermogravimetry Studies, Microporous and Mesoporous Materials. 100 (2007) 27-34.

[8] K. Maquelin, C. Kirschner, L.-P. Choo-Smith, N. van Den Braak, H.P. Endtz, D. Naumann, G.J. Puppels, Identification of Medically Relevant Microorganisms by Vibrational Spectroscopy., Journal of Microbiological Methods. 51 (2002) 255-71.

[9] A. Omoike, J. Chorover, Adsorption to Goethite of Extracellular Polymeric Substances from *Bacillus subtilis*, Geochimica Et Cosmochimica Acta. 70 (2006) 827-838.

[10] A. Omoike, J. Chorover, Spectroscopic Study of Extracellular Polymeric Substances from *Bacillus subtilis*: Aqueous Chemistry and Adsorption Effects., Biomacromolecules. 5 (2004) 1219-1230.

[11] C. Pettinari, C. Santini, IR and Raman Spectroscopy of Inorganic, Coordination and Organometallic Compounds, in: J. Lindon (Ed.), Encyclopedia of Spectroscopy and Spectrometry, Oxford, Elsevier, 1999: pp. 1021-1034.

[12] P.-P. Knops-Gerrits, D. De Vos, E.J.P. Feijen, P.A. Jacobs, Raman Spectroscopy on Zeolites, Microporous Materials. 8 (1997) 3-17.

[13] P.C. Stair, Advances in Raman Spectroscopy Methods For Catalysis Research, Current Opinion in Solid State and Materials Science. 5 (2001) 365-369.

[14] D.A. Skoog, D.M. West, F.J. Holler, Fundamentals of Analytical Chemistry, 7th ed., Saunders College Publishing, 1996.

[15] J.A. Holcombe, Fluorescence and Emission Spectroscopy, Theory, in: J. Lindon (Ed.), Encyclopedia of Spectroscopy and Spectrometry, Oxford, Elsevier, 1999: pp. 560-565.

[16] S.J. Hill, A.S. Fisher, Atomic Absorption , Methods and Instrumentation, in: J. Lindon (Ed.), Encyclopedia of Spectroscopy and Spectrometry, Oxford, Elsevier, 1999: pp. 24-32.

[17] D. Louër, Powder X-Ray Diffraction, Applications, in: J. Lindon (Ed.), Encyclopedia of Spectroscopy and Spectrometry, Oxford, Elsevier, 1999: pp. 1865-1875.

[18] M. Guisnet, F.R. Ribeiro, Zeólitos - Um Nanomundo ao Serviço da Catálise, Lisboa, Fundação Calouste Gulbenkian, 2004.

[19] H. Figueiredo, B. Silva, M.M.M. Raposo, A.M. Fonseca, I.C. Neves, C. Quintelas, T. Tavares, Immobilization of Fe(III) Complexes of Pyridazine Derivatives Prepared from Biosorbents Supported on Zeolites, Microporous and Mesoporous Materials. 109 (2008) 163-171.

[20] H.S. Abbo, S.J.J. Titinchi, Synthesis and Catalytic Activity of Cu(II), Fe(III) and Bi(III) Complexes of Thio-Schiff Base Encapsulated in Zeolite-Y for Hydroxylation of Phenol, Topics in Catalysis. 53 (2010) 254-264.

[21] H. Figueiredo, B. Silva, C. Quintelas, M.M.M. Raposo, P. Parpot, A.M. Fonseca, A.E. Lewandowska, M.A. Bañares, I.C. Neves, T. Tavares, Immobilization of Chromium Complexes in Zeolite Y Obtained From Biosorbents: Synthesis, Characterization and Catalytic Behaviour, Applied Catalysis B: Environmental. 94 (2010) 1-7.

(this page is intentionally left blank)

CHAPTER 3

EXPERIMENTAL PROCEDURES

CHAPTER 3 – EXPERIMENTAL PROCEDURES

This chapter covers all aspects and details related to the execution of the experimental work. Work carried out during this study is divided into three main areas: *biotreatment of Cr(VI) solutions by the bacterium-zeolite system*, *preparation of heterogeneous catalysts by immobilization of chromium in zeolite* and *catalytic reactions in liquid phase*.

3.1 Biotreatment of Cr(VI) solutions

This section presents the experimental procedures used for the treatment of Cr(VI) solutions, to be detailed in Chapter 4.

3.1.1 Studies with low biomass concentration

Initial studies on the remediation of hexavalent chromium (Cr(VI)) were carried out using the *Arthrobacter viscosus* bacterium supported on two mordenite type (MOR) zeolites with different acidity behaviour.

Arthrobacter viscosus was obtained from the Spanish type-culture collection and previously grown in suspension, before addition to the reactor. The bacteria were grown for 24 h at 28 ºC using the culture medium described in table 3.1 (as suggested by the supplier), with pH set to 7.0:

Table 3.1: Composition of the *Arthrobacter viscosus* culture medium.

Component	Concentration (g/L)
Glucose	10
Peptone	5
Malt extract	3
Yeast extract	3
Agar (plate use only)	15

MOR zeolites, NH_4^+-stabilized MOR (HMOR) and Na^+-stabilized MOR (NaMOR) were purchased from Zeolyst International, with the respective references CBV 21A and CBV 10A. Zeolites in powder form were calcined under a dry air flow (50 mL/min) with a heating rate of 5 ºC/min until a maximum temperature of 500 ºC, which was kept for 8 h (according to Figure 3.1).

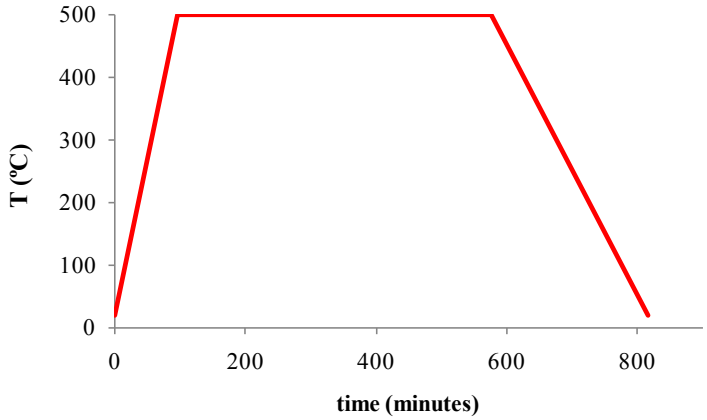

Figure 3.1: Temperature programme for the calcination of zeolites.

The zeolite CBV 21A was available in the ammonium form. After heating, ammonium is transformed into NH_3 and H^+. NH_3 desorbs and the presence of protons increases the number of acid sites. The protonic form of MOR (HMOR) was obtained after the calcination. Specific details of these zeolites are presented in table 3.2.

The treatment of Cr(VI) solutions was performed in batch conditions in 250 mL Erlenmeyer flasks. Each reactor contained 1.0 g of either HMOR or NaMOR zeolite and 15.0 mL of previously grown *Arthrobacter viscosus* suspension. 150 mL of a $K_2Cr_2O_7$ (Riedel, analytical grade) solution in deionised water, with concentrations of 20, 40, 60, 80, 100 and 120 mg_{Cr}/L, were later added to each reactor. All concentrations were tested in triplicate.

The flasks were kept at 28 ºC with moderate agitation on an orbital incubator for 8 days. Samples were collected regularly throughout the experiment by transferring 1.0 mL of the reactor content to a sample tube, which was centrifuged and the supernatant solution was analysed for Cr(VI) by the 1,5-diphenylcarbazide method (detailed further in this section). pH was allowed to change freely and was monitored regularly.

3.1.2 Studies with high biomass concentration

The bulk of the work on treatment of Cr(VI) was conducted with improved biosorption conditions. It was found that, in order to improve the Cr(VI) reducing capacity of the *Arthrobacter viscosus* – zeolite system, a pH of 4.0 and a biomass concentration of 5 g/L yielded the best results [1,2]; therefore, all work in this section was carried out under those conditions. Two different operating modes were employed: *single-step batch experiments* (as the previous studies) and *sequential batch reactor experiments*.

In all conditions, a total of four different zeolite structures were tested, possessing either FAU framework (faujasite type zeolite) or MOR framework (mordenite type zeolite). They were supplied by Zeolyst International. The specifications of the zeolites were obtained from the supplier for MOR zeolites (HMOR and NaMOR) and FAU zeolites (HY and NaY) were characterized by different techniques (table 3.2).

Table 3.2: Specifications of the zeolite samples used in this work.

Zeolite name	Framework type	Stabilizing Ion	Si/Al ratio	Total surface area (m^2/g)	Suplier reference
HY	FAU	H^+	2.80[a]	665[c]	CBV 400
NaY		Na^+	2.83[a]	787[c]	CBV 100
HMOR	MOR	NH_4^+	10.00[b]	500[b]	CBV 21A
NaMOR		Na^+	6.50[b]	425[b]	CBV 10A

[a]Total Si/Al ratio determined from ICP-AES.
[b]Data from Zeolyst International.
[c]Determined by nitrogen adsorption.

Single-step batch reactor operation

All single-batch reactors used correspond to 250 mL Erlenmeyer flasks containing 1.0 g of supporting zeolite, 150 mL of Cr(VI) solution and 15.0 mL of concentrated biomass suspension.

The biomass suspension was processed previously. *Arthrobacter viscosus* was grown in 500 mL of the culture medium (table 3.1) for 24 h at 28 ºC, in an orbital incubator with moderate agitation (150 rpm). Afterwards, this volume was divided and transferred to 2 flasks containing fresh culture medium and the contents were allowed to a second growth

cycle for 48 h, under the same conditions of the first growth cycle. After achievement of the second cycle, the biomass is centrifuged in 250 mL flasks on a Sigma 4K15 centrifuge (set at a maximum RCF of 8000). The supernatant is stored in a sterilized flasks and an adequate volume was used to resuspend the centrifuged biomass pellets. This volume was calculated as to set the biomass concentration in each reactor to 5.0 g/L.

The single-batch experiments were conducted with all zeolites and two Cr(VI) solutions, with concentrations of 50 and 100 mg_{Cr}/L, prepared from $K_2Cr_2O_7$. All assays were conducted in duplicate. Flasks were kept in an orbital incubator set at 28 ºC with moderate agitation (125 rpm) for 27 days. pH was set to 4.0 on the initial stages with H_2SO_4 4.0 or 1.0 M, and constantly monitored and controlled thereafter. Samples were withdrawn, centrifuged and the supernatant solution was analysed for both Cr(VI) and total Cr concentrations by the 1,5-diphenylcarbazide method.

One long-term experiment was conducted with NaY zeolite. The process was the same as described above, with the exception of experimental time which was set to 165 days.

Sequential-batch reactor (SBR) operation

A sequential-batch reactor (SBR), as described in this work, corresponds to three 250 mL Erlenmeyer flasks containing 1.0 g of zeolite and 15.0 mL of concentrated biomass suspension (prepared as detailed previously) through which a Cr(VI) solution is passed sequentially, with a residence time of 96 h for each reactor.

The first step in the SBR operation is prepared identically to the single-step batch experiments. 150 mL of a 100 mg_{Cr}/L Cr(VI) solution is transferred to a reactor containing the zeolite and biomass suspension. The pH is set immediately to 4.0 with H_2SO_2 4.0 or 1.0 M (when necessary). After 96 h, the solution was recovered by centrifugation on a Sigma 4K15 centrifuge (set at maximum RCF of 7000). The volume of the supernatant solution was measured on a sterilized graduated cylinder and transferred to the second reactor, where it is treated for another 96 h. The centrifugation process was repeated for the start of the third cycle.

All zeolites were tested in duplicate in all process cycles. The reactors were kept at 28 ºC in an orbital incubator with moderate agitation (125 rpm). The pH was constantly monitored

and corrected to 4.0 as necessary using H_2SO_2 1.0 M. Samples were collected regularly, centrifuged and the supernatant solution was analysed for both Cr(VI) and total Cr concentrations using the 1,5-diphenylcarbazide method.

3.1.3 Definition of sample nomenclature

Samples collected from the different Cr(VI) treatment studies bear reference to the employed zeolite, with the "Cr" prefix. Samples of FAU zeolites are named "CrNaY" or "CrHY", while samples from mordenite zeolites are referred to as "CrMOR" or "CrHMOR".

Adding to the reference name, every sample possesses a distinctive suffix. The following suffixes are applied:

- (samples from single-step batch reactors): reference to the initial chromium concentration of the solution tested (example: CrHMOR 80 refers to a HMOR zeolite used in the biotreatment of a 80 mg_{Cr}/L solution);
- CrNaY sample recovered from the long-duration experiment was given the reference "CrNaY EXT" (as for "extended duration")
- (samples from sequential batch reactors): the suffix "SBR" is applied instead of the initial chromium concentration of the experiment. According to the reactor cycle, SBR 1, SBR 2 or SBR 3 suffixes are employed (example: the HY zeolite recovered from the second cycle reactor is named $CrHY_{SBR}$ 2).

3.2 Preparation of the heterogeneous catalysts

All solid samples described in this section are recovered from the Cr(VI) biotreatment experiments, consisting of the biomass-zeolite system. Some exceptions (the preparation of Cr(III) catalysts by ion-exchange) are mentioned wherever necessary.

The full experimental results from this section will be detailed in Chapter 5.

3.2.1 Recovery and treatment of used biomass-zeolite

The different Cr-zeolite concentrations and processes (single-batch or SBR cycle) are treated individually.

After the achievement of the Cr(VI) biotreatment studies, the residual solid was recovered by centrifugation using a Sigma 4K15 centrifuge, set at a maximum RCF of 6000. The supernatant solution is discarded or stored for analysis (as necessary) and the solid phase is dried in an oven at 105 ºC (normal atmosphere). After 24 h drying, the solids are ground and calcined using the same temperature program as described in Figure 3.1, under a dry air flow at 40 mL/min.

3.2.2 Synthesis of the heterogeneous catalysts

Early studies on the synthesis of heterogeneous catalysts were based on zeolitic samples from previous studies [3-5].

For all catalysts prepared in this work, the chromium obtained after the biotreament was entrapped in zeolite by the *flexible ligand* method using specific heterocyclic derivative ligands. The overall preparation can be summarized as follows for NaY as example:

I- Reduction of Cr(VI) to Cr(III) by *Arthrobacter viscosus* supported on NaY

II- Ion-exchange of Cr(III) ions in zeolite obtained by biosorption process

$$Na_{53}Y + xCr^{3+} \leftrightarrow Cr_xNa_{53-3x}Y + 3xNa^{+} \quad [1]$$

III- *In situ* immobilization of the Cr complex

$$Cr_xNa_{53-3x}Y + \text{excess L} \leftrightarrow [Cr(L_n)]_xNa_{53-3x}Y \quad [2]$$

where x represents the atom fraction of Cr^{3+} ions migrating into the zeolite and L represents the heterocyclic derivative ligand coordinated to the chromium center. The heterocyclic derivative ligands used in this work were: 1-(2-pyridylazo)-2-naphthol (PAN) and diphenyltriazene derivatives ligands.

Immobilization with PAN ligand

A single Cr-containing NaY zeolite from previous studies was used in this work, named "CrNaY* 100" (the asterisk is for the distinction between this sample and the CrNaY 100 sample obtained from high biomass concentration studies), with a chromium loading of

0.14 % (w/w). PAN ligand (Aldrich) was used as received and the corresponding molecular structure can be found in Figure 3.2.

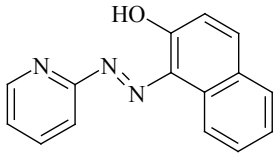

Figure 3.2: Molecular structure of the 1-(2-pyridylazo)-2-naphthol (PAN) ligand.

The immobilization process consisted in three steps: *in-situ synthesis, Soxhlet extraction* and *stabilization with sodium ions (Na^+)*.

The in-situ synthesis of the complex was carried out using 0.5 g of calcined Cr-zeolite and 0.76 mol of PAN ligand. The CrNaY* 100 sample was previously dried at 150 ºC under vacuum for 12 h. The solid was transferred into 100 mL round flask with 50 mL of tetrahydrofuran (THF). The mixture was refluxed for 12 h and the solids were recovered by filtration and dried at 60 ºC overnight.

Soxhlet extraction was performed to remove uncoordinated PAN molecules, Cr-PAN complexes that formed on the outer surface of the zeolite and possible THF molecules retained by the framework. The extraction was carried out with 60 mL ethanol during 12 h, after which the solid was collected and dried overnight at 60 ºC. The final step of the process was stabilization with an aqueous NaCl solution (0.01 M) to remove uncoordinated Cr ions, for 24 h. The solid was recovered by filtration and dried overnight at 90 ºC under vacuum.

Immobilization with diphenyltriazene derivative ligands

The ligand compounds used in this work were synthesized in the Chemistry Department of the University of Minho. The structures, codenames and correspondent nomenclature are presented in Figure 3.3.

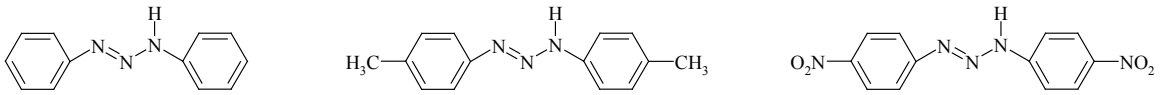

diphenyltriazene (DPT) di(4-methyl-phenyl)-triazene (MeDPT) di(4-nitro-phenyl)-triazene (NODPT)

Figure 3.3: Structures and nomenclature of the diphenyltriazene ligands.

Selected Cr(VI) treatment samples were used as supports for the encapsulation of Cr complexes, with the corresponding ligands indicated in table 3.3. Additionally, a Cr(III)-NaY sample was prepared for comparison purposes. This sample was prepared by allowing 2.5 g of calcined NaY zeolite to contact 150 mL of a $CrCl_3.6H_2O$ solution (85 mg_{Cr}/L), under agitation at room temperature for 72 h. The solid was recovered by filtration and dried at 200 ºC overnight.

Table 3.3: Combination of supports/ligands used in this work.

Support	Tested ligands
CrNaY 100	DPT, MeDPT, NODPT
CrNaY SBR 1	DPT
CrHY SBR 1	DPT
Cr(III)-NaY	DPT

The immobilization of Cr complexes in FAU type zeolites was carried out in a similar process as to the preparation of Cr-PAN complexes, using the same three steps.

For the *in-situ* synthesis, 1.0 g of the support (previously dried at 150 ºC under vacuum) was refluxed with 0.28 mmol of ligand in 100 mL of ethanol (99.9 %) for 24 h. The solid was recovered by filtration and dried at 60 ºC overnight. Soxhlet extraction was performed with dichloromethane (50 mL) for 5 h and the solid was dried at 60 ºC overnight before the stabilization with a $NaNO_3$ 0.01 M solution. The solid was recovered by filtration, washed with distilled water and dried overnight at 60 ºC.

3.3 Catalytic reactions

Evaluation of the performance of the prepared catalysts was conducted by two reactions: oxidation of cyclohexene and oxidation of cyclohexanol. Full results will be detailed in Chapter 6.

Oxidation of cyclohexene

The experimental conditions for the cyclohexene oxidation reaction were adjusted throughout the work. The previous conditions were based on the work of Nunes *et al.* [6]. The selected oxidant was *tert*-butylhydroperoxide (*t*-BuOOH) (Aldrich), commercially available in a 5.0-6.0 M solution in decane. The same solvent was chosen for the reaction (Aldrich, p.a.), due to its high boiling point. Cyclohexene was purchase from Aldrich (GC grade, 99%) and toluene was purchased from Riedel (p.a.) and used as internal standard for GC analysis. Both compounds were stored in darkness and in closed glass bottles with dry 4A molecular sieves (BDH Limited).

The reaction was carried out in 50 mL three-way round flasks, immersed in an oil bath thermostated fitted with a water condenser. The reaction mixture used in all experiments was the following:

Table 3.4: Reaction mixture for the oxidation of cyclohexene.

Compound	Quantity (mL)	Purpose
Decane	5.8	solvent
Cyclohexene	0.2 (2 mmol))	substrate
Toluene	0.4	GC internal standard
t-BuOOH (5.0 – 6.0 M in decane)	2.0 (≈ 12 mmol)	oxidant

The general procedure is as follows: 50 mg of chosen catalyst are previously dried at 105 ºC under vacuum for a minimum of 12 h and allowed to cool down (also under vacuum) to the reaction temperature prior to use. Decane, cyclohexene and toluene are transferred into the reactor already at the selected reaction temperature. Agitation is provided by a magnetic stirrer set at 100 rpm. After a short mixing time, a sample of this initial solution is collected before the addition of the catalyst. After transferring the catalyst, the reactor is sealed with a

rubber septum and allowed to mix for 20 min, when the *t*-BuOOH oxidant is transferred dropwise with a glass syringe. The addition of the oxidant marks the start of the reaction (t = 0 s). The reaction is allowed to run for 23 h (or otherwise specified). With the exception of the initial solution sample, all samples are collected with a disposable syringe and filtered with 0.20 μm pore size syringe filters.

Whenever necessary, the solid contents were recovered by filtration with a 10-16 μm pore glass filter, washed with ethanol and acetone and dried at 105 ºC under vacuum.

The conversion of the substrate in the reaction is given by equation 3.1.

$$X_{Cyclohexene} = 100.\frac{\left(A_{Cyclohexene} / A_{Toluene} \right)_i}{\left(A_{Cyclohexene} / A_{Toluene} \right)_{t=0}} \qquad \text{(eq. 3.1)}$$

where X is the reaction conversion and A represents peak area from GC analysis of either cyclohexene or toluene. The initial and final samples were analysed in triplicate for each reaction and the conversion was determined from the average result. The error is determined by the *t*-student distribution for a 95 % confidence level. If a catalyst is tested more than once, the overall average and error are determined from all individual analytical results.

The determination of reaction selectivity for each oxidation product is given by equation 3.2.

$$S_a = 100.\frac{A_a}{A_a + A_b + ... + A_n} \qquad \text{(eq. 3.2)}$$

where S is selectivity, A is the peak area from GC analysis of the sample and *a, b,...,n* represent the several reaction products.

Oxidation of cyclohexanol

The second catalytic reaction covered in this work is the oxidation of cyclohexanol. The same experimental apparatus used in the oxidation of cyclohexene was used for this study and the only difference was the composition of the reaction mixture. Since cyclohexanol is

more polar than cyclohexene, a change in solvent was required and the selected option was diethylketone (DEK) (Aldrich, 98 %, reagent grade). This solvent presents good solubility for the reaction components and a high boiling point (105 ºC). Cyclohexanol was purchased from Panreac (99 %, synthesis grade) and chlorobenzene (Acros Organics, spectroscopy grade) was selected as internal standard for GC analysis. Both compounds were stored in dark and in closed glass bottles with dry 4A molecular sieves (BDH Limited). The same oxidant was used (*t*-BuOOH, 5.0 – 6.0 M in decane, Aldrich). The reaction mixture used in all experiments was the following:

Table 3.5: Reaction mixture for the oxidation of cyclohexanol.

Compound	Quantity (mL)	Purpose
Diethylketone	5.0	solvent
Cyclohexanol	0.3 (2.9 mmol)	substrate
Chlorobenzene	0.4	GC internal standard
tBuOOH (5.0 – 6.0 M in decane)	2.0 (≈ 12 mmol)	oxidant

The same overall procedure and sampling employed in the oxidation of cyclohexene was used for this reaction. The determination of reaction yield was determined using equation 3.3

$$X_{Cyclohexanol} = 100.\frac{\left(A_{Cyclohexanol} / A_{Chlorobenzene} \right)_i}{\left(A_{Cyclohexanol} / A_{Chlorobenzene} \right)_{t=0}} \qquad \text{(eq. 3.3)}$$

where X is reaction conversion and A represents the peak area from GC analysis of either cyclohexene or toluene. The initial and final samples were analysed in triplicate for each reaction and the conversion was determined from the average result. The error is determined by the *t*-student distribution for a 95% confidence level. If a catalyst is tested more than once, the overall average and error are determined from all individual analytical results. The determination of product selectivity was not carried out as this is a single-product oxidation reaction.

Evaluation of chromium leaching from the catalyst was performed for this reaction. Liquid samples from end-of-reaction experimental time were digested with nitric acid (HNO_3, 66%, p.a.) in a microwave and analysed for total Cr by AAS.

3.4 Analytical conditions

The determination of Cr(VI) and total Cr concentration in all samples from Cr(VI) biotreatment studies was carried out using the 1,5-diphenylcarbazide colorimetric method. This is one of the longstanding analysis method for Cr(VI) [7] and has become a standard method [8], successfully employed for the determination of Cr(VI) and total Cr in samples from biosorption studies [9,10]. Liquid samples were diluted according to the initial Cr concentration of the essay (1:50 and 1:100 for initial concentrations of 50 mg_{Cr}/L or 100 mg_{Cr}/L, respectively). For the determination of total Cr, samples were previously digested with excess $KMnO_4$ to oxidize any other Cr oxidation state to Cr(VI). Absorbance was measured at 540 nm wavelength in a 1 cm cell, averaging three readings per sample. Calibration curves were performed using Cr(VI) standard solutions that received the same treatment as samples.

Determination of total Cr in microwave digested samples was performed by AAS in a Varian SpectrAA-250 spectrometer, with acetylene/air supported flame. Acid digestion was performed with HNO_3 on a CEM MDS-2000 microwave (0.5 mL of sample for 10.0 mL of acid).

FTIR spectra of solid samples were collected on a Bomen MB104 spectrometer. Samples were ground with dry KBr ia a sample:KBr mass proportion of 1:100 (possibly increasing KBr ratio if saturation of signal is detected). Spectra were collected by averaging 10 scans per sample, with a resolution of 4 cm^{-1}.

Raman spectra of solid samples were obtained with a Perkin-Elmer 400F Ramanstation spectrometer, fitted with an infrared laser (λ = 785 nm) able to supply a maximum power at sample of 100 mW. All samples were analysed in powder form with individual adjustments to laser power, exposition time and number of expositions per sample being carried out as necessary to reduce background fluorescence.

TGA analysis was conducted on a Shimadzu TGA-50 equipment. Samples were placed in aluminium crucibles (maximum operating temperature of 600 ºC), with sample masses ranging from 2.5 to 3.5 mg. Every analysis was conducted with constant heating of 6 ºC/min to a maximum temperature of 580 ºC, under a 50 mL/min dry N_2 flow.

Nitrogen adsorption isotherms were performed on a Micromeritics ASAP-2000 automatic instrument. All samples were previously degassed at 140 ºC for 2 h.

GC analysis of liquid samples from the catalytic reactions was performed on a SRI Instruments 8610C gas chromatograph, equipped with a Quadrex 007 5%-methyl-phenyl silicone capillary column (30 m length per 0.25 mm internal diameter) and a FID detector. Temperature programs and carrier gas pressure (dry N_2) were adjusted to enable good separation of products, especially substrate and oxidation products. All monitored components were identified from the retention times of the corresponding GC-grade standards and confirmed by coupled GC-MS spectroscopy (Varian 4000 Performance).

3.5 Material conditioning and waste management

All glassware and materials used for handling, testing and storing of aqueous Cr(VI) solutions were previously washed with diluted nitric acid and rinsed with deionised water.

All glassware and materials used in the preparation of culture media, bacterial growth or for the concentration of biomass suspensions were previously sterilized in autoclave at 121 ºC for 20 min.

All glassware and materials used in catalytic reactions were previously treated with diluted nitric acid in an ultrasound bath for 10-15 mins and rinsed with deionised water.

Liquid medium wastes were stored according to their specific nature and collected for treatment by a specialized company. Cr(VI) solutions and wastes generated by the 1,5-diphenylcarbazide colorimetric method were stored altogether. The liquid contents collected from the catalytic reactions were stored as non-halogenated solvents waste.

3.6 References

[1] B. Silva, H. Figueiredo, I.C. Neves, T. Tavares, The role of pH on Cr (VI) Reduction and Removal by Arthrobacter Viscosus, International Journal of Chemical and Biomolecular Engineering. 43 (2009) 59-62.

[2] H. Figueiredo, B. Silva, C. Quintelas, I.C. Neves, T. Tavares, Effect of the Supporting Zeolite Structure on Cr Biosorption: Performance of a Single Step Reactor and of a Sequential Batch Reactor-a Comparison Study, Chemical Engineering Journal. 163 (2010) 22-27.

[3] H. Figueiredo, B. Silva, C. Quintelas, M.M.M. Raposo, P. Parpot, A.M. Fonseca, A.E. Lewandowska, M.A. Bañares, I.C. Neves, T. Tavares, Immobilization of Chromium Complexes in Zeolite Y Obtained From Biosorbents: Synthesis, Characterization and Catalytic Behaviour, Applied Catalysis B: Environmental. 94 (2010) 1-7.

[4] H. Figueiredo, I.C. Neves, C. Quintelas, T. Tavares, M. Taralunga, J. Mijoin, P. Magnoux, Oxidation Catalysts Prepared From Biosorbents Supported on Zeolites, Applied Catalysis B: Environmental. 66 (2006) 274-280.

[5] H. Figueiredo, M.M.M. Raposo, A.M. Fonseca, I.C. Neves, C. Quintelas, T. Tavares, Encapsulated Pyridazine Cr(III) Complexes Prepared From Biosorbents Supported in Zeolites, in: J. Cejka, I. Zilková, P. Nachtigall (Eds.), Molecular Sieves: From Basic Research To Industrial Applications, Proceedings Of the 3rd International Zeolite Symposium (3rd FEZA), Elsevier, 2005: pp. 1073-1080.

[6] N. Nunes, R. Amaro, F. Costa, E. Rombi, M.A. Carvalho, I.C. Neves, A.M. Fonseca, Copper(II)–Purine Complexes Encapsulated in NaY Zeolite, European Journal of Inorganic Chemistry. 2007 (2007) 1682-1689.

[7] R.T. Pflaum, L.C. Howick, The Chromium-Diphenylcarbazide Reaction, Journal of the American Chemical Society. 78 (1956) 4862–4866.

[8] D. Eaton, L.S. Clesceri, A.E. Greenberg, Standard Methods for the Examination of Water and Wastewater, 19th ed., Washington D.C., American Public Health Association (APHA), 1995.

[9] D. Park, S.-R. Lim, Y.-S. Yun, J.M. Park, Reliable Evidences That the Removal Mechanism of Hexavalent Chromium by Natural Biomaterials is Adsorption-coupled Reduction., Chemosphere. 70 (2007) 298-305.

[10] D. Park, Y.-S. Yun, J.Y. Kim, J.M. Park, How to Study Cr(VI) Biosorption: Use of Fermentation Waste for Detoxifying Cr(VI) in Aqueous Solution, Chemical Engineering Journal. 136 (2008) 173-179.

(this page is intentionally left blank)

CHAPTER 4

BIOTREATMENT OF Cr(VI) SOLUTIONS

CHAPTER 4 – BIOTREATMENT OF Cr(VI) SOLUTIONS

This chapter presents the experimental results and related discussion on the development of the *Arthrobacter viscosus*-zeolite system and its performance on the treatment of Cr(VI) solutions.

The contents of this chapter are divided in three sections. The first, referred to as previous work, presents an historical overview of the early experiments and results obtained with the *A. viscosus*-FAU zeolite system, which were conducted previously to this PhD research plan, albeit of great importance for the development of this work. This section is followed by the initial studies with free pH and studies with optimized biomass and pH conditions, both belonging to the actual scope of this plan.

4.1 Previous work on the *Arthrobacter viscosus*–zeolite system

The first studies on the properties of *Arthrobacter viscosus* as an adequate biosorbent for Cr(VI) were performed using granular activated carbon (GAC) as the biofilm support [1]. The usage of natural zeolites instead of activated carbon arose from the possible synergistic effects between biomass and zeolites [2,3], the lower cost of zeolites *vs.* GAC, as well as the known sorption properties of zeolites towards metals in solution. Natural zeolite clinoptilolite was used either individually or mixed with GAC for supporting an *A. viscosus* biofilm to treat Cr(VI) solutions and it was found that, although individually inferior in performance to a GAC system, the combination of both supports enhanced Cr(VI) removal [4].

The option for synthetic zeolites as biosorbent supports came later with the intentional aim of using the exhausted supports in catalytic applications. Those studies were conducted in batch conditions using faujasite (FAU) zeolite structures (NaX or NaY) that showed capacity for partial treatment of Cr(VI) solutions with concentrations up to 250 mg_{Cr}/L. The maximum Cr removal was 20 %, which was achieved with both zeolites [5,6]. The results demonstrated that the intrinsic inability of these zeolites for the capture of Cr(VI)

anionic species could be overcome by their reduction to Cr(III) ions, which was performed by the bacteria. Figure 4.1 presents a schematic view of the process.

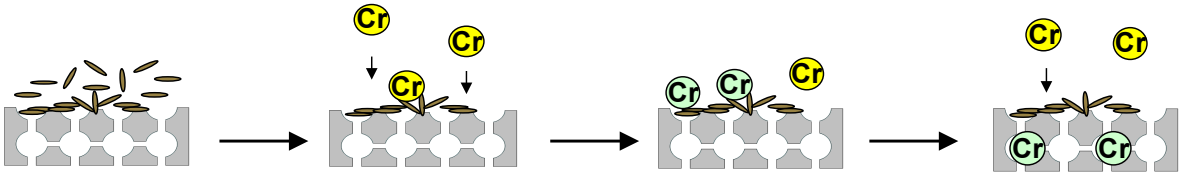

Figure 4.1: Schematic view of the Cr(VI) biotreatment by the *A. viscosus*-Y zeolite system. From left to right: 1) biomass deposition of Y zeolite, 2) Cr(VI) (yellow colour) biosorption by the biomass, 3) bioreduction to Cr(III) (green colour) and 4) ion-exchange of Cr^{III} by the zeolite. Illustration is not in scale.

The system was also tested for cationic species such as Fe(III) and Cr(VI), coupled with Cr(VI) solutions [7-9], and it showed good affinity for these species, both in presence and absence of competing Cr(VI) compounds. Structurally, the cristallinity of framework structure and chemical composition of the zeolites were preserved throughout the biosorption process, allowing their recovery for future use in catalysis.

The relative lower removal capacity of *A. viscosus* -NaX or -NaY system, when compared to GAC, was subject of further studies. First, zeolites lack the same Cr(VI) affinity as GAC offers. This renders the zeolite based system largely dependent on the Cr(VI) reduction capacity of the biomass. Secondly, GAC offers a much larger surface area that is also more easily available to the bacteria, allowing more efficient deposition of the latest (biofilm formation) which can assist the transfer process of reduced Cr species to the support [4,5].

In order to overcome this limitation, a modification of NaY zeolite was performed using alkali-treatment. The intention was to increase the roughness of the outer zeolite surface, thus increasing the availability of fixation sites for the bacteria. The zeolite was treated with sodium hydroxide (NaOH) solutions under reflux for 1 hour. It was found that this treatment selectively attacks the Si tetrahedra while conserving the Al-based structures. The decrease in Si/Al ratio was confirmed: from an initial 2.88 value to final values of 2.51 for bulk Si/Al ratio and 1.89 for exclusive framework Si/Al ratio [10]. Biosorption data revealed that an increase in Cr removal was possible by this modification; however, later retention of the Cr ions in the zeolite was affected by the alkali treatment, which was

undesirable for the downstream catalytic application. Moreover, given the added complexity and increase in cost for large scale modification treatment of the zeolite, this approach was left behind in favour of improving biosorption performance, which marked the starting point of the studies, conducted under the scope of this work.

4.2 Initial studies with free pH

The studies presented in this section involve pH mediation by the biomass-zeolite system, without external contribution. Although the supports were selected in order to have a deliberate influence on pH, the absence of external control means that these studies are considered operating under free pH conditions.

From the early studies, it was perceived that the biomass-zeolite system required a notorious capacity for Cr(VI) reduction in order to increase Cr retention. Looking into the factors that contribute to the redox properties of Cr(VI), a relevant dependence on availability of H^+ ions and electron donors is easily noticed from the formal reduction equation of dichromate in acidic medium (eq. 4.1):

$$Cr_2O_7^{2-} + 14H^+ + 6e^- \Leftrightarrow 2Cr^{3+} + 7H_2O \qquad \text{(eq. 4.1)}$$

The formal electrode potential for this reaction is quite high, at +1.330 V [11], which explains the proneness of dichromate to be reduced. The dependency on proton availability was mentioned in the studies of Park *et al.* [12,13]. Since the electron source on equation 4.1 can be any of the different electron donor groups present in the complex nature of the cellular surface, limiting electron availability to biomass itself, a control on pH could possibly induce better Cr(VI) reduction performance. This could be achieved by external control of the pH of the solution; however, an alternative for internal pH regulation was considered by selective choice of the supporting zeolite, replacing alkali-metal containing zeolites for their hydrogen-containing counterparts.

Taking into account the ionization equilibrium of water molecules (eq. 4.2), the presence of an alkali-metal containing zeolite (example: NaY) increases the pH of the solution [14], as it is able to exchange H^+ ions from water (eq. 4.3).

$$H_2O \Leftrightarrow H^+ + OH^- \quad \text{(eq. 4.2)}$$

$$Na^+ - Y + H_2O \Leftrightarrow H^+ - Y + Na^+ + OH^- \quad \text{(eq.4.3)}$$

Conversely, the hydrolysis of a HY zeolite results in no change in H^+ concentration (eq. 4.4). Nevertheless, provided other cations are present in solution, such as K^+ from the potassium dichromate salt, release of H^+ ions from the HY zeolite into solution is possible, thus lowering the pH of the solution (eq. 4.5).

$$\underset{(1)}{H^+} - Y + \underset{(2)}{H_2O} \Leftrightarrow \underset{(2)}{H^+} - Y + \underset{(1)}{H^+} + OH^- \quad \text{(eq. 4.4)}$$

$$H^+ - Y + K^+ \Leftrightarrow K^+ - Y + H^+ \quad \text{(eq. 4.5)}$$

Free pH assays were conducted with two mordenite (MOR) zeolites, namely NaMOR and HMOR, according to their chemical composition. Although the first studies were conducted on NaX or NaY zeolites, the change in support was also tested in this experiment, in order to evaluate possible differences promoted by the structural nature of each zeolite, albeit possessing the same pore opening size (12 O openings). The biomass-MOR zeolite systems were tested for the treatment of Cr(VI) solution in the 20-120 mg_{Cr}/L range for an experimental period of 192 hours. The different zeolites promoted distinct pH profiles, as intended, which are presented in Table 4.1.

Table 4.1: Measured pH values for the different solutions.

Solution (mg_{Cr}/L)	Cr^{VI} Solution pH	HMOR		NaMOR	
		Initial	Final	Initial	Final
20	5.21	3.60	3.35	7.03	7.85
40	5.20	3.52	3.27	6.31	8.19
60	4.30	3.53	3.21	6.22	7.83
80	5.02	3.29	3.10	6.08	5.41
100	4.83	3.39	3.11	6.12	5.18
120	4.72	3.31	3.07	6.09	5.34

Both zeolites induced instant shift in pH condition upon addition of Cr(VI) solution, as it can be seen from the pH values of the initial measurements. This set of data also shows the distinct behaviour of HMOR and NaMOR zeolites: HMOR zeolite instantly lowered the pH of Cr solutions to pH less than 4, which decreased slightly towards the end of the experiment. NaMOR zeolite increased the initial pH of the solution and for concentrations below 60 mg_{Cr}/L the pH increased until the end of the assays, while for the higher concentrations the pH tended to return to the original value of the parent Cr(VI) solutions. A possible explanation for this inversion in pH behaviour on the higher chromium concentrations could be the release of early-exchanged H^+ ions with the more concentrated K^+ ions (in these solutions) or even the higher concentration of Cr(III) species which also compete with the existing charge-balancing cations that could displace some H^+ ions initially exchanged.

The difference in pH behaviour had an impact on Cr(VI) reduction efficiency. Results for Cr(VI) removal (in terms of C/Cº: instant over initial Cr concentration ratio) are presented in Figure 4.2.

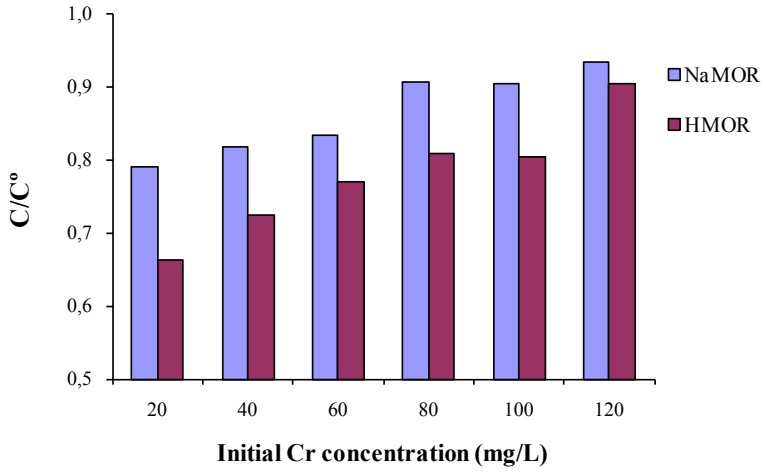

Figure 4.2: C/Cº ratios for the different solutions tested and for the two zeolitic supports.

As it can be seen in Figure 4.2, Cr(VI) C/Cº ratios are lower when the HMOR support is used in all Cr solutions, therefore indicating that the lower pH of the solution favours Cr(VI) reduction. Table 4.2 presents the results for Cr(VI) removal and Cr uptake (defined as mass of removed Cr per mass of dry zeolite):

Table 4.2: Removal and uptake of Cr(VI) by the biomass-MOR zeolite system, after an experimental period of 192 hours.

Solution (mg_{Cr}/L)	Cr(VI) Removal (%)		Cr uptake ($mg_{Cr}/g_{zeolite}$)	
	NaMOR	HMOR	NaMOR	HMOR
20	21.0	33.7	0.72	1.15
40	18.2	27.7	1.43	2.18
60	16.6	22.9	1.86	2.57
80	9.4	19.2	1.31	2.68
100	9.6	19.6	1.71	3.49
120	6.7	9.5	1.31	1.86

The maximum observed Cr removal was 33.7 % of the initial amount, obtained for the least concentrated solution. For the 100 mg_{Cr}/L solution, a removal of 20 % was obtained with HMOR zeolite, which is comparable to the results obtained with NaY or NaX zeolites [5,6]. However, for NaMOR zeolite, the removal of Cr(VI) was less than 10 % which, comparatively to NaY or NaX based system, is quite low. This is due to the smaller ion-exchange capacity of MOR zeolites compared to FAU zeolites (2.29 against 3.39 meq/g, respectively) [15]. Nevertheless, this limitation still allows the performance of HMOR to be comparable to NaY and NaX zeolites – in fact, it even stresses out the influence of the availability of H^+ ions on Cr(VI) reduction and removal, as this low ion-exchange capacity zeolite is still able to achieve comparable Cr(VI) removal.

The Langmuir adsorption model (eq. 4.6) fitted successfully the Cr(VI) adsorption data of HMOR-based system. For NaMOR, a slight deviation is observed. Figure 4.3 presents the plotted fitting of the model (in linear form) to the experimental data, while the calculated parameters are presented in Table 4.3.

$$q = q_{\max} \cdot \frac{bC_{eq}}{1 + bC_{eq}} \qquad \text{(eq. 4.6)}$$

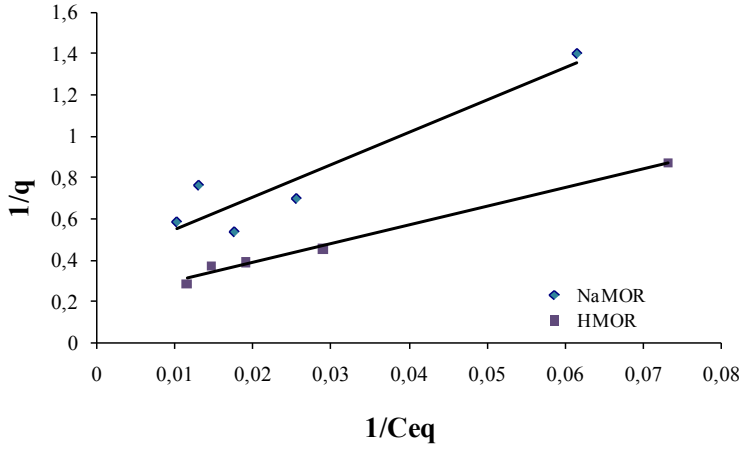

Figure 4.3: Fitting of the Langmuir adsorption model to the experimental data.

Table 4.3: Fitting parameters for the Langmuir model, for both supports tested.

Zeolite	Maximum uptake (q_{max}), $mg_{Cr}/g_{zeolite}$	Affinity Coefficient (b), $(mg/L)^{-1}$	r^2
NaMOR	2.54	0.025	0.890
HMOR	4.77	0.023	0.991

The successful application of the Langmuir adsorption model to the experimental data obtained with the HMOR-based sorbent goes in line with the overall Cr(VI) removal by the adsorption-coupled reduction (ACR) mechanism proposed by Park *et al.* [12]. Other publications on Cr(VI) biosorption by *Arthrobacter* sp. also reported the successful fitting of the Langmuir or Langmuir-based adsorption models [16].

In the adsorption-coupled reduction mechanism, the importance of both solution pH and biomass concentration has been stressed out [13]. While the first factor was investigated in this experiment, biomass concentration was not controlled up to this point. Moreover, the biomass adsorption of Cr(VI) appears to be the limiting step for the ACR mechanism, in terms of the amount of reduced Cr(III) that is generated. Although the support-regulated pH proved to be useful in increasing the efficiency of the system in terms of Cr(VI) removal, a major performance breakthrough to the initial tests was not achieved. Therefore, a study on

the influence of the concentration of *A.viscosus* was needed, which led to the work presented in the next section of this chapter.

4.3 Studies with optimized biomass and pH conditions

This section is adapted from Figueiredo, Silva, Quintelas, Neves and Tavares, Chemical Engineering Journal 163, 22-27, 2010 [17].

An evaluation of the biomass concentration used in previous studies with both FAU and MOR zeolite structures was performed based on estimations, as the exact determination of biomass contents by thermal or spectroscopic techniques is rendered difficult when zeolite particles are present in the medium. Thus, is was observed that the initial culture medium could grow a biomass concentration of 2.5 to 3.0 $g_{biomass}$/L in 24 hours (values for dry biomass concentration), which upon transfer to the reactor would be diluted to values between 0.22 and 0.27 $g_{biomass}$/L. This is a range of very low concentrations when compared to the literature, where concentrations up to 20 g/L were tested to treat Cr(VI) solutions. Therefore, a higher concentration of biomass was required to allow a greater capacity of Cr(VI) treatment.

Initial studies on the influence of pH and biomass concentration on Cr(VI) reduction by a suspension of *Arthrobacter viscosus* was reported by Silva *et al.* [18]. After using biomass concentrations in the 1-5 mg/L range (dry biomass weight), it was found that the highest concentration allowed the best results in terms of Cr(VI) reduction and Cr uptake. Additionally, pH influence studies were carried out with biomass concentration of 5 g/L. The solutions were maintained at pH values of 1, 2, 3 or 4 and the initial concentration of Cr(VI) in each reactor was 100 mg/L. It was confirmed that Cr(VI) reduction by the bacteria was highly pH-dependant and pH 1 proved to be the best pH for Cr(VI) reduction. However, in terms of total Cr removal and uptake by the biomass, pH 4 yielded the best results. This is due to the fact that at a lower pH, the protonation of several functional groups on the cell's surface occurs. The increased abundance of positive charges on the cellular surface limits the affinity for the formed cationic Cr(III) species, which therefore remain in solution at low pH.

After these studies, the operational parameters of pH 4 and biomass concentration of 5 g/L were set as "standard" for the upcoming experiments. Although a lower pH favours Cr(VI) reduction, the stability of the zeolite under strong acidic conditions would be a concern, as it is known that a strong acidic environment promotes the dealumination of the zeolite structure [19,20]. Moreover, as reported previously, a pH of 4 would allow greater contribution of the biomass to Cr uptake. Also, a lower ionic strength of the solution would favour the ion-exchange of the formed Cr(III) species by the zeolite.

The experimental work carried out using these optimized conditions was performed in single batch or sequential batch operation. A total of four different zeolites were used, namely FAU zeolites (HY and NaY) and MOR zeolites (HMOR and NaMOR).

4.3.1 Single-batch studies

The single-batch studies with FAU and MOR zeolites were the first to be conducted under the set pH and biomass concentration parameters. Cr(VI) solutions of 50 and 100 mg_{Cr}/L were tested. However, the different systems responded differently to the pH maintenance which was carried out through the experiments. H-stabilized zeolites allowed a much swifter initial setting and subsequent maintenance, whereas Na-stabilized FAU and MOR zeolites required a higher amount of acid for the initial setting of pH 4 (mostly NaY), although the following maintenance was similar to the H-zeolites counterparts. In terms of biomass concentration, the initial concentration of each system was determined by the dry weight method before the biomass suspension was added to the reactor and concentrations ranged from 4.7 to 4.9 $g_{biomass}/L$ (dry weight).

Figures 4.4 and 4.5 present the evolution of Cr(VI) in each reactor, expressed as instant over initial Cr(VI) concentration (C/C^o), for the solutions of 50 and 100 mg_{Cr}/L, respectively.

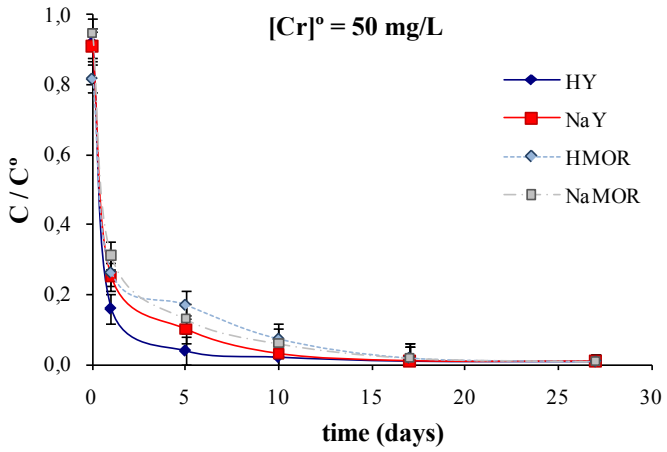

Figure 4.4: Evolution of Cr(VI) concentration for the different supports tested, for an initial Cr concentration of 50 mg/L.

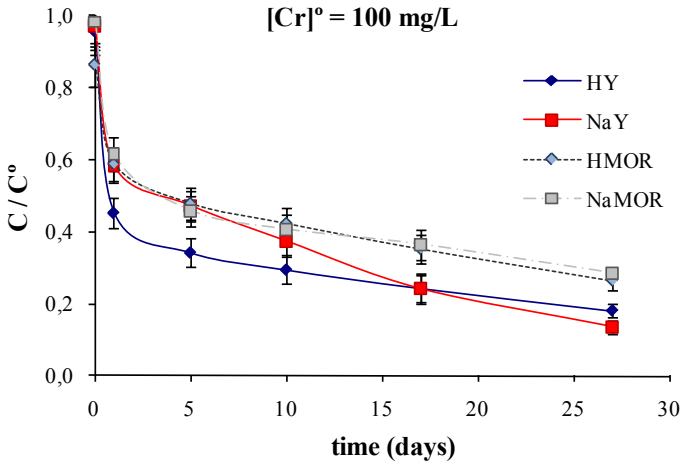

Figure 4.5: Evolution of Cr(VI) concentration for the different supports tested, for an initial Cr concentration of 100 mg/L.

Figures 4.4 and 4.5 show that the optimized conditions enabled the different biomass-zeolite systems to achieve a much higher Cr(VI) reduction. With the higher concentration of biomass, Cr(VI) evolution presents typical biosorption kinetics, with a fast initial stage (observed in the first 24 h) corresponding to processes involving the external cell, and a second slower stage which is dependent on intra-cellular processes or cellular metabolism [4].

The experimental data for the 50 mg/L solution show that the different zeolites present slight differences in terms of Cr(VI) concentration along time, decreasing steadily until

total reduction is achieved in 17 days for all zeolites tested. However, the HY-based system presented the lowest Cr(VI) concentration throughout this experiment.

Differences in performance of each support were made more noticeable using the higher Cr(VI) initial concentration. MOR zeolites presented similar Cr(VI) reduction performance, which is explained by their smaller capacity of ionic exchange when compared to FAU zeolites. This limits the interference in Cr(VI) reduction due to H^+ consumption by NaMOR. The differences between the FAU zeolites are more striking, with HY being a more adequate support for the initial reduction of Cr(VI). This is due to the availability of H^+ ions in the biomass-HY system, as the NaY counterpart consumes some of these ions in the initial stages (which was observed during setting of the initial pH), decreasing Cr(VI) reduction. However, in the longer term, the biomass-NaY system was able to achieve the highest removal of Cr(VI) in this study, surpassing the HY counterpart after 17 days. The reason for this higher second phase rate of Cr(VI) removal can be due to a more efficient ion-exchange with the formed Cr(III) species (since Na^+ is more prone to ion-exchange than H^+), or could be related to a side-process involving the beneficial presence of Na^+ ions in terms of swifter cellular growth or surface regeneration, which would assist Cr(VI) reduction by replacing exhausted electron-donor groups.

Analysis of total Cr confirmed the existence of free Cr(III) species in solution. Figure 4.6 presents the concentration of total Cr at the end of experimental time and Table 4.4 presents Cr removal and uptake by the different systems and initial Cr concentration.

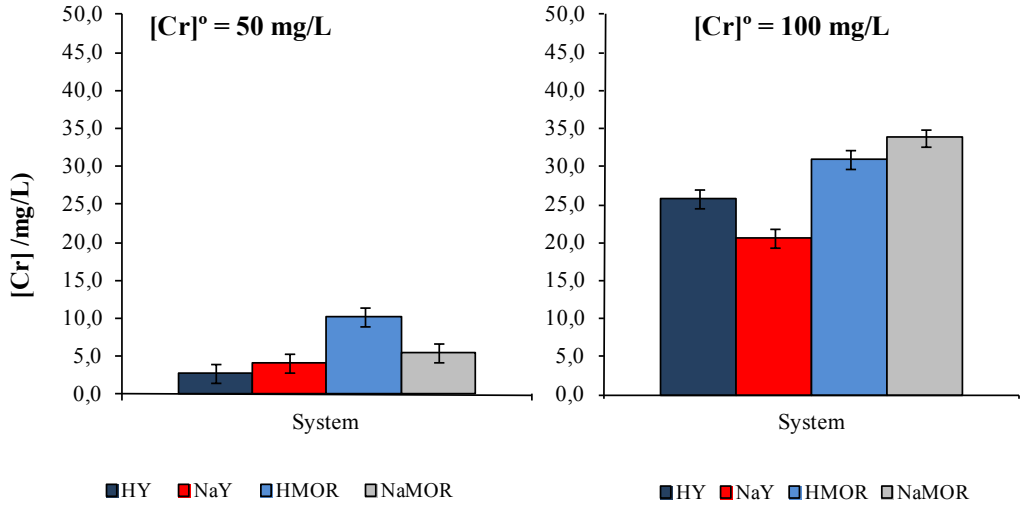

Figure 4.6: Total Cr concentration after 27 days for all supports tested, for the different Cr solutions.

Table 4.4: Removal and uptake of total Cr for the different biomass-zeolite systems.

Initial Cr concentration (mg/L)	Support	Cr removal (%)	Cr Uptake ($mg_{Cr}/g_{zeolite}$)
51.4	HY	93.4	7.2
	NaY	90.8	7.0
	HMOR	77.8	6.0
	NaMOR	88.2	6.8
100.5	HY	71.6	10.8
	NaY	77.6	11.7
	HMOR	65.6	9.9
	NaMOR	63.0	9.5

Looking at the results obtained for the 50 mg_{Cr}/L solution, it is noticed that despite complete Cr(VI) reduction was achieved in all systems, a fraction of reduced Cr remains in solution. The presence of Cr(III) species in solution is most likely due to coordination of the latest with biomolecules such as cellular metabolites or EPS fragments, which is quite prone to occur [21,22]. The coordination with these compounds would render their size large enough to block accessibility to the zeolite structure, thus remaining in solution. The Y zeolites achieved comparable performance in terms of removal and uptake whereas NaMOR zeolite appears to be more effective than it HMOR counterpart. The initial stages of Cr(VI) evolution (Fig. 4.4) show that NaMOR presented a higher reduction capacity through the experimental period, which could explain this difference.

For the higher Cr concentration, the differences in Cr removal between HY and NaY become greater. NaY zeolite was able to achieve the highest removal and uptake of this study, mostly due to a greater reduction rate observed in the secondary stage of biosorption. The experimental results for the MOR pair reveal that the performance of these supports is comparable.

Since NaY zeolite was found to be the most efficient support for Cr(VI) treatment, a long-term study was carried out with this support in order to determine the possibility of achieving complete Cr(VI) reduction from a 100 mg_{Cr}/L solution. The assay was carried out during 161 days. Figure 4.7 presents the evolution of Cr(VI) and total Cr in solution, for this support.

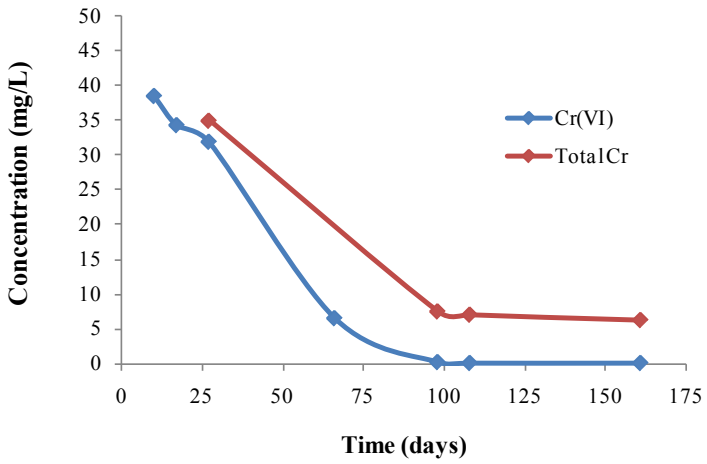

Figure 4.7: Evolution of Cr(VI) and total Cr for the long-term essay with NaY zeolite.

This experiment confirmed that complete reduction of a 100 mg_{Cr}/L solution can be achieved by the biomass-NaY system, provided a long enough experimental period is used which, in this case, was 98 days. However, after complete reduction is achieved, the concentration of total Cr remains constant throughout the experiment, which indicates that a near-equilibrium state is reached and further ion-exchange of Cr(III) species may have ceased. The final Cr uptake was 13.9 $mg_{Cr}/g_{zeolite}$, the highest uptake achieved in single-batch studies. Cr removal was 93.7 % of the initial Cr.

In general terms, the utilization of improved biomass and pH conditions allowed a drastic increase in the performance of the *A.viscosus*-zeolite system in Cr(VI) reduction, total Cr removal and uptake. However, the drawbacks of very long experimental periods and the fact that total Cr and Cr(VI) concentrations are out of legislation parameters still remain.

A different approach was tested and the biosorption system was used in a sequential batch process, instead of the single-batch assays carried out up to this point which leads to the next section of this chapter.

4.3.2 Sequential batch reactor studies

The decision of operating the biomass-zeolite system in sequencing batch reactors (SBR) mode was based on the previous knowledge acquired from the single batch studies with optimized biosorption parameters. Looking at the performance of the system for the 100

mg_{Cr}/L solution in terms of Cr(VI) evolution (Figure 4.5), it was noted that the concentration of this species decreases up to 50 % in 24 hours, followed by a long second stage of reduction which continued throughout the experimental period. To take advantage of the higher reduction capacity during the early operational stages, the usage of a sequence of additional reactors could decrease the experimental time required for total Cr(VI) reduction.

It was decided to start the SBR experiment with a 100 mg_{Cr}/L solution and with the same initial procedure as for the single-batch experiments. However, after a pre-established period of 4 days, the solution would be transferred to another reactor containing fresh biomass and equivalent mass of zeolite support. This procedure would be repeated in a third cycle, so that the overall experimental period would consist of three cycles of 4 days. The evolution of Cr(VI) concentration is presented in Figures 4.8 and 4.9, in the form of instant over initial Cr(VI) concentration (C/Cº).

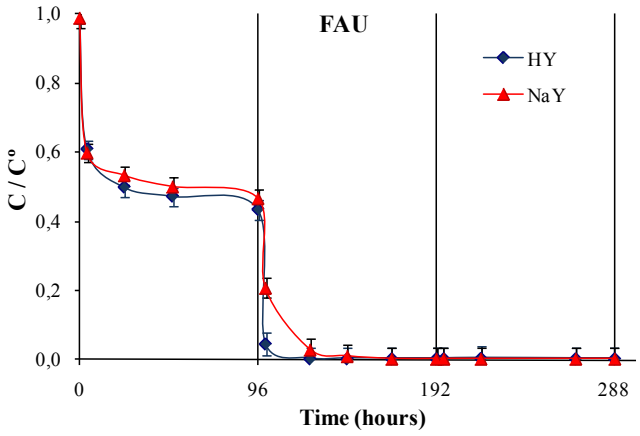

Figure 4.8: Evolution of Cr(VI) through the different reactor cycles for FAU (HY and NaY) supports (change in reactor is signalled by the vertical lines).

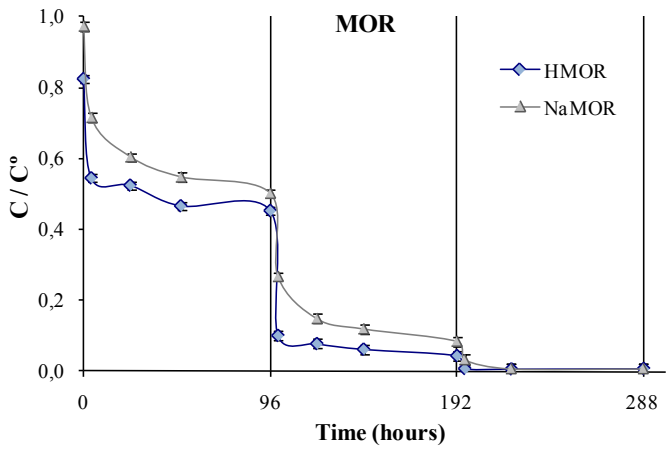

Figure 4.9: Evolution of Cr(VI) through the different reactor cycles for MOR (HMOR and NaMOR) supports (change in reactor is signalled by the vertical lines).

The evolution of Cr(VI) concentration shows that complete reduction was achieved in the given experimental period of 12 days. For FAU zeolites, complete reduction was observed during cycle 2, whereas MOR zeolites required an additional third cycle to achieve total reduction. Again, the lower ion-exchange capacity is probably the main cause for the lower efficiency of based-MOR systems, which was also observed in single-batch studies.

For both zeolite structures, the supports containing H^+ ions perform better than the Na^+ equivalents. The same principia that governed Cr(VI) reduction dynamics in single batch-studies explain the higher reduction achieved with the acidic support, as the availability of H^+ ions in the supports has a beneficial effect. The HY-based system was the first to register complete Cr(VI) reduction, 24 hours before the NaY-based system. MOR systems only achieved total reduction at the initial stages of cycle 3. These results are in accordance to the initial evolution of Cr(VI) in single-batch studies, where the HY-based system outperformed the remaining supports on the first 5 days of experimental time.

The determination of total Cr concentration was made for each solution at the end of each cycle. The total Cr concentration at the end of each cycle is presented in Figure 4.10, while Table 4.5 presents Cr the removal efficiency and uptake achieved by each system.

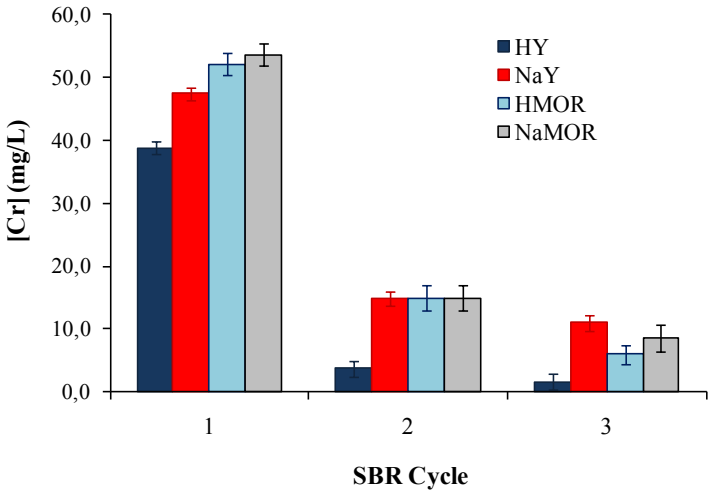

Figure 4.10: Total Cr concentration at the end of each cycle, for all the tested supports.

Table 4.5: Total Cr removal after cycle 3 and Cr uptake, for each support tested.

Support	Overall Cr removal after cycle 3 (%)	Cr Uptake ($mg_{Cr}/g_{zeolite}$)			
		Cycle 1	Cycle 2	Cycle 3	Accumulated
HY	98.2	8.3	5.2	0.3	13.8
NaY	87.3	6.7	4.6	0.4	11.7
HMOR	93.4	6.5	5.3	1.3	13.1
NaMOR	90.5	6.2	5.5	0.8	12.5

The experimental data reveal that the third cycle is less efficient in terms of removal of the reduced Cr(III) species. As it was the case for the single-batch studies, a reason for the less efficient ion-exchange of Cr(III) species could be the formation of coordination compounds with biomolecules present in solution. Although the solid contents of each system are removed at the end of cycles, cellular metabolites or EPS fragments still remain in solution and after 3 consecutive cycles, the increasing concentration of these compounds could ease the formation of Cr(III) complexes which will have a detrimental effect in Cr removal by the systems.

The HY-based system was able to achieve a total Cr concentration below 2.0 mg/L which, coupled to the absence of Cr(VI), means that this solution is now in accordance with the legislation parameters for concentration in an effluent. The remaining zeolites were able to achieve removal ratios ranging from 87 to 94 %. The cumulative uptake values are also

higher than the obtained in single-batch studies; however, end-of-cycle Cr uptake values are considerably lower.

4.3.3 Cr loading of the zeolitic supports

After the achievement of the studies on biotreatment of Cr(VI) solutions, it was concluded that FAU zeolite structures showed better performance, compared to MOR zeolite structures. In single batch operation, the based-NaY system achieved the best removal and uptake of Cr, while the SBR intrinsic dynamics render HY zeolite as the best support for the biotreatment system.

The evaluation of Cr loading on the FAU supports was conducted by chemical analysis of the calcined solid samples from single and sequencing batch studies. Samples from single-batch studies were collected from the 100 mg_{Cr}/L initial solution assays, namely CrNaY, CrHY and CrNaY EXT (from the extended study of 167 days). Additionally, a comparison with a sample from previous studies, conducted without pH control, under low biomass concentration and from an initial 100 mg_{Cr}/L solution, was added to this study, being named CrNaY*. Samples from SBR studies are marked as $CrHY_{SBR}$ and $CrNaY_{SBR}$. Table 4.6 presents the obtained Cr loading of all samples.

Table 4.6: Cr loading on selected supports, recovered from Cr(VI) biotreatment studies.

Sample	Cr loading (%, w/w)	
(single batch studies)		
CrNaY* (*previous studies* [5])	0.14	
CrHY	0.54	
CrNaY	0.75	
CrNaY EXT	0.94	
(sequencing batch studies)	*cycle*	
$CrHY_{SBR}$	*1*	0.59
	2	0.45
	3	0.04
$CrNaY_{SBR}$	*1*	0.46
	2	0.36
	3	0.05

The first sample in Table 4.6, CrNaY* presents a Cr loading of 0.14 %, whereas the equivalent CrNaY presents almost five times more Cr, which is a good indication of the difference in performance which is achieved using optimized biosorption conditions.

The comparison of the Cr loading on single-batch and SBR studies presented interesting data on the dynamics of both systems. The Cr loading in NaY supports increases with the solution contact period, which is in accordance to the previously stated higher affinity for ion-exchange of reduced Cr species. The secondary reduction stage presented higher rates of reduction when NaY supports were used and the Cr loading in $CrNaY_{SBR}$, CrNaY and CrNaY EXT confirm that tendency, with increasing the Cr loading with contact period.

HY-based systems presented different results. Comparing CrHY and $CrHY_{SBR}$, which were submitted to the same initial conditions, it is observed that the Cr loading is similar (0.59 and 0.54%), even if $CrHY_{SBR}$ only contacted the metal solution during 4 days and CrHY contacted it during 27 days. This means that the ion-exchange of the reduced Cr species only takes place on the early stages, probably due to a fast equilibrium being achieved between the H^+ ions present in the solution and the remaining cations. Since this support also registered the higher initial rate of Cr(VI) reduction, it is likely that these early reduced species might be also included in this swift equilibrium with the H^+ ions from the zeolite.

4.4 Conclusions

From the results presented in this chapter, it was possible to conclude that the biotreatment of Cr(VI) species by the *Arthrobacter viscosus* bacterium is strongly dependent on the support, solution pH and biomass concentration.

While the chemical composition of the zeolite may affect the pH of the solution, an external control is preferable as the free pH studies with MOR zeolite structures demonstrated that, despite the support action on the solution, the pH of each solution varied through a wide range. However, the contribution of the chemical composition of the support, although seemingly minor to the solution pH, proved to be also influent on the performance of the system, in terms of Cr(VI) reduction efficiency.

It was possible to achieve an increase in Cr(VI) reduction and overall removal efficiency using optimized pH and biomass concentration parameters. Single-batch studies showed that the biotreatment of the Cr(VI) solutions occurred in two distinct stages, as a normal biosorption kinetics. The first stage is fast and takes place on the first 24 hours of treatment, whereas the second stage, which is considerably slower, continued throughout the remaining experimental period. To this extent, zeolites containing H^+ ions registered a higher Cr(VI) reduction rate in the first stage. However, NaY zeolite with presented the highest upkate. Ultimately, this zeolite was able to achieve the highest removal and uptake for the 100 mg_{Cr}/L solution. The required experimental periods for complete Cr(VI) reduction from initial Cr concentrations of 50 and 100 mg/L were 17 and 98 days, respectively.

The operation in SBR allowed a balanced exploitation of the fast initial rates of reduction which were observed in each reactor in single batch studies, in order to overcome the need for long experimental periods. HY zeolite was the best support, ultimately achieving Cr(VI) and total Cr concentrations within legislation limits. The remaining supports also improved Cr removal when compared to the experimental data from single-batch studies, for an initial Cr concentration at 100 mg/L and 27 days of assay.

The evaluation of Cr(VI) and total Cr concentrations in both single and sequencing batch reactors offered different perspectives in terms of treatment dynamics. Single batch processes ultimately allowed a higher loading of metal to the zeolite matrix, which is

potentially useful for the downstream catalytic studies. SBR reactors lacked sufficient contact to achieve comparable Cr loadings on NaY zeolite. However, the metal loading on HY zeolite was comparable in either single or sequential batch studies, which allows concluding that the removal of Cr by this support is fast, occurring only within the first four days of assays.

4.5 References

[1] C. Quintelas, T. Tavares, Removal of Chromium (VI) and Cadmium (II) From Aqueous Solution by a Bacterial Biofilm Supported on Granular Activated Carbon, Biotechnology Letters. 23 (2001) 1349–1353.

[2] E. Sánchez, R. Roque-Malherbe, Zeolite as Support Material in Anaerobic Wastewater Treatment, Biotechnology Letters. 9 (1987) 671–672.

[3] Z. Milán, E. Sánchez, R. Borja, P. Weiland, M. Cruz, Synergistic Effects of Natural and Modified Zeolites on the Methanogenesis of Acetate and Methanol, Biotechnology Letters. 23 (2001) 559–562.

[4] S. Lameiras, C. Quintelas, T. Tavares, Biosorption of Cr (VI) Using a Bacterial Biofilm Supported on Granular Activated Carbon and on Zeolite, Bioresource Technology. 99 (2008) 801-806.

[5] H. Figueiredo, I.C. Neves, C. Quintelas, T. Tavares, M. Taralunga, J. Mijoin, P. Magnoux, Oxidation Catalysts Prepared From Biosorbents Supported on Zeolites, Applied Catalysis B: Environmental. 66 (2006) 274-280.

[6] H. Figueiredo, M.M.M. Raposo, A.M. Fonseca, I.C. Neves, C. Quintelas, T. Tavares, Encapsulated Pyridazine Cr(III) Complexes Prepared From Biosorbents Supported in Zeolites, in: J. Cejka, I. Zilková, P. Nachtigall (Eds.), Molecular Sieves: From Basic Research To Industrial Applications, Proceedings Of the 3rd International Zeolite Symposium (3rd FEZA), Elsevier, 2005: pp. 1073-1080.

[7] H. Figueiredo, B. Silva, M.M.M. Raposo, A.M. Fonseca, I.C. Neves, C. Quintelas, T. Tavares, Immobilization of Fe(III) Complexes of Pyridazine Derivatives Prepared From Biosorbents Supported on Zeolites, Microporous and Mesoporous Materials. 109 (2008) 163-171.

[8] B. Silva, H. Figueiredo, C. Quintelas, I.C. Neves, T. Tavares, Iron and Chromium Removal from Binary Solutions of Fe(III)/Cr(III) and Fe(III)/Cr(VI) by Biosorbents Supported on Zeolites, Materials Science Forum. 588 (2008) 463-467.

[9] B. Silva, H. Figueiredo, C. Quintelas, I. Neves, T. Tavares, Zeolites as supports for the Biorecovery of Hexavalent and Trivalent Chromium, Microporous and Mesoporous Materials. 116 (2008) 555-560.

[10] H. Figueiredo, B. Silva, C. Quintelas, M.F.R. Pereira, I.C. Neves, T. Tavares, Biosorption of Hexavalent Chromium Based on Modified Y Zeolites Obtained by Alkaline Treatment, Environmental Engineering and Management Journal. 9 (2010) 305-311.

[11] D.A. Skoog, D.M. West, F.J. Holler, Fundamentals of Analytical Chemistry, 7th ed., Saunders College Publishing, 1996.

[12] D. Park, S.-R. Lim, Y.-S. Yun, J.M. Park, Reliable Evidences That the Removal Mechanism of Hexavalent Chromium by Natural Biomaterials is Adsorption-coupled Reduction., Chemosphere. 70 (2007) 298-305.

[13] D. Park, Y.-S. Yun, J.Y. Kim, J.M. Park, How to Study Cr(VI) Biosorption: Use of Fermentation Waste for Detoxifying Cr(VI) in Aqueous Solution, Chemical Engineering Journal. 136 (2008) 173-179.

[14] H.S. Sherry, Ion Exchange, in: S.M. Auerbach, K.A. Carrado, P.K. Dutta (Eds.), Handbook Of Zeolite Science and Technology, New York, Basel, Marcel Dekker, Inc., 2003.

[15] V.J. Inglezakis, The Concept of "Capacity" in Zeolite Ion-exchange Systems., Journal Of Colloid and Interface Science. 281 (2005) 68-79.

[16] N. Tsibakhashvili, T. Kalabegishvili, L. Mosulishvili, E. Kirkesali, S. Kerkenjia, I. Murusidze, H.-Y. Holman, M.V. Frontasyeva, S.F. Gundorina, Biotechnology of Cr(VI) Transformation Into Cr(III) Complexes, Journal Of Radioanalytical and Nuclear Chemistry. 278 (2008) 565-569.

[17] H. Figueiredo, B. Silva, C. Quintelas, I.C. Neves, T. Tavares, Effect of the Supporting Zeolite Structure on Cr Biosorption: Performance of a Single Step Reactor and of a Sequential Batch Reactor-a Comparison Study, Chemical Engineering Journal. 163 (2010) 22-27.

[18] B. Silva, H. Figueiredo, I.C. Neves, T. Tavares, The role of pH on Cr (VI) Reduction and Removal by *Arthrobacter Viscosus*, International Journal Of Chemical and Biomolecular Engineering. 43 (2009) 59-62.

[19] A. Omegna, M. Haouas, A. Kogelbauer, R. Prins, Realumination of Dealuminated HZSM-5 Zeolites by Acid Treatment: a Reexamination, Microporous and Mesoporous Materials. 46 (2001) 177-184.

[20] L. Cherif, Structural Evolution of Calcium-exchanged $(NH_4)_2SiF_6$-dealuminated Y Zeolite After Various Chemical Treatments, Colloids and Surfaces A: Physicochemical and Engineering Aspects. 220 (2003) 83-89.

[21] G.J. Puzon, A.G. Roberts, D.M. Kramer, L. Xun, Formation of Soluble Organo-chromium(III) Complexes After Chromate Reduction in the Presence of Cellular Organics, Environmental Science and Technology. 39 (2005) 2811-2817.

[22] G.J. Puzon, R.K. Tokala, H. Zhang, D. Yonge, B.M. Peyton, L. Xun, Mobility and Recalcitrance of Organo-chromium(III) Complexes, Chemosphere. 70 (2008) 2054-2059.

(this page is intentionally left blank)

CHAPTER 5

PREPARATION OF CHROMIUM CATALYSTS FROM BIOSORPTION SUPPPORTS

CHAPTER 5 – PREPARATION OF Cr CATALYSTS FROM BIOSORPTION SUPPORTS

This chapter presents experimental results and related discussion on the development of the Cr heterogeneous catalysts. Also, this chapter bridges the two distinct fields covered in this study: Cr(VI) biotreatment and liquid-phase catalysis in oxidation reactions.

Despite FAU and MOR zeolites were used throughout the biotreatment experiments, only FAU zeolites were recovered for the preparation of encapsulated catalysts by the *flexible ligand method*. This results from their favourable microporous structure, where the supercages with tetrahedrally-oriented 12-ring pore openings and a 3-dimensional channel system offer the ideal support for encapsulation of metal complexes. MOR zeolite presents a 2-dimensional channel system with 12-ring channels connected by short alternating 8-ring channels, of which only the 12-ring channel is accessible. Consequently, the channel system has effectively one dimension. Therefore, these structures were dropped in favour of FAU zeolites. Nevertheless, Cr-MOR zeolites could be tested as catalysts for gas-phase reactions which are outside the scope of this work.

The overall process tested in this project may be summarized as follows:

I- Reduction of Cr(VI) to Cr(III) by *Arthrobacter viscosus* supported on NaY

II- Ion-exchange of Cr(III) ions in zeolite obtained by biosorption process (example of a NaY zeolite)

$$Na_{53}Y + xCr^{3+} \leftrightarrow Cr_xNa_{53-3x}Y + 3xNa^{+} \qquad \text{(eq. 5.1)}$$

III- *In situ* encapsulation of the Cr complex

$$Cr_xNa_{53-3x}Y + \text{excess L} \leftrightarrow [Cr(L_n)]_xNa_{53-3x}Y \qquad \text{(eq. 5.2)}$$

where x represents the atom fraction of Cr^{3+} ions migrating into the zeolite and L represents the heterocyclic ligand coordinated to the chromium center.

5.1 Recovery of the biosorption supports and characterization

The recovery of the solid residues of the several Cr(VI) biotreatment assays was initially performed by vacuum filtration using a 10-16 μm pore sintered glass filter. This process was mainly used for the recovery of CrNaY and CrNaX zeolites from the experiments with low biomass concentration. Due to operational limitations, such as decrease in rate of filtration due to sedimentation of fine solids over the glass filter with filtration time, this process was dropped in favour of centrifugation of the whole reactor contents. All solid samples recovered from biotreatment studies within optimized conditions were recovered by centrifugation, discarding the supernatant. Either filtrated or centrifuged, all recovered samples were individually dried after collection at moderate temperature (typically below 60 ºC), ensuing calcination at 500 ºC for 8 hours, in order to remove the whole biomass from the zeolite.

For all Cr-zeolite samples, the zeolitic hosts change their colour after calcination. While parent FAU or MOR zeolites are white, collected samples from biosorption present a light brown colour (from the biomass contents), which upon calcination changes to a pale yellow colour.

Scanning electronic microscopy (SEM) was used to characterize the collected samples. Figure 5.1 presents SEM images of parent zeolite, as-recovered biotreatment samples and calcined samples (example of sample CrNaY*). Calcined samples present the same morphology of parent zeolites, with the hexagonal shaped crystals, which are typical of FAU-type zeolites, being conserved throughout the process.

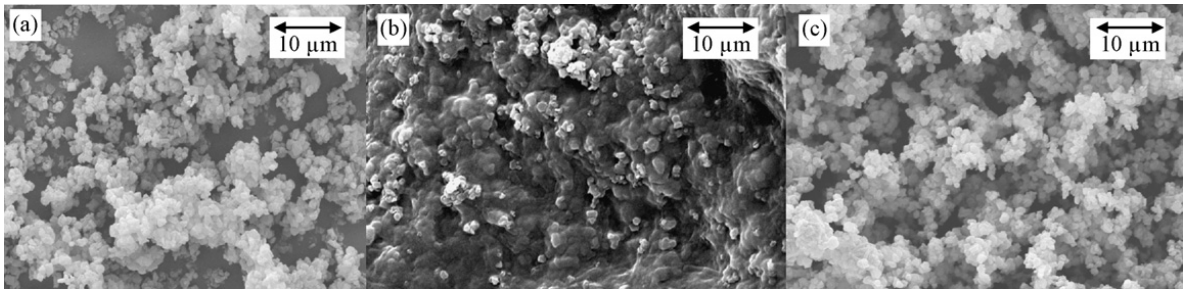

Figure 5.1: SEM images of: NaY (a) and CrNaY* prior to calcination (b) and after calcination (c), with magnification of 3000x (imported from [1]).

The same behaviour was observed on calcined samples which were recovered from studies with concentrated biomass. Figures 5.2 presents SEM images of CrHY after calcination, coupled to the energy-dispersive spectroscopy (EDS) spectrum. Amongst the spectral signals for Si and Al, the *Kα* line for Cr was detected at 5.41 keV [2], as well as the signal for P, detected at 2.03 keV [3]. The presence of this element is likely to be due to the higher biomass concentration that the sample contained before calcination, forming phosphorous residues on the surface of the zeolite during the thermal treatment.

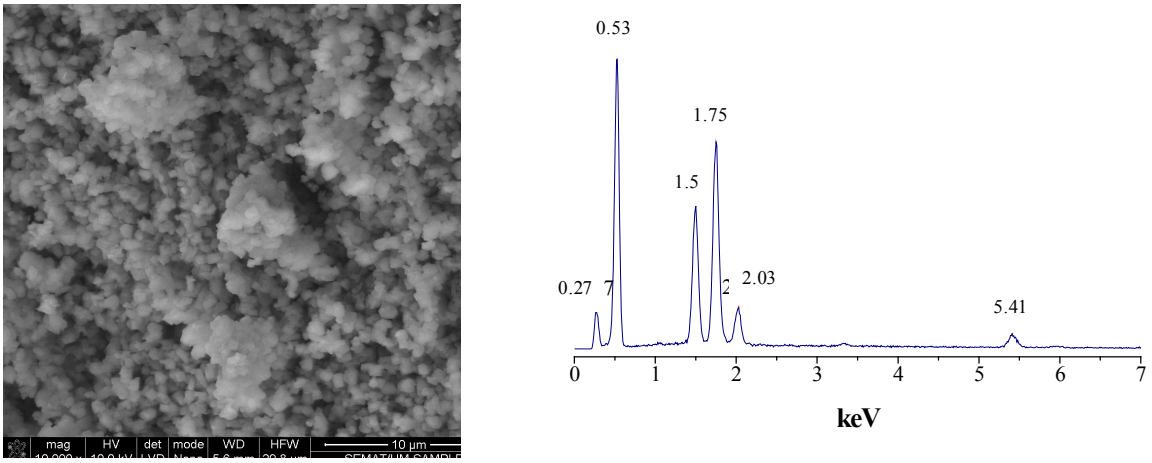

Figure 5.2: SEM image of calcined CrHY (left) with magnification 10.000x and the respective EDS spectrum (right).

TGA analysis confirmed that the calcination process ensured an efficient removal of the biomass. Figure 5.3 presents the comparison of the thermograms of NaY zeolite and CrNaY*, before and after calcination. While the calcined sample presents the same thermal behaviour of NaY zeolite, with a single-stage weight loss due to the loss of water from the structure, as-recovered sample presents a second weight loss which is attributed to the decomposition of the biomass. This occurs at *circa* 300 ºC and accounts for 5% of the sample mass.

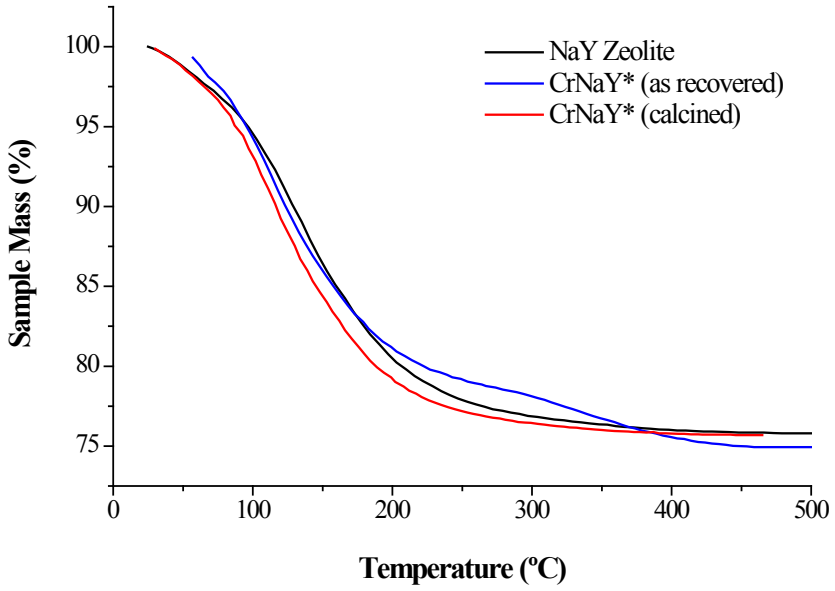

Figure 5.3: TGA curves for NaY zeolite and CrNaY*, before and after calcination.

Chemical analysis of the calcined samples confirmed both the presence of chromium in the structure, as well as the absence of nitrogen, which is an important indicator of successful biomass removal during calcination. Moreover, the absence of nitrogen in the Cr-containing hosts is useful for future chemical analysis of the prepared heterogeneous catalysts, to be discussed later. Carbon appears as a trace residue in samples that were recovered from studies using high biomass concentration, being this fact responsible for the presence of the carbonaceous residue from incomplete C oxidation after calcination.

Table 5.1 presents the data from the combined chemical analysis performed on the supports which were selected under the scope of this work, including two Cr(III)-NaY samples prepared by ion-exchange, which were used for the purpose of comparison.

Table 5.1: Chemical analysis of the supports used for the preparation of heterogeneous catalysts.

Support	Elemental content (%, w/w)	
	Cr	C
NaY	0.00	0.00
CrNaY*	0.14	0.00
CrNaY	0.75	0.16
$CrNaY_{SBR}$	0.46	0.22
$CrHY_{SBR}$	0.59	0.43
Cr(III)-NaY_1	0.62	0.00
Cr(III)-NaY_2 (non calcined)	0.36	0.00

From the structural point of view, infrared spectroscopy (FTIR) and X-ray diffraction (XRD) analysis confirmed the integrity of the crystalline FAU matrix. FTIR spectra for CrNaY* before and after calcination are presented in Figure 5.4, combined with the FTIR spectrum of dry *Arthrobacter viscosus* bacteria. The bands in the 1250-1000 cm^{-1} and 4000-3250 cm^{-1} regions, seen in both spectra of CrNaY*, indicate that the structure is kept unchanged during the process. The only significant difference between these spectra is the band at 1400 cm^{-1} observed in as-recovered CrNaY* (as indicated by the arrows in Figure 5.4), which disappears after calcination. This band is due to carboxylate groups ($R\text{-}COO^-$) [4], resulting from the presence of the *Arthrobacter viscosus* biomass.

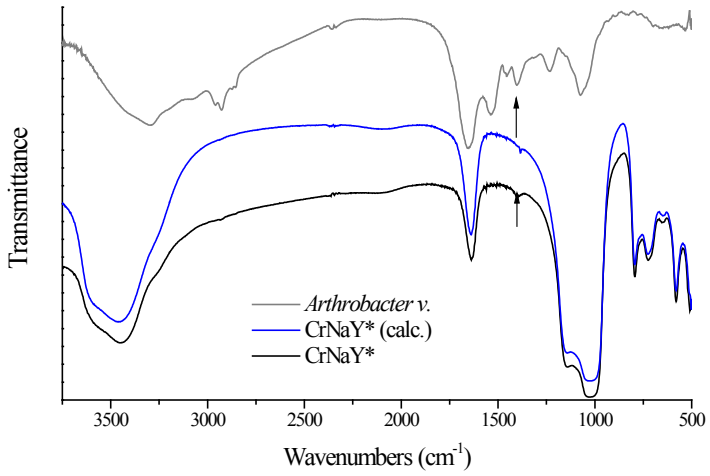

Figure 5.4: FTIR spectra of dry *Arthrobacter viscosus* and CrNaY* before and after calcination.

XRD analysis of the different solid samples further confirmed that the crystalline structure is maintained throughout the biosorption process. Figure 5.5 presents XRD diffractograms of parent NaY zeolite and calcined CrNaY*. No shifts in peak positions or new peaks were detected, confirming that the crystalline matrix was not damaged. Further determination of framework Si/Al ratios showed a very slight decrease in NaY-based samples, from 2.80 on parent NaY samples to 2.70 in calcined biosorption samples. The same results were obtained with similar samples, either originating from Cr(VI) or Cr(III) biotreatment [1,5–7] or from Fe(III) biotreatment [8]. This proves that the robustness of the zeolitic matrix is sufficient to ensure that no damage occurs during the various processes from biotreatment to recovery. The only case where structural damage was observed during Cr(VI) biotreatment was the alkali-modified zeolites, when the modified surface endured further loss of Si from the framework, as determined by XRD [9].

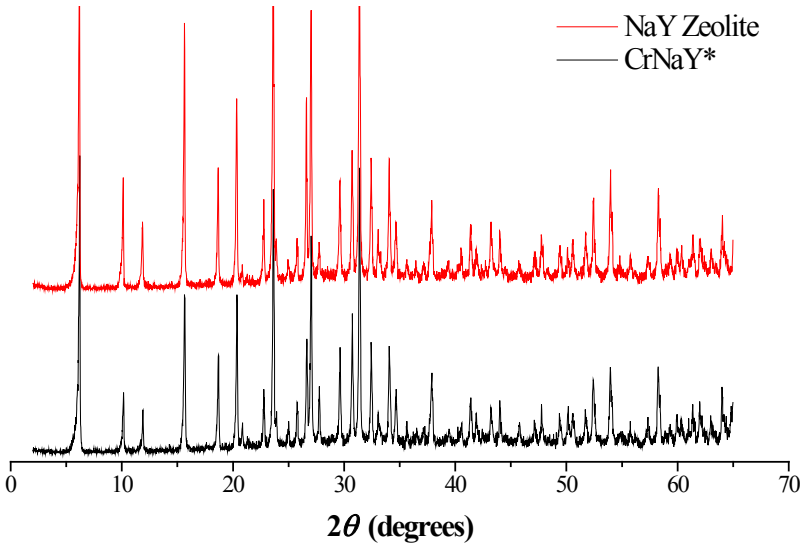

Figure 5.5: XRD analysis of parent NaY and calcined CrNaY*.

In conclusion, the combined analytical data confirm that the supports maintained their structural integrity, while efficiently removing the biomass and ensuring the retention of Cr species. Therefore, the recovered supports offer good properties for the preparation of heterogeneous catalysts by *in-situ* synthesis.

5.2 Preparation of heterogeneous catalysts with N-heterocyclic ligands

The first studies on the preparation of heterogeneous Cr catalysts from recovered biosorption supports, using *the flexible ligand* method, were based on the CrNaY* support.

For the coordination of the Cr(III) ions within the framework, a total of four heterocyclic ligands were selected (structures presented in Figure 5.6), namely 3-methoxy-6-chloropyridazine (PyMe), 3-ethoxy-6-chloropyridazine (PyEt), 3-piperidino-6-chloropyridazine (PyP) and 1-(2-pyridylazo)-2-naphthol (PAN). All ligands used in this work are able to diffuse freely through the FAU zeolite pores. The chloropyridazine derivatives were synthesized on the Chemistry Department at University of Minho and the synthesis process was previously reported [8]. PAN ligand is a commercially available product from Aldrich.

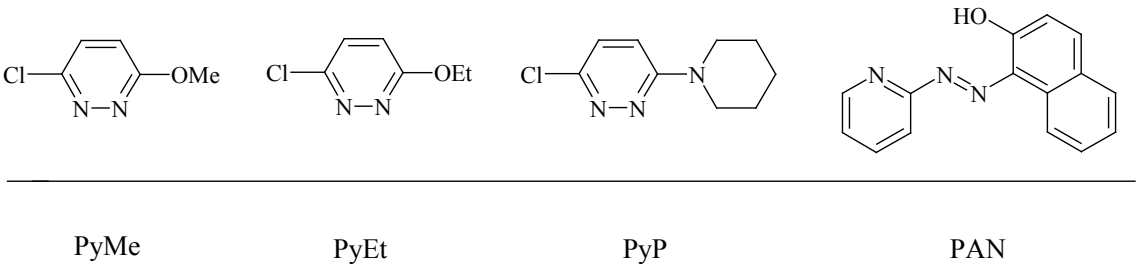

PyMe PyEt PyP PAN

Figure 5.6: Heterocyclic ligands used for the encapsulation of chromium on CrNaY*.

The structures of the heterocyclic ligands are different. The selected ligands present different atoms which are available for coordination. In the case of pyridazine derivatives, the coordinating nitrogen atoms are part of the aromatic ring. However, the coordination with PAN ligand involves the nitrogen atoms from the azo group and the oxygen atom.

Pyridazine compounds have been widely referred as interesting ligands for metal coordination. Pyridazine ligands are able to bridge two metal ions and their strong magnetic mediation properties allow them to stabilize low oxidation states of metal ions [10,11].

The heterogeneous catalysts were prepared by the flexible ligand method in three steps: *in-situ* complex synthesis, liquid-solid extraction and stabilization. In the first step, the solution containing the specific ligand and Cr-containing support is refluxed and the

molecules of the first diffuse through the zeolitic framework and reach the Cr(III) ions. The second step consists of a liquid-solid Soxhlet extraction, where the uncoordinated molecules are removed (such as merely adsorbed species), as well as eventual Cr (III) complexes not encapsuled in the supercages. The final step is a charge-balancing procedure, where the samples are allowed to be ion-exchanged with a diluted NaCl solution, in order to compensate eventual charge deficits in the formed coordination compounds.

5.2.1 Encapsulated Cr-Pyridazine catalysts

Cr-Pyridazine complexes encapsulated in CrNaY* matrix were the first heterogeneous catalysts to be prepared and studied. Full details on the characterization of these catalysts has been reported [1,6,12] and are summarized in this section. The characterization of the compounds included several analytical techniques such as FTIR, XRD, TGA and chemical analysis.

Chemical analyses were performed and the presence of C and N was detected in the prepared catalysts. While the presence of carbon can be due to solvent molecules as well as to ligand molecules, the presence of nitrogen is a clear indicator that pyridazine molecules were successfully coordinated with chromium and the complex was entrapped in the zeolitic matrix.

FTIR spectra of the Cr-pyridazine catalysts, coupled to XRD data, revealed that the zeolite structure is not affected by the encapsulation of the metal complex. The detection of new bands in FTIR analysis was hampered by the inherent crystalline rigidity of the zeolitic matrix that limits vibrational states of molecules within it, coupled to the low loading of organic compounds (less than 3.0 %, determined by TGA), altogether limiting the detection of Cr complexes to very weak signals.

TGA analyses presented the most significant data on metal complex encapsulation. Figure 5.7 presents the comparison of the thermogravimetric curves for Cr-PyEt complex ([Cr-PyEt]NaY*) and parent CrNaY* host. The thermogram of the heterogeneous catalyst presents two distinct mass loss stages, whereas for parent CrNaY* host, only water loss is observed below, 200 ºC. The mass loss that starts at 500 ºC is attributed to the decomposition of the encapsulated complex, which decomposes at such high temperatures

due to thermal shielding from the zeolitic structure. The same TGA behaviour has been reported for metal complexes immobilized in NaY zeolite [13–15].

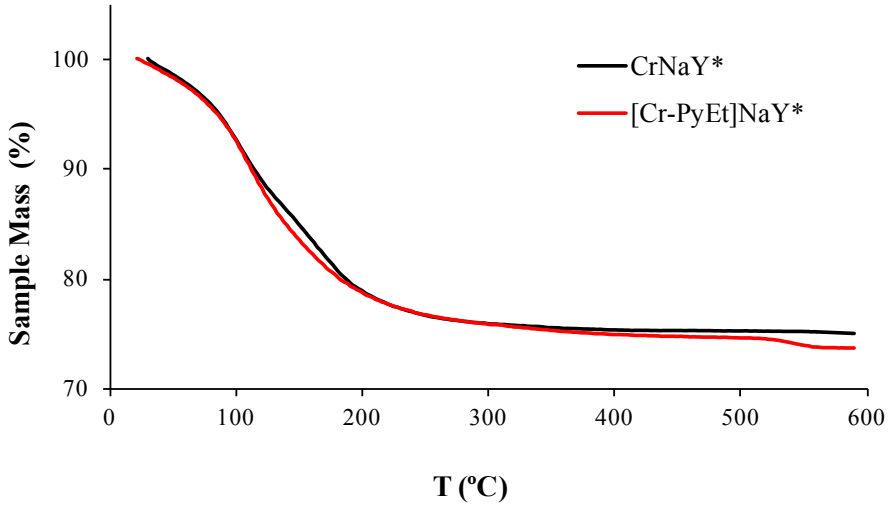

Figure 5.7: TGA curves for CrNaY* host and [Cr-PyEt]NaY* catalyst.

Table 5.2 presents combined chemical composition and TGA data of the several immobilized pyridazine complexes.

Table 5.2: Chemical composition and TGA data for immobilized Cr-Pyridazine catalysts.

Ligand	Host	Elemental Composition (%)			TGA data	
		Cr[a]	C[b]	N[b]	Complex mass (%) (w/w)	Decomposition T (ºC)
PyMe	CrNaY*	0.09	0.82	0.05	2.7	540
	Cr(III)-NaY_1	0.58	0.65	0.03	2.5	537
PyEt	CrNaY*	0.13	n.d.	n.d.	2.0	543
PyP		0.09	0.67	0.04	1.0	546

[a]Cr loading on FAU supports determined by ICP-AES analysis.
[b]Carbon and nitrogen loadings obtained by elemental analysis.

It was observed that the mass of complex was dependent on the ligand structure. PyMe was able to form the biggest mass of complex with 2.7 % and its PyP counterpart was only able to form 1.0 %. The bulk size of the different substitution groups (-OMe, -OEt and –

$N(CH_2)_5$) is the main responsible for the decrease in mobility through the zeolite pores, which in turn limits the ability of the ligand to coordinate with the metal ions.

Comparing the Cr(III)-NaY_1 support with CrNaY*, it is seen that the same ligand molecule was able to form a comparable amount of complex in supports with striking differences in terms of Cr loading. This indicates that most of the Cr(III) ions in Cr(III)-NaY_1 support are inaccessible to the ligand molecules. The fact that this fraction could still be present at certain sites of the zeolite cannot be ruled out. Y zeolite has two sites inside the hexagonal prism and the sodalite cages where cations can be accommodated and solvated by the zeolite oxygen atoms, but they cannot participate in the formation of the complexes due to steric constraints [16]. Only Cr(III) ions located inside the supercages are available to interact with ligands, forming the complex [17].

Further analyses brought additional data on the nature of the chromium species on the surface of Cr(III)-NaY_1 support. Raman signals for Cr(VI) species were detected (Figure 5.8). The presence of dichromate species is confirmed by the Raman shifts at 902 and 952 cm^{-1} from Cr-O vibrations of dichromate ions [18]. Signals for Cr(III) species are expected at 550 cm^{-1} and are absent from the spectra, mainly due to masking by the strong signal at 500 cm^{-1} which is the characteristic peak for FAU zeolites [19]. This means that superficial Cr(III) species were oxidized to Cr(VI), which is an occurrence previously reported when Cr(III) ion-exchanged NaY zeolites were calcined in the presence of O_2 [20].

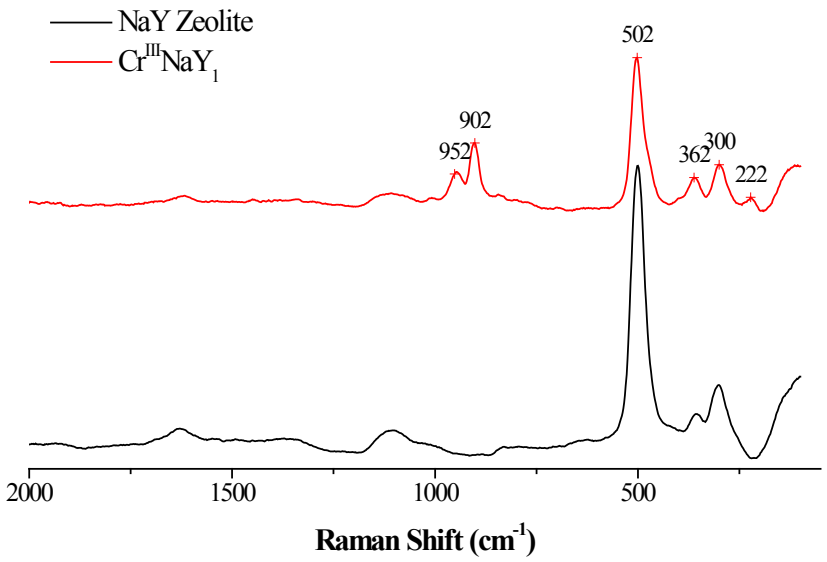

Figure 5.8: Raman spectra of NaY zeolite and Cr(III)-NaY_1.

It was not possible to obtain any information on the valence of the innermost Cr ions from Raman analysis; however, the fact that Cr complexes were encapsulated in this support indicates that Cr(III) species were likely to be present within of the framework.

5.2.2 Encapsulated Cr-PAN catalyst

The encapsulation of chromium complexes in CrNaY* support was also performed with the PAN ligand. As it was shown in Figure 5.6, this molecule presents some differences when compared to the pyridazine derivatives, as the N=N bond is not part of a heterocyclic group.

After the *in-situ* synthesis of the CrPAN complex, the color of CrNaY* changed from pale yellow to purple. The characterization of [CrPAN]NaY* through FTIR, TGA and chemical analysis indicated a similar behaviour to the one previously observed for the encapsulated Cr-pyridazine complexes. TGA analysis yielded the most significant result as it confirmed the presence of encapsulated complexes with 1.0 % of total sample mass. Chemical analysis revealed that the Cr contents of this catalyst were 0.07%, a decrease from the original 0.14% of the parent host. Although not quantified, it is likely that the loss of Cr happened during stabilization with NaCl.

The characterization of [CrPAN]NaY* through diffuse reflectance UV spectroscopy (DR-UV) brought to light some new information on the valence of the Cr ions, presented in Figure 5.9.

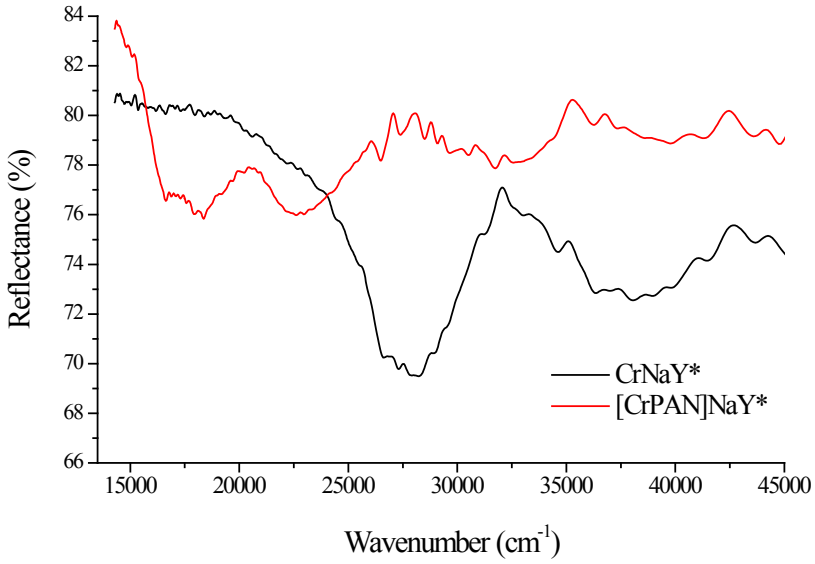

Figure 5.9: DR-UV spectra of CrNaY* and [CrPAN]NaY*.

The DR-UV spectra of CrNaY* is mainly dominated by a peak at 28000 cm^{-1} and a broad band centred at 38000 cm^{-1}. These signals have been described as indicative of monochromate species on the surface of the support [21], formed during calcination of the zeolitic support. This was previously observed from the Raman signals of Cr(III) ion-exchanged Cr(III)-NaY_1 zeolite. The spectrum of the immobilized complex presents differences compared to the parent host, such as the broad band centered at 23000 cm^{-1} indicating the presence of di- or polychromates [20]. Monochromate species are less evident in the DR-UV spectra of the encapsulated complex, maybe due to simple leaching during the flexible ligand method, as it may be concluded from the decrease in Cr loading (0.14 % to 0.07 %). However, the most significant differences in the DR-UV spectra are the peaks appearing between 15000 and 18000 cm^{-1}, seen in the encapsulated complex. These are due to the *d-d* transitions of Cr(III) species [18,20] and their DR-UV signal became more intense upon coordination with the ligand due to their stabilization.

The presence of Cr(III) ions was also confirmed by cyclic voltammetry. Solid samples of [CrPAN]NaY* were deposited in carbon Toray (as well as parent NaY) and the respective voltammograms are presented in Figure 5.10. While parent NaY zeolite does not present any redox process in the range from -1.5 to +1.5 V *vs*. saturated calomel electrode (SCE), it was found that the samples of encapsulated complex were electroactive, with a reversible

redox process observed on the wave occurring between -0.20 V and +0.25 V (*vs.* SCE). This is attributed to the redox couple Cr(III)/Cr(II) and the peak positions and shape are not affected by the variation of scan rates, which indicates reproducibility of the electrode reaction. Moreover, the same phenomenon was reported by Koley *et al*. in their study with Cr(III)-*salen* complexes [22].

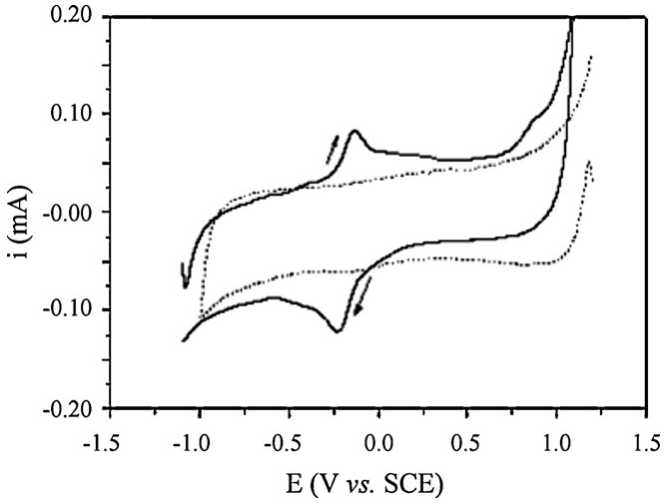

Figure 5.10: Cyclic voltammograms for NaY zeolite (dashed line) and [CrPAN]NaY* catalyst (dark line). Image imported from reference [1].

5.3 Preparation of heterogeneous catalysts with diphenyltriazene ligands

This section details the studies of the encapsulation of chromium complexes on the supports recovered from the Cr(VI) biotreatment under optimized conditions. These supports differ from the early used, as the loading of chromium on the matrix is considerably higher, as the comparison between CrNaY* (0.14 %) and CrNaY (0.75 %) clearly demonstrates.

The study of the encapsulation of Cr-PAN complex raised interesting questions concerning the nature of the chromium species present in the zeolite moiety after calcination of the recovered supports. Indications of potential Cr(III) oxidation to Cr(VI) after calcination were observed from Raman and DR-UV spectroscopy (Figures 5.8 and 5.9). In order to have a better understanding of the higher Cr loading supports, a XPS study was conducted

with CrNaY and $CrHY_{SBR}$. The respective chromium high resolution spectra are presented in Figure 5.11.

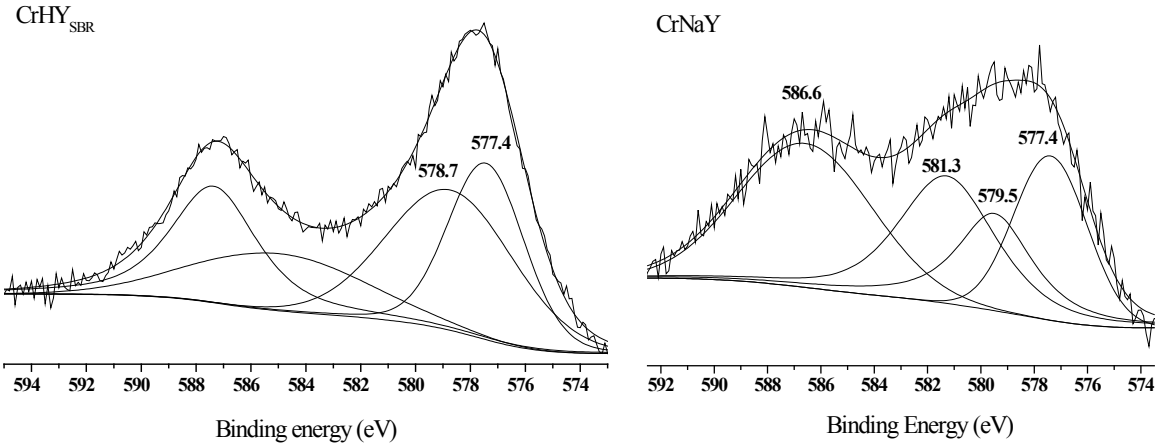

Figure 5.11: XPS spectra and respective peak fitting of the Cr2p region of calcined $CrHY_{SBR}$ and CrNaY samples.

Peak fitting of the XPS spectra was conducted with the XPS PEAK 4.1 software, for a fitting of 4 peaks. Both spectra are dominated by the typical signals of Cr(III) ions at binding energies of 587 and 577 eV, corresponding to the $Cr2p_{1/2}$ and $Cr2p_{3/2}$ orbitals, respectively [23]. The correspondent signals for Cr(VI) species are expected at slightly higher binding energy, as observed in the spectra for CrNaY. The shape of the spectra appears to be wider, compared to $CrHY_{SBR}$ and a shoulder is visible at 581 eV. Software fitting of this peak shows signals for Cr(VI) which are expected at 580 eV [18]. It is likely that these Cr(VI) species might be situated in the external surface of the zeolite – as it was seen in Chapter 4. CrNaY presented a two-step Cr(VI) reduction process while $CrHY_{SBR}$ presented a swift Cr(VI) reduction in less than 48 hours. The presence of Cr(VI) in the external surface of the zeolite is due to the calcination treatment, where a fraction of the exchanged Cr(III) species would be re-oxidized to Cr(VI). This fact was reported by Weckhuysen *et al.*, where Cr(III) ion-exchanged Y zeolites would form chromate species upon calcination in a oxygen-rich atmosphere [20]. Since the recovered biosorption supports were calcined under dry air flow, it is likely that a partial oxidation occurs and the supports contain both Cr(VI) and Cr(III) species.

A new series of ligands was, then, selected to perform the encapsulation of Cr complexes in these supports and their structures are presented in Figure 5.12. For this work, a series of diphenyltriazene derivatives were employed, namely 1,3-diphenyltriazene (DPT), 1,3-bis(*p*-methylphenyl)triazene (MeDPT) and 1,3-bis(*p*-nitrophenyl)triazene (NODPT). All ligands could be chelated by 1,3 nitrogen atoms.

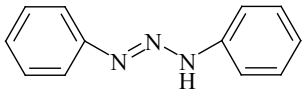

DPT

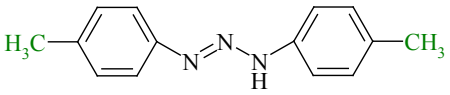

MeDPT

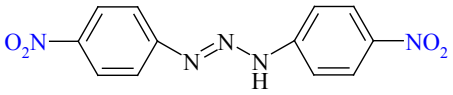

NODPT

Figure 5.12: Structures of the different ligands used for the immobilization of chromium on the supports with higher loading of the metal.

These ligands were synthesized in the Chemistry Department at University of Minho using previously described methods in the literature [24,25]

The coordination of chromium by these ligands is strongly affected by the substitution in the *para*-aryl position. The nitro group in *para* position of the aromatic ring decreases the coordination of triazenido as a result of its electro-withdrawing ability. However, the methyl group in *para* position increases the electronic density in the central triazenido group, resulting in enhanced coordination. The chemical environment for the coordination also has an important role for the final complexes, since it is necessary to assure that deprotonation of the acidic hydrogen occurs in the triazene group [26].

DPT ligand was used on all four hosts for comparison, namely CrNaY, $CrHY_{SBR}$, $CrNaY_{SBR}$ and Cr(III)-NaY_2 supports. The latest sample was prepared by ion-exchange and was not calcined in order to avoid oxidation of the exchanged Cr(III) ions, as previously witnessed in section 5.2. Additionally, in order to compare the effect of molecular structure of the ligand on the efficiency of chromium complex encapsulation, the two remaining ligands (MeDPT and NODPT) were used for encapsulation on the same host, CrNaY, since this one presents the highest chromium loading.

Catalysts prepared using DPT ligand promoted a colour change of the supports to dark grey, whereas MeDPT ligand promoted a change to light brown colour. NODPT did not promote any visible change in the coloration of the host.

The characterization of the heterogeneous catalysts included the same techniques previously employed (FTIR, TGA and chemical analysis). Raman spectroscopy and determination of BET area of the prepared catalysts were also performed.

The analysis of the solid samples by vibrational spectroscopy techniques confirmed that the ligands were present in the matrix, with the exception of NODPT. Figure 5.13 presents the FTIR spectra of the different catalysts prepared from CrNaY host.

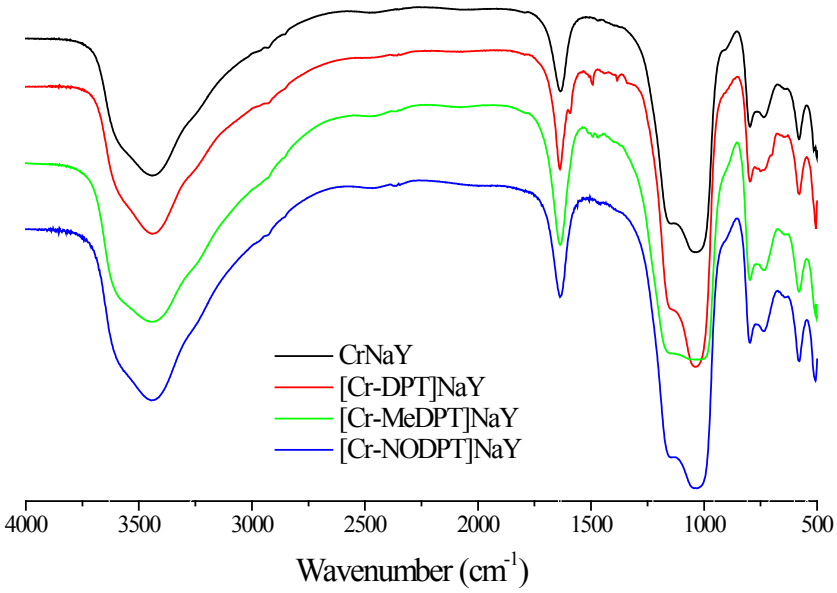

Figure 5.13: FTIR spectra of the three catalysts prepared from the different ligands and CrNaYhost.

All FTIR spectra are dominated by the strong bands attributable to the zeolite structure. No shift or broadening of the zeolite vibration bands is observed upon incorporation of the chromium complexes. FTIR spectrum of CrNaY is characterized by a very intense broad band at ca. 3460 cm^{-1} with a poorly resolved shoulder at ca. 3600 cm^{-1} which can be attributed to the hydroxyl groups in the supercages and in the sodalite cages respectively

The spectra of CrNaY and of the catalysts provide evidence that the zeolite framework is preserved throughout calcination and immobilization of the triazenido derivative chromium

complex. The spectra of [Cr-DPT]NaY and [Cr-MeDPT]NaY show the bands at 1492 and 1593 cm^{-1}, attributed to the ν(N---N---N) of the triazene group which proves that these ligands were successfully coordinated within the zeolite framework. Figure 5.14 presents the Raman spectra of the different catalysts prepared from CrNaY host.

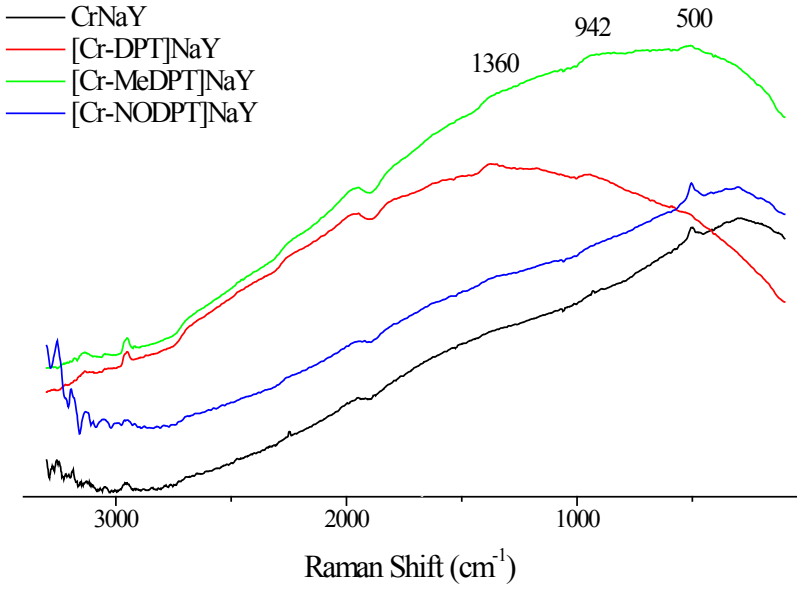

Figure 5.14: Raman spectra of the catalysts prepared with CrNaY host.

The same indications are given by Raman spectroscopy. All Raman spectra are dominated by the strong background fluorescence which is common in zeolite samples [27]. However, some of the immobilized complex samples present changes in the shape of the spectra, mainly on the samples with DPT and MeDPT ligands. In these spectra, it is possible to identify peaks at 1360 and 942 cm^{-1}, while the spectrum of [Cr-NODPT]NaY is similar to CrNaY. The first signal corresponds to the D-band of carbon compounds [28] while the second peak is attributed to surface Cr(VI) species [18]. The presence of these species is related to the calcination conditions that favour the oxidation of Cr(III) to Cr(VI).

The confirmation of encapsulated Cr complexes was given by the combined TGA–BET area analysis. Table 5.3 presents the combined data from TGA (extracted from Figure 5.15), chemical analysis and BET area determination of all catalyst samples.

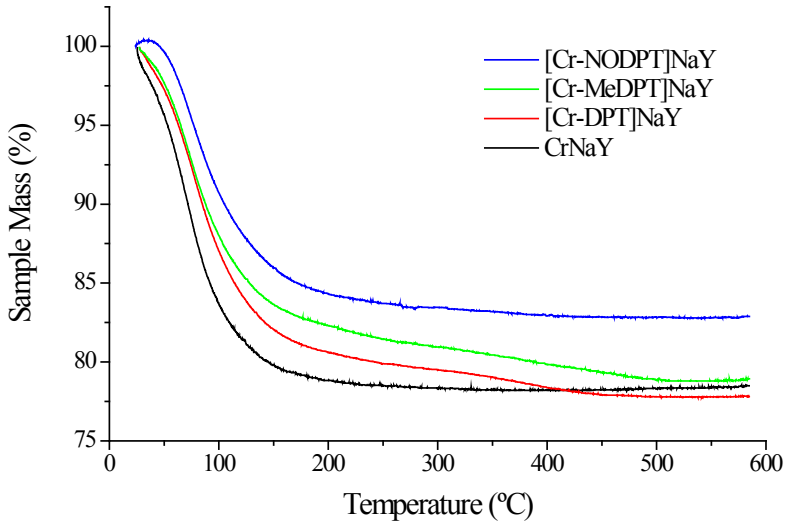

Figure 5.15: Thermogravimetric analysis of the three catalysts prepared with different ligands and CrNaY host.

Table 5.3: Chemical, thermogravimetric and textural analyses data for all the catalysts and hosts.

		Elemental analysis (%, w/w)				TGA analysis	BET Surface Area ($m^2.g^{-1}$)
Support	Ligand	Cr[a]	C[b]	N[b]	Cr/N	Loss of mass at temp. > 250 ºC (%, w/w)	
CrNaY	---	0.75	0	0	---	---	562.85
	DPT	0.71	0.75	0.19	3.74	2.5	195.79
	MeDPT	0.71	1.23	0.20	3.55	2.1	317.15
	NODPT	0.72	0.10	0.02	14.5	0.2	562.48
$CrNaY_{SBR}$	---	0.46	0	0	---	---	590.34
	DPT	0.47	0.32	0.05	9.40	0.8	539.64
$CrHY_{SBR}$	---	0.59	0	0	---	---	495.65
	DPT	0.55	1.04	0.29	1.89	2.5	201.19
Cr(III)-NaY_2	---	0.36	0	0	---	---	622.67
	DPT	0.38	0.07	0.02	15.3	0.2	580.33

[a]Cr loading on FAU supports determined by ICP-AES analysis.
[b]Carbon and nitrogen from Cr complexes obtained by elemental analysis.

Thermogravimetric analysis provided further indication that immobilization of Cr-DPT and Cr-MeDPT complexes was achieved. TG and DTG curves of all samples show a weight loss at 110 ºC which is attributed to the loss of water molecules present in the framework of the zeolite. After the synthesis of the complex, the catalysts based in DPT and MeDPT ligands present a second weight loss, taking place at a higher temperature around 380 ºC, attributed to the decomposition of the organic matter from the complexes. Comparing the complexes formed with DPT ligand, the extent of the secondary weight loss varied with the different supports. This ligand was able to form up to 2.5 % (w/w) mass of chromium complex within CrNaY and $CrHY_{SBR}$. Despite having different chromium loadings, the formation of complex with DPT ligand was comparable between these two supports.

The thermogravimetric analysis of [Cr-NODPT]-NaY is similar to the CrNaY host indicating that the complex is not obtained, in agreement with other characterization techniques. The different weight loss observed for the catalysts confirm that the NODPT ligand is not coordinated with the chromium.

Concerning the other hosts in study ($CrHY_{SBR}$, $CrNaY_{SBR}$ and $Cr^{III}NaY_2$), only $CrHY_{SBR}$ support was able to perform comparatively to CrNaY, in terms of immobilization of chromium complex. In the case of the chromium complex formed in $CrNaY_{SBR}$ and Cr(III)-NaY_2 supports, the TGA results show that the lower amount of formed complex is related to the lower loading of chromium in these supports.

The immobilization of the chromium complexes in the supports was confirmed by the analytical data of carbon, nitrogen and metal. High Cr/N ratios were obtained, observed for different catalysts, which suggests the presence of a fraction of uncoordinated chromium ions. It is assumed that one part of these ions could be located in framework sites that are inaccessible for the ligands [16]. However, the lower nitrogen amount in the [Cr-NODPT]NaY catalyst comfirm that the complex with NODPT ligand was not achieved. These results are due to the decrease of the electron-donor strength of the triazenido ligand by the NO_2 group in *para* position of the aromatic ring in acidic medium [26].

The low amount of formed chromium complex is related to the presence of the different chromium species in the biosorption-recovered Y supports. The Cr(VI) species detected in XPS and Raman do not coordinate with the triazenido ligands which means that only a small fraction of chromium takes part in the synthesis of the complex, being this fraction Cr(III) species.

For all catalysts, the total surface areas (S_{BET}) were calculated by applying the BET equation and the data show a reduction in area upon coordination, when compared to the

respective parent supports. This is further indication of successful immobilization [13]. However, for the catalysts obtained from CrNaY (with both DPT and MeDPT) and $CrHY_{SBR}$ the decrease in BET area is significant.

The chemical analysis of the supports and respective catalysts revealed that no significant loss of chromium occurred during the *in-situ* synthesis, which means that the overall catalytic activity of each support is not significantly changed.

5.4 Conclusions

The results presented in this chapter allowed concluding that the recovered Cr(VI) biotreatment supports may be potentially used as catalysts for liquid-phase oxidation reactions.

Different ligands were employed for the immobilization of Cr complexes in FAU supports. All ligands present nitrogen atoms for coordination in different chemical structures, pyridazine, azo and triazenido groups. Analytical results from different techniques demonstrated the presence of ligand molecules in the framework and this was possible by coordination with the chromium ions present in the zeolitic moiety.

Diphenyltriazene ligands were successfully employed for the *in-situ* synthesis of chromium complexes on the supports recovered from assays performed under optimized conditions, which allowed higher loading of the metal.

5.5 References

[1] H. Figueiredo, B. Silva, C. Quintelas, M.M.M. Raposo, P. Parpot, A.M. Fonseca, A.E. Lewandowska, M.A. Bañares, I.C. Neves, T. Tavares, Immobilization of Chromium Complexes in Zeolite Y Obtained From Biosorbents: Synthesis,

Characterization and Catalytic Behaviour, Applied Catalysis B: Environmental. 94 (2010) 1-7.

[2] P. Echlin, Low-Voltage Energy-Dispersive X-ray Microanalysis of Bulk Biological Materials, Microscopy and Microanalysis. 4 (1999) 577–584.

[3] S.-Y. Li, J. Millstone, C. Mirkin, V. Dravid, Detection of Phosphorus in Biological Samples with Analytical Electron Microscopy, Microscopy and Microanalysis. 13 (2007) 456-457.

[4] S. Comte, G. Guibaud, M. Baudu, Biosorption Properties of Extracellular Polymeric Substances (EPS) Resulting From Activated Sludge According to Their Type: Soluble or Bound, Process Biochemistry. 41 (2006) 815-823.

[5] H. Figueiredo, I.C. Neves, C. Quintelas, T. Tavares, M. Taralunga, J. Mijoin, P. Magnoux, Oxidation Catalysts Prepared From Biosorbents Supported on Zeolites, Applied Catalysis B: Environmental. 66 (2006) 274-280.

[6] H. Figueiredo, M.M.M. Raposo, A.M. Fonseca, I.C. Neves, C. Quintelas, T. Tavares, Encapsulated Pyridazine Cr(III) Complexes Prepared from Biosorbents Supported in Zeolites, in: J. Cejka, I. Zilková, P. Nachtigall (Eds.), Molecular Sieves: From Basic Research to Industrial Applications, Proceedings of the 3rd International Zeolite Symposium (3rd FEZA), Elsevier, 2005: pp. 1073-1080.

[7] B. Silva, H. Figueiredo, C. Quintelas, I. Neves, T. Tavares, Zeolites as Supports for the Biorecovery of Hexavalent and Trivalent Chromium, Microporous and Mesoporous Materials. 116 (2008) 555-560.

[8] H. Figueiredo, B. Silva, M.M.M. Raposo, A.M. Fonseca, I.C. Neves, C. Quintelas, T. Tavares, Immobilization of Fe(III) Complexes of Pyridazine Derivatives Prepared From Biosorbents Supported on Zeolites, Microporous and Mesoporous Materials. 109 (2008) 163-171.

[9] H. Figueiredo, B. Silva, C. Quintelas, M.F.R. Pereira, I.C. Neves, T. Tavares, Biosorption of Hexavalent Chromium Based on Modified Y Zeolites Obtained by Alkaline Treatment, Environmental Engineering and Management Journal. 9 (2010) 305-311.

[10] H. Khanmohammadi, M. Darvishpour, New Azo Ligands Containing Azomethine Groups in the Pyridazine-based Chain: Synthesis and Characterization, Dyes and Pigments. 81 (2009) 167-173.

[11] C.D. Brandt, P.G. Plieger, R.J. Kelly, D.J. de Geest, D.K. Kennepohl, S.S. Iremonger, S. Brooker, Dinickel(II), Dizinc(II) and Dilead(II) Complexes of a Pyridazine-containing Schiff-base Macrocycle, Inorganica Chimica Acta. 357 (2004) 4265-4272.

[12] H. Figueiredo, Reutilização Catalítica de Biossorventes Suporteados em Zeólitos, University of Minho, Master Thesis. 2007.

[13] H.S. Abbo, S.J.J. Titinchi, Metallo Salicylidenetriazol Complexes Encapsulated in Zeolite-Y: Synthesis, Physicochemical Properties and Catalytic Studies, Topics in Catalysis. 53 (2010) 1401-1410.

[14] P. Chutia, S. Kato, T. Kojima, S. Satokawa, Synthesis and Characterization of Co(II) and Cu(II) Supported Complexes of 2-pyrazinecarboxylic Acid for Cyclohexene Oxidation, Polyhedron. 28 (2009) 370-380.

[15] M.R. Maurya, A.K. Chandrakar, S. Chand, Oxidation of Phenol, Styrene and Methyl Phenyl Sulfide with H_2O_2 Catalysed by Dioxovanadium(V) and Copper(II) Complexes of 2-aminomethylbenzimidazole-based Ligand Encapsulated in Zeolite-Y, Journal of Molecular Catalysis A: Chemical. 263 (2007) 227-237.

[16] M. Álvaro, B. Ferrer, H. García, A. Sanjuán, Heterogeneous Gif Oxidation of Cyclohexane Using Fe^{3+}-picolinate Complex Encapsulated Within Zeolites, Tetrahedron. 55 (1999) 11895-11902.

[17] N. Xiao, Q. Xu, J. Sun, J. Chen, Unusual reactions of [{μ-(phthalazine-N^2:N^3)}Fe_2(μ-CO)$(CO)_6$] with Organolithium Reagents. A Novel Coordination Mode of 1,2-diazane Diiron Carbonyl Compounds, Dalton Transactions (Cambridge, England : 2003). (2006) 603-608.

[18] B.M. Weckhuysen, I.E. Wachs, R.A. Schoonheydt, Surface Chemistry and Spectroscopy of Chromium in Inorganic Oxides., Chemical Reviews. 96 (1996) 3327-3350.

[19] P.-P. Knops-Gerrits, D. De Vos, E.J.P. Feijen, P.A. Jacobs, Raman Spectroscopy on Zeolites, Microporous Materials. 8 (1997) 3-17.

[20] B.M. Weckhuysen, H.J. Spooren, R.A. Schoonheydt, A Quantitative Diffuse Reflectance Spectroscopy Study of Chromium-containing Zeolites, Zeolites. 14 (1994) 450-457.

[21] B.M. Weckhuysen, R.A. Schoonheydt, J.-M. Jehng, I.E. Wachs, S.J. Cho, R. Ryoo, S. Kijlstra, E. Poels, Combined DRS-RS-EXAFS-XANES-TPR Study of Supported Chromium Catalysts, Journal of the Chemical Society, Faraday Transactions. 91 (1995) 3245.

[22] M.K. Koley, S.C. Sivasubramanian, B. Varghese, P.T. Manoharan, A.P. Koley, Synthesis and Characterization of Two Stable Paramagnetic Octahedral Chromium(IV) Complexes With Dianionic Tridentate SNO Donor Ligands and of a Chromium(III) Complex With a ONO Donor Ligand, Inorganica Chimica Acta. 361 (2008) 1485-1495.

[23] D. Park, Y.-S. Yun, J.M. Park, XAS and XPS Studies on Chromium-binding Groups of Biomaterial During Cr(VI) Biosorption., Journal of Colloid and Interface Science. 317 (2008) 54-61.

[24] M. Menon, A. Pramanik, S. Chattopadhyay, N. Bag, A. Chakravorty, Chemistry of [Ru(1,3-diaryltriazenide)$_2$(PPh$_3$)$_2$]z (z = 0,+). A Hindered Ru(II),(III)N^2P^2 Family with Valence-Independent Geometry, Inorganic Chemistry. 34 (1995) 1361-1367.

[25] A.F.M.J. Van der Ploeg, G. Van Koten, K. Vrieze, Synthesis of novel dinuclear formamidino and triazenido compounds {[2,6-(Me$_2$NCH$_2$)$_2$C$_6$H$_3$](*p*-tolNYNR)PtAgBr} (Y=CH,N) Containing a Platinum-silver Bond, Inorganic Chemistry. 21 (1982) 2026-2031.

[26] J.J. Nuricumbo-Escobar, C. Campos-Alvarado, G. Ríos-Moreno, D. Morales-Morales, P.J. Walsh, M. Parra-Hake, Binuclear Palladium(I) and Palladium(II) Complexes of Ortho-functionalized 1,3-bis(aryl)triazenido Ligands., Inorganic Chemistry. 46 (2007) 6182-6189.

[27] Y. Huang, R.M. Paroli, A.H. Delgado, T.A. Richardson, An FT-Raman Study of Solid-state Ion Exchange in Zeolites, Spectrochimica Acta Part A: Molecular and Biomolecular Spectroscopy. 54 (1998) 1347-1354.

[28] B. Kwiecinska, I. Suárez-Ruiz, C. Paluszkiewicz, S. Rodriques, Raman Spectroscopy of Selected Carbonaceous Samples, International Journal of Coal Geology. 84 (2010) 206-212.

CHAPTER 6

ASSEMENT OF THE CHROMIUM CATALYSTS IN LIQUID-PHASE OXIDATION REACTIONS

CHAPTER 6 – ASSESSMENT OF THE Cr CATALYSTS IN LIQUID-PHASE OXIDATION REACTIONS

This chapter presents the experimental results obtained from the catalytic experiments conducted with the chromium catalysts, previously described in Chapter 5.

There was a previous catalytic evaluation of the as-recovered Cr(VI) biotreatment supports, conducted on the gas-phase oxidation of 1,2-dichlorobenzene, using CrNaY and CrNaX supports [1]. The performance of the several Cr catalysts in liquid-phase was evaluated in two different oxidation reactions, namely, the oxidation of cyclohexene and the oxidation of cyclohexanol. Both reactions were referred to in Chapter 1 (see section 1.3.4).

6.1 Oxidation of cyclohexanol

The oxidation of cyclohexanol using *tert*-butylhydroperoxide (TBHP) as the oxygen source follows the typical reaction pathway for an oxidation of a secondary alcohol, with the formation of the corresponding ketone, which in this case is cyclohexanone (Figure 6.1).

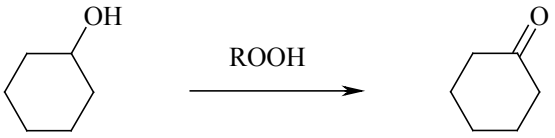

Figure 6.1: Peroxide oxidation of cyclohexanol into cyclohexanone.

The experimental work on this reaction was conducted later to the studies on cyclohexene oxidation. Due to the exhaustion of the Cr-chloropiridazine and Cr-PAN catalysts on those studies, only the Cr-diphenyltriazene catalyst series allowed a comprehensive study for the oxidation of cyclohexanol. Therefore, only the experimental results with these catalysts will be presented in this section.

A series of blank reactions were carried out to test the stability of the solvents and of the GC internal standards to the THBP oxidant. Diethylketone (DEK) was chosen as solvent for the reaction due to its intermediate polarity and high boiling point (105 ºC), which is useful given the chosen reaction temperature (later discussed). Due to the same fact, chlorobenzene was chosen as GC internal standard as it has high stability at the reaction temperature *vs*. other tested compounds (cyclohexane and toluene). This compound was also used as solvent and GC standard for this reaction by Laha and Gläser [2] and Sakthivel [3].

The selection of temperature was based on the comparison between the conversion achieved by two catalysts of distinct natures, CrNaY host and the corresponding encapsulated complex of [Cr-MeDPT]NaY. The catalytic results are presented in Figure 6.2.

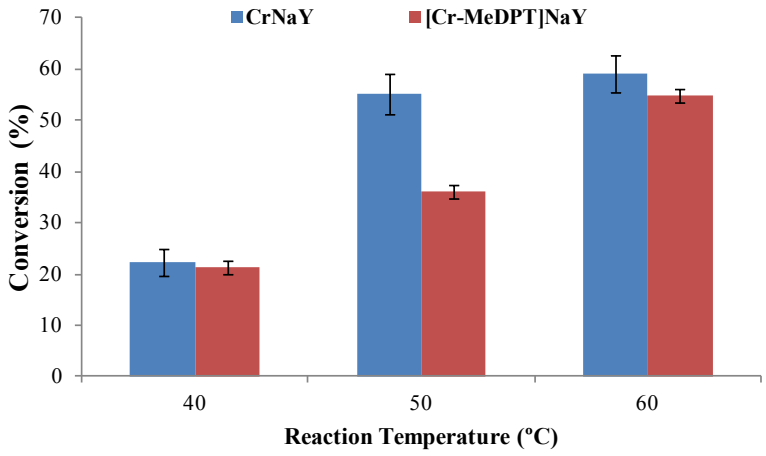

Figure 6.2: Conversion of cyclohexanol by CrNaY and [Cr-MeDPT]NaYcatalysts, for the tested temperature range, after 23 hours of reaction.

The temperature range between 40-60 ºC was selected to assure mild oxidation conditions while avoiding decomposition of the TBHP oxidant. This compound is known to be more stable than H_2O_2 while being environmentally safe [4], withstanding reaction temperatures up to 120 ºC (reported by Sakthivel *et al.* [3]). The data presented in Figure 6.2 shows that the maximum cyclohexanol conversion was achieved at 60 ºC for both catalysts tested. Although the increase in cyclohexanol conversion between 50 and 60 ºC is minor for

CrNaY, a significant increase was observed for [Cr-MeDPT]NaY. For this fact, all reactions were carried out at 60 ºC.

The reaction time was set at 23 hours. However, some reactions were allowed to proceed during 48 hours and an increase in *circa* 5% of cyclohexanol conversion was observed (compared to the conversion after 23 hours). Despite the non-equilibrium conditions, the experimental time of 23 hours was deemed sufficient and was used throughout the experiments.

The complete study on the activity of the different catalysts is presented in Table 6.1. The catalysts may be separated into three main groups: biosorption supports from the high-biomass concentration studies (also named *hosts*); the encapsulated Cr-diphenyltriazene complexes and the supports prepared by ion-exchange with Cr(III). Experimental results for a non-catalyzed reaction as well as the blank reactions with calcined NaY and HY zeolites were also included. The turn-over number (TON) was also determined, being defined as the ratio between the moles of converted cyclohexanol molecules and the initial moles of chromium ions available in the catalyst. This figure indicates the average catalytic cycles performed by each active metal centre.

Table 6.1: Conversion of cyclohexanol and turn-over numbers (TON) for the different catalysts tested.

Catalyst	Cyclohexanol conversion (%)	Analytical error *(%)*	Cr loading of catalyst (%, w/w)	TON[a]
Blank reaction	18.6	± *3.5*	---	---
NaY	15.8	± *5.3*	---	---
HY	14.2	± *1.4*	---	---
CrNaY	61.2	± *1.2*	0.75	246.2
[CrDPT]NaY	57.3	± *3.0*	0.71	243.4
[CrMeDPT]NaY	54.1	± *1.7*	0.81	201.4
[CrNODPT]NaY	63.5	± *2.8*	0.72	266.0
CrNaY EXT	61.8	± *3.1*	0.94	198.2
$CrNaY_{SBR}$	56.8	± *4.5*	0.46	372.5
$[CrDPT]NaY_{SBR}$	49.1	± *4.6*	0.47	314.9
CrHY	50.7	± *4.2*	0.54	283.2
$CrHY_{SBR}$	48.0	± *1.1*	0.59	245.4
$[CrDPT]HY_{SBR}$	42.9	± *2.9*	0.55	235.4
$Cr(III)\text{-}NaY_1$ (calcined)	51.9	± *4.3*	0.62	252.5
$Cr(III)\text{-}NaY_2$	42.6	± *1.0*	0.36	357.1
$[Cr(III)\text{-}DPT]NaY_2$	38.3	± *0.9*	0.38	304.0

[a]The turnover number (TON) was determined from the converted cyclohexanol moles over the initial molarity of chromium on the respective catalyst.

The data presented in Table 6.1 will be discussed comparing the three different catalyst types.

Analysing the conversion values for the zeolitic hosts, it is possible to conclude that the NaY or HY zeolites do not contribute to cyclohexanol conversion as NaY- or HY-catalyzed reactions achieved a conversion comparable to the blank reaction. On the other hand, the

biosorption samples confirmed that the presence of chromium resulted in a significant increase in conversion. Therefore, the presence of chromium ions on the support greatly increases the cyclohexanol conversion.

Comparing the performance of the four biosorption supports (CrHY, $CrHY_{SBR}$, CrNaY and $CrNaY_{SBR}$) plus the CrNaY EXT sample, it is possible to notice some aspects. The first is related to the NaY-based catalysts, where the chromium loading of the supports does not promote a linear response in terms of catalytic activity. This is highlighted in Figure 6.3, where the catalytic activity of the NaY- and HY-based catalysts is plotted *vs*. the Cr loading of the support.

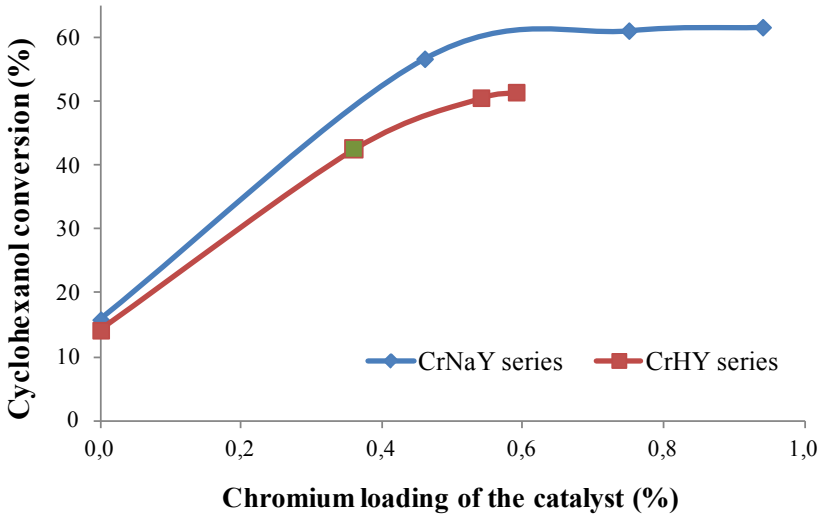

Figure 6.3: Cyclohexanol conversion *vs*. chromium loading of the different biosorption supports.

In the NaY series, it is visible that the cyclohexanol conversion increases with the Cr loading of the support until a conversion of *circa* 62% is achieved with the CrNaY and CrNaY EXT supports. Despite the higher loading of metal on the last support, the activity is comparable to the first, meaning that the accessible Cr active sites are equally available. This could be explained by the dynamics of Cr(VI) biotreatment on these supports (presented in Chapter 4): for $CrNaY_{SBR}$, the chromium ions are mostly located at the outermost zeolite surface, since the residence time of 4 days did not allow an efficient ion-exchange of the bioreduced Cr(III) species. For CrNaY and CrNaY EXT, the contact time of the Cr(VI) solution allowed the slower secondary ion-exchange process to take place, also allowing difusion of the reduced Cr into the framework.

For the CrNaY hosts from biosorption treatments, both Cr(VI) and Cr(III) species were observed on the surface after the calcination of the samples, as it was seen in Chapter 5. XPS studies of these supports show that both Cr(VI) and Cr(III) species are present in the external surface or close to the surface of CrNaY. This could explain the higher activity of the CrNaY hosts when compared to the CrHY samples, since Cr(VI)-containing catalysts are known to be very active on the peroxide oxidation of primary and secondary alcohols [5,6]. An important fraction of the Cr(III) species is located in the zeolite framework of the hosts and these are also contributing to the overall conversion, as witnessed in the CrHY and Cr(III)-NaY_2 samples . However, some ions can be inaccessible to the reactants, being present at certain sites of the zeolite that cannot be ruled out, such as within the hexagonal prisms or sodalite cages [7,8]. The TON values of the three CrNaY-based supports also sustain this interpretation, as they decrease with the increase in Cr loading. This indicates that not all of the loaded chromium is active on this reaction.

By the same XPS study described in Chapter 5, $CrHY_{SBR}$ host presented a clear spectrum for Cr(III) species, meaning that the surface would lack the same amount of Cr(VI) active sites as CrNaY counterparts. This explains the low conversion observed for CrHY supports. Since CrHY and $CrHY_{SBR}$ present comparable chromium loadings and conversion values, Cr(III)-NaY_2 sample was included in the plot presented in Figure 6.3 and appears to follow the same tendency as CrHY supports. This further sustains the Cr(III) nature of the catalytic active sites. Therefore, considering the two different plots in Figure 6.3, it may be assumed that the CrNaY plot represents a catalytic process with the combined contribution of Cr(VI) and Cr(III) active centres, whereas the CrHY plot represents a process with a predominantly Cr^{III}-mediated process.

Looking at the performance of the encapsulated chromium complexes, the catalytic activity decreases when compared to the corresponding hosts. Although some authors comment that zeolite-encapsulated metal complexes can achieve higher catalytic activity than the equivalent homogenous complexes [9,10], these results raised some questions on the possible leaching of active metal centres into the reaction medium. This is mainly brought up by the fact that CrNaY and [Cr-NODPT]NaY achieved identical conversion, whereas [Cr-DPT]NaY and [Cr-MeDPT]NaY presented a slight decrease in conversion. Since it was seen in Chapter 5 that no encapsulation took place when NODPT ligand was used with CrNaY, it is clear that the [Cr-NODPT]NaY catalyst may be very similar to the parent host. Moreover, since the chromium ions are encapsulated in the other catalysts with DPT and

MeDPT ligands, it is likely that the conversion of the parent Cr-zeolite hosts might be due to leaching of chromium ions to the reaction medium. In order to confirm this, acid digestion of the reaction medium after conclusion of the reaction, was performed and the determination of chromium content was conducted by AAS. The results for this analysis are presented in Figure 6.4.

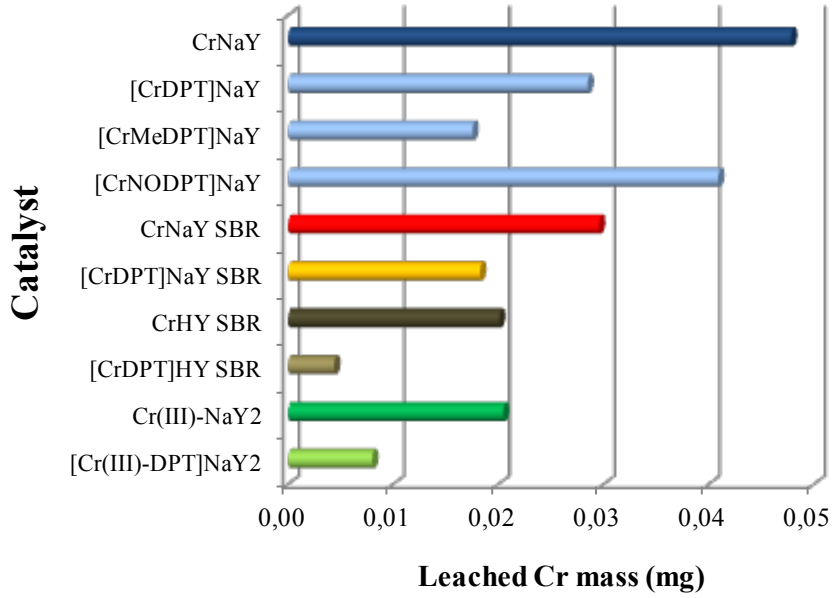

Figure 6.4: Leached Cr mass for the different catalysts.

As it can be seen in Figure 6.4, leaching of chromium was observed for the different catalysts, maybe with the exception of the almost negligible leaching observed for [Cr-DPT]HY_{SBR}. It can also be seen that the other encapsulated complexes minimized the leaching of metal from their respective hosts. Some additional conclusions can also be inferred from this analysis.

Firstly, comparing $CrNaY_{SBR}$ and $CrHY_{SBR}$, it can be seen that although the chromium loading is higher on the last support, it is the first that presents a higher leaching during reaction. This is in accordance with the previously commented dynamics of the Cr(VI) biotreatment studies indicating a higher dispersion of metal on the $CrNaY_{SBR}$ surface, while for CrHY it was more efficiently ion-exchanged. It is likely that the superficial chromium species are more susceptible to removal by the TBHP oxidant, as Sheldon *et al.* referred for the cleavage of Si-O-Cr bonds being responsible for the loss of heterogeneous

character on CrAPO catalysts [11–13]. In the $CrHY_{SBR}$ host, the chromium ions are located within the framework, being less exposed to a leaching action by the peroxide. This explains the lesser extent of chromium loss when compared to the CrNaY hosts.

Another fact that can be observed in Figure 6.4 is that NaY-based catalysts are more prone to leaching. CrNaY and $CrNaY_{SBR}$ are amongst the most susceptible catalysts, while comparing to the ion-exchanged Cr(III)-NaY_2 support to $CrHY_{SBR}$, the amount of leached metal is similar even if the CrHY support presents a higher chromium loading. This can be mainly due to the preferable deposition of chromium on the NaY-supports during the Cr(VI) biotreatment assays. These chromium species, even when coordinated with the diphenyltriazene ligands, are more exposed to the TBHP oxidant than the encapsulated complexes, and this may lead to break-down of the metal-zeolite interaction.

In order to evaluate the effect of chromium leaching on the reusability of the catalysts, a recycling test was conducted using the most active host (CrNaY) and its corresponding encapsulated [Cr-DPT]NaY catalyst. The catalysts were removed from the reaction medium by filtration and dried before the following reaction. This process resulted in a significant loss of mass from cycle to cycle; nevertheless, it was possible to conduct the reactions with the available catalyst mass and the result is presented in Figure 6.5.

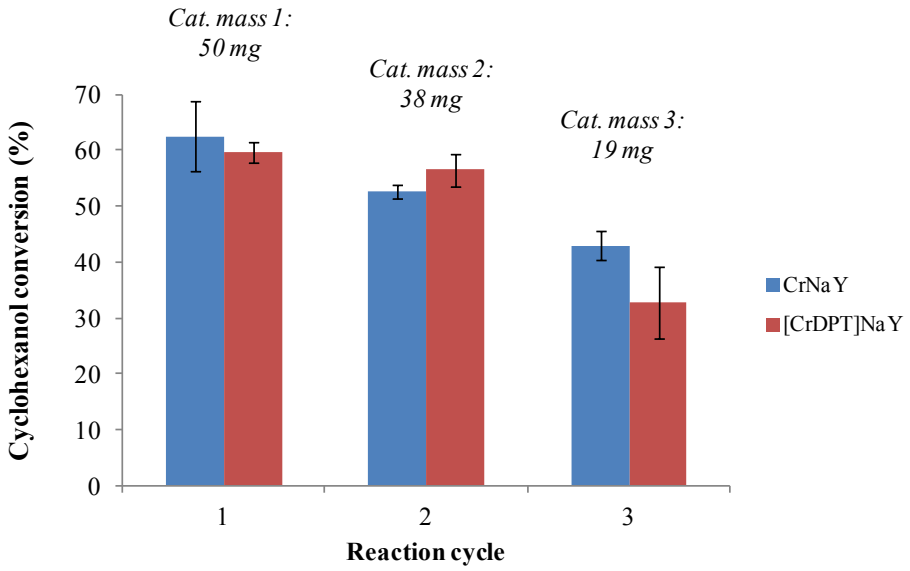

Figure 6.5: Conversion of cyclohexanol for CrNaY and [Cr-DPT]NaY for the different catalytic cycles. Average catalyst masses are indicated on top of each cycle.

The recycling experiment confirmed that both non-immobilized and immobilized catalyst maintain catalytic activity for this reaction for 3 consecutive cycles. However, while CrNaY presents a decrease in conversion from cycle 1 to 2, [CrDPT]NaY is able to perform the same conversion after 2 cycles.

In conclusion, the oxidation of cyclohexanol allowed a catalytic evaluation of the Cr-containing biosorption supports and the corresponding immobilized catalysts. Leaching of chromium ions was observed from the biosorption supports, which has decreased upon encapsulation of the Cr ions with diphenyltriazene ligands. To this extent, [Cr-DPT]HY$_{SBR}$ was the best catalyst in terms of stability. Nevertheless, both immobilized and non-immobilized catalysts exhibited activity for the reaction for 3 consecutive reaction cycles.

6.2 Oxidation of cyclohexene

The second reaction considered is the oxidation of cyclohexene with TBHP for the evaluation of the different catalysts prepared in this work. According to works presented by different authors, this reaction is known to generate several reaction products [4,14–17]. A summary of those is presented in Figure 6.6.

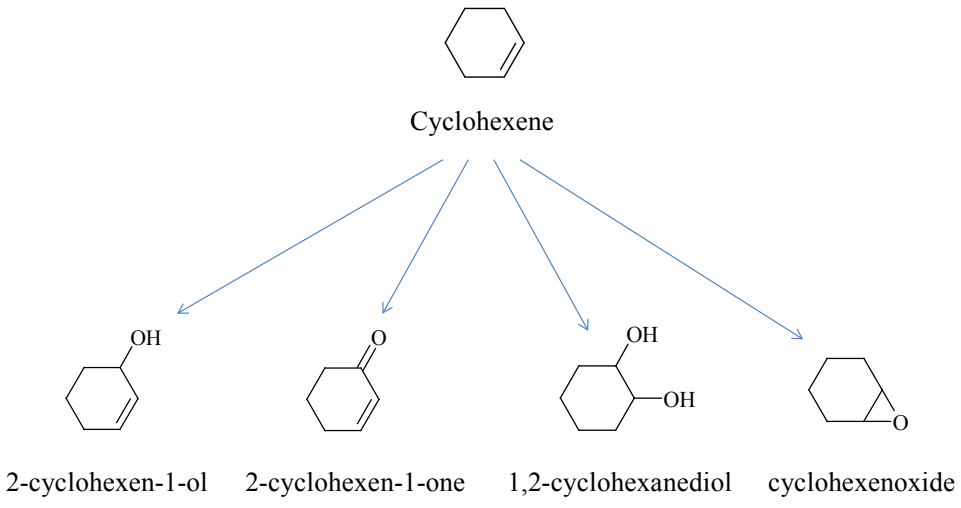

Figure 6.6: Oxidation products for the peroxide oxidation of cyclohexene.

The oxidation of cyclohexene with peroxides may undergo different pathways, with epoxidation of C-C bonds competing with allylic oxidation of C-H bonds [18]. The extent of each pathway depends on several reaction conditions, such as the choice of peroxide oxidant, solvent and catalyst.

The oxidation of cyclohexene was carried out to evaluate the catalytic performance of the different biotreatment supports and immobilized Cr complexes. This was conducted in two distinct phases. In the first one, the reaction conditions and analytical routines were developed using the immobilized Cr-pyridazine and Cr-PAN catalysts, as well as the corresponding supports, collected from the early studies in Cr(VI) biotreatment. In a second phase, the immobilized Cr-diphenyltriazene and the respective hosts were tested for this reaction. This will be covered in two separate sections.

6.2.1 Oxidation of cyclohexene using encapsulated Cr-pyridazine and Cr-PAN complexes

(Note: studies presented in this section have been previously reported in Figueiredo, Silva, Quintelas, Raposo, Parpot, Fonseca, Lewandowska, Bañares, Neves and Tavares, Applied Catalysis B: Environmental 94, 2010, 1-7 [19]).

The oxidation of cyclohexene with Cr-pyridazine and Cr-PAN complexes marked the first liquid-phase catalytic test of the materials prepared from Cr(VI) biotreatment studies. To this extent, most of the reaction conditions and analytical routines were selected using as-recovered Cr(VI) biotreatment supports from early studies, such as CrNaY*. Another support extensively used was the ion-exchanged Cr(III)-NaY_1, in the calcined form.

The definition of reaction conditions was based on the works of Nunes *et al*. [16]. The chosen solvent for this reaction was the same solvent on which the TBHP oxidant was commercially provided, decane. Additional factors such as its known chemical inertness and high solubility for cyclohexene contributed for this option. Toluene was used as GC internal standard. Blank reactions were conducted in order to assure that the observed reaction products were originated exclusively from the oxidation of cyclohexene and not from solvent or toluene. This last one has been used as solvent for this reaction [18]. The initial tests were conducted at a temperature of 30 ºC; however, it would soon be increased to 40 ºC to allow higher conversion of cyclohexene.

The experimental time was set at 23 hours of reaction, as early results showed no further conversion of cyclohexene beyond this point. Figure 6.7 shows an example of time-dependency of the conversion of cyclohexene using Cr(III)-NaY_1 support as catalyst, which was found to be the most active in this study (see Table 6.2).

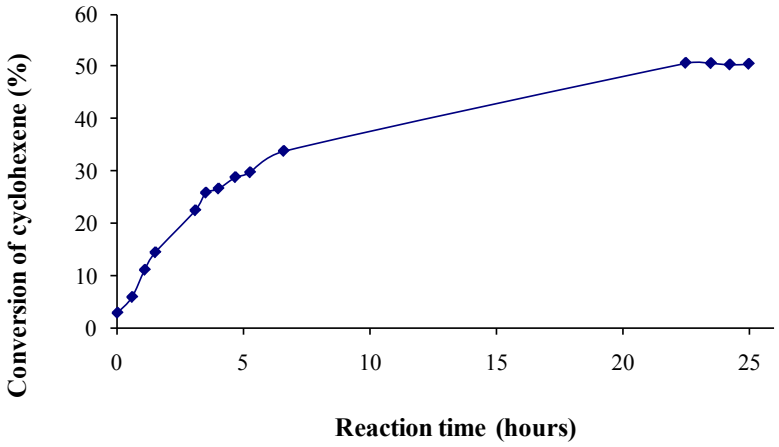

Figure 6.7: Time dependency of the conversion of cyclohexene with Cr(III)-NaY_1 catalyst.

The first results showed the absence of cyclohexeneoxide (ChO) amongst the reaction products. The main products obtained from the oxidation were 2-cyclohexen-1-ol (ChOl) and 2-cyclohexene-1-one (ChOne). The formation of a third product that did not match any of the standards for the oxidation products presented in Figure 6.6 was observed. This product was identified by GC-MS, corresponding to *tert*-butyl-cyclohexylperoxide (Ch-TBHP) and was found to behave as an intermediary product towards the formation of ChOl and ChOne, as it is presented in Figure 6.8. As it can be seen, Ch-TBHP is the first product to be formed and the formation of the other two, ChOl and ChOne, increases upon the consumption of the intermediary. The formation of this intermediary product was also reported by other authors [14,20].

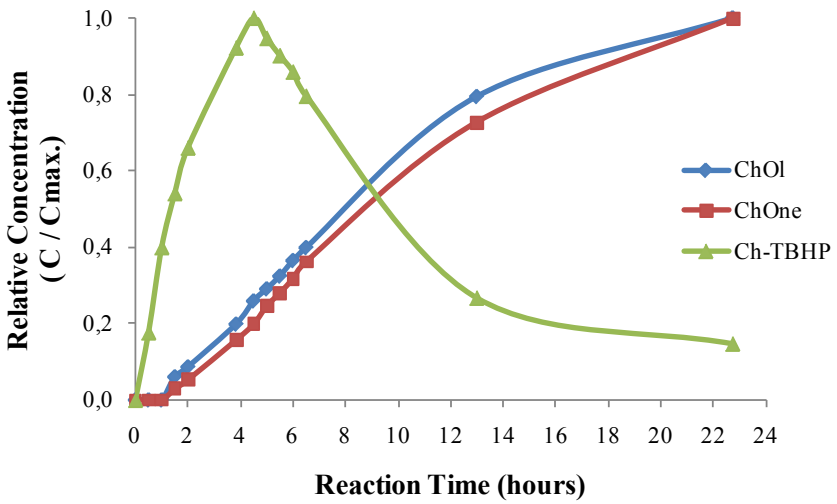

Figure 6.8: Evolution of the reaction products for the oxidation of cyclohexene with TBHP, using $Cr^{III}NaY_1$ catalyst. Evolution of products is calculated as instant over maximum concentration (C/C_{max}) during the experimental time.

The complete results for the oxidation of cyclohexene are presented in Table 6.2.

Table 6.2: Conversion of cyclohexene, product selectivity and turn-over numbers for the Cr-pyridazine and Cr-PAN encapsulated complexes and their respective hosts.

Catalyst	Conversion (%)	Analytical error (%)	Selectivity (%)			Cr loading of catalyst (%)	TON
			ChOl	ChOne	Ch-TBHP		
blank reaction	16.2	± *5.5*	0.0	0.0	100.0	---	---
NaY	14.2	± *8.6*	0.0	0.0	100.0	---	---
CrNaY*	40.3	± *4.9*	0.0	34.3	65.7	0.14	614
$Cr^{III}NaY_1$ (calc.)	51.2	± *3.9*	20.1	79.9	0.0	0.62	160
[Cr-PyMe]NaY*	27.6	± *4.6*	0.0	17.0	83.0	0.09	647
[Cr-PyP]NaY*	30.3	± *6.5*	0.0	21.5	71.5	0.09	717
[Cr-PAN]NaY*	31.8	± *5.0*	0.0	21.5	78.5	0.07	851
[Cr(III)-PyMe]NaY_1	37.9	*4.4*	9.5	44.5	46.0	0.58	127

The experimental results show that while NaY zeolite is inactive for the oxidation of cyclohexene, the presence of chromium on the CrNaY*, Cr(III)-NaY_1 supports and respective encapsulated complexes increases cyclohexene conversion. Additionally, the selectivity appears to be dependent on the quantity of metal of the support.

Comparing the CrNaY* and calcined Cr(III)-NaY_1 supports with parent NaY zeolite, it is clearly noticeable that the selectivity towards ChOl and ChOne depends on the availability of chromium on the support. This is further evidenced by the absence of the Ch-TBHP intermediary using the Cr(III)-NaY_1 support. A previous study by Buijs *et al.* highlighted the activity of Cr(VI) catalysts on the decomposition of cyclohexyl-hydroperoxide into cyclohexanone [21], and this process appears to be valid for this reaction as well. Since the calcined Cr(III)-NaY_1 support presented superficial Cr(VI) species (commented in Chapter 5), the contribution of all chromium species may be responsible for the high cyclohexene conversion achieved with this support. Moreover, the higher selectivity towards ChOne over ChOl may also be due to secondary oxidation of the ChOl product into ChOne, in a similar process to the previously observed for the oxidation of cyclohexanol to cyclohexanone (section 6.1).

Comparing the product selectivity to the reported in literature, it is possible to find divergent results. As an example, the work of Adam and Fook referred the use of a Cr-silica catalyst prepared by treatment with a Cr(III) solution and subsequent calcination at 500 ºC, which was used for the oxidation of cyclohexene with H_2O_2 oxidant, reaching a maximum conversion of 31 %. The main reaction product was ChOne while ChOl was produced in a lesser extent (*circa* 60% to 20%, respectively) [22]. A study by Abbo *et al.* reported that ChOl was the main product from the oxidation of cyclohexene with H_2O_2 using a Cr(III) complex encapsulated in NaY zeolite [17]. This could mean that Cr(III) species are less active on the formation of ChOne or this ion lacks the activity of Cr(VI) for the secondary oxidation of ChOl to ChOne, which could be responsible for the observations of Adam and Fook.

Despite the lower cromium loading on CrNaY* comparatively to Cr(III)-NaY_1, the evaluation of the respective TON shows that the catalytically active centres are more accessible in the biosorption support than in the ion-exchange catalyst. This is due to the ion-exchange of Cr(III) ions occurring in different sites on the zeolite framework, some of which are inaccessible to cyclohexene. On another perspective, it is likely that the

chromium species in CrNaY* might be found on the surface or within the near-surface framework, since this support was recovered from assays using low biomass concentration, limiting the extent of the reduction of Cr(VI) to Cr(III). As consequence, less exchangeable chromium was available to the zeolite, allowing a higher dispersion on the framework surface. Moreover, the dispersion of metal on the surface of CrNaY* may prevent the formation of polynuclear chromium species.

Comparing the performances of the encapsulated chromium complexes, a decrease in cyclohexene conversion face to the respective parent hosts was observed. As it was previously commented for the oxidation of cyclohexanol in section 6.1, it is likely that this decrease might be due to a limitation of chromium leaching to the reaction medium. Furthermore, as it was previously commented in Chapter 5, the encapsulated complexes presented a loss of the Cr(VI) signals of CrNaY* (from DR-UV data), which would explain the smaller activity on the oxidation of cyclohexene. Nevertheless, the selectivity towards ChOne is still maintained.

The catalytic performance of the three encapsulated complexes in CrNaY* is comparable in terms of cyclohexene conversion and product selectivity. [Cr-PAN]NaY* achieved the highest TON of this study, whereas [Cr-PyMe]NaY* and [Cr-PyP]NaY* presented a slight increase of TON compared to the parent host. This suggests that the encapsulation of Cr-complexes renders the metal centres more accessible and active for the oxidation reaction. For the ion-exchange catalysts, the encapsulation of Cr-PyMe also resulted in a decrease of conversion and the selectivity was affected by the loss of activity on the decomposition of the intermediary Ch-TBHP product. This could be due to the effectiveness in preventing leaching of active chromium centres into the reaction medium, as previously commented on the activity of the Cr(III)-NaY_1 host.

From the results indicated in Table 6.2 and Figure 6.8 it is evident that ChOne is selectively formed in the presence of Cr(III)-NaY_1 . The evolution of the allylic oxidation products for this host shows that chromium improves the ChOne production, reducing the selectivity towards ChOl. Ch-TBHP is an intermediary product of the reaction and the appearance of this product is an indication of radicalar reaction pathway [23,24]. The selectivity analysis shows that Ch-TBHP is an unstable product, while ChOne appears as a secondary and stable product. The reaction mechanism proposed for the formation of the allylic oxidation products, ChOne and ChOl, is related to the cage controlled metal-OH chemistry rather

than to free radical mechanism. The overall mechanism for the oxidation of cyclohexene proceeds through a radical mechanism, as presented in figure 6.9 [16,23,24]:

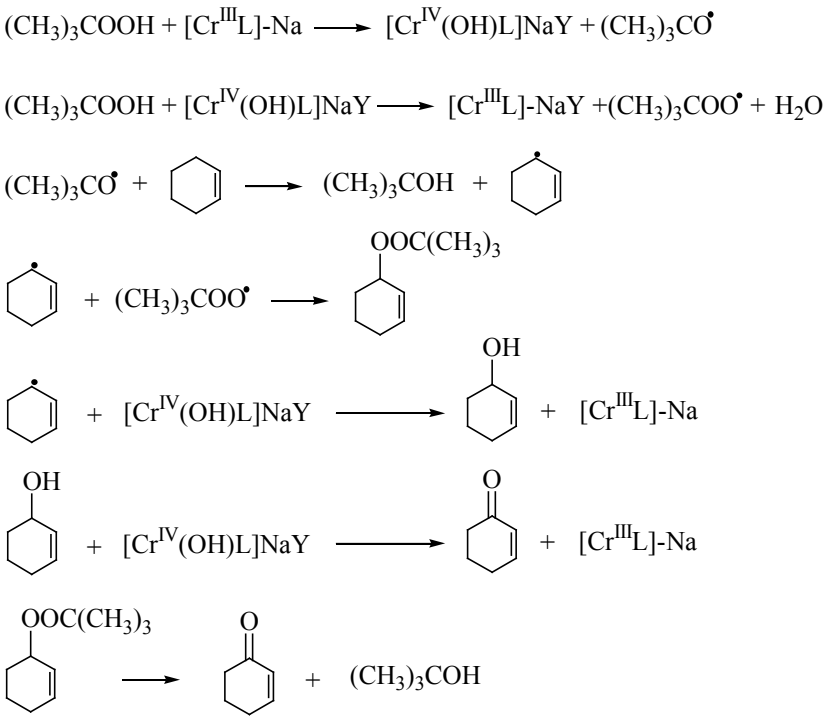

Figure 6.9: Reaction mechanism for the oxidation of cyclohexene. Image imported from reference [19].

6.2.2 Oxidation of cyclohexene using encapsulated Cr-diphenyltriazene complexes

The second phase of the study on catalytic oxidation of cyclohexene consisted in the use of Cr(VI) biotreatment supports recovered from optimized biosorption conditions and the encapsulated Cr-diphenyltriazene derivatives that were prepared from those supports.

The same reaction conditions were kept, with the exception of reaction temperature, which was increased from 40 to 50 ºC, as commented for cyclohexanol (Figure 6.2). A temperature-dependence study was conducted, with resulting data are presented in Figure 6.10.

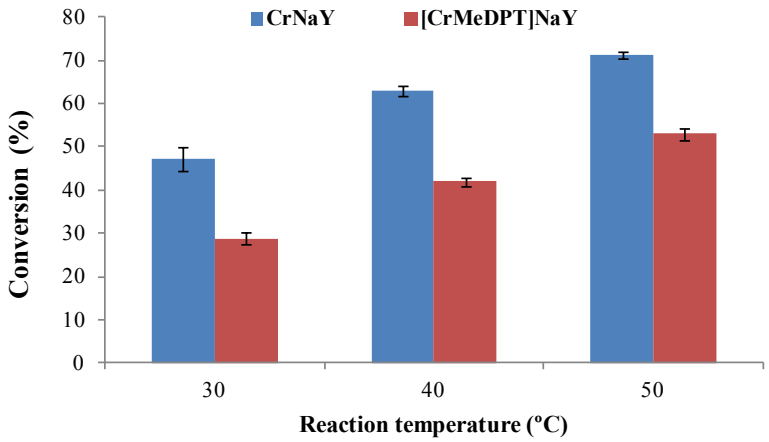

Figure 6.10: Conversion of cyclohexene with TBHP using CrNaY and [CrMeDPT]NaY catalysts, for different temperatures.

As it can be seen in Figure 6.10, the conversion of cyclohexene increases with the increase in temperature, for both catalysts. In parallel to the temperature effect in cyclohexanol conversion, the conversion of cyclohexene with the CrNaY host presents a slight increase from 40 to 50 ºC, more significant for the immobilized complex, justifying the selection of 50 ºC as the reaction temperature for the ensuing studies. The complete experimental results for all the different catalysts are presented in Table 6.3.

Table 6.3: Conversion, product selectivity and turn-over numbers for the oxidation of cyclohexene.

Catalyst	Conversion (%)	Analytical error (%)	Product selectivity (%)			Cr loading of catalyst (%)	TON
			ChOl	ChOne	Ch-TBHP		
blank reaction	16.9	± *5.9*	---	---	100.0	---	---
NaY	14.1	± *2.2*	---	---	100.0	---	---
HY	28.7	± *4.8*	---	---	100.0	---	---
CrNaY	69.0	± *1.8*	21.6	67.8	10.7	0.74	189.6
[Cr-DPT]NaY	56.0	± *1.5*	12.2	69.4	18.5	0.71	164.0
[Cr-MeDPT]NaY	55.1	± *2.5*	15.1	74.0	10.8	0.81	140.4
[Cr-NODPT]NaY	60.4	± *3.1*	15.4	71.6	13.0	0.72	173.2
CrNaY EXT	75.9	± *0.8*	22,4	59,1	18,5	0.94	166.7
$CrNaY_{SBR}$	61.2	± *1.0*	16.7	68.9	14.3	0.46	277.5
$[CrDPT]NaY_{SBR}$	60.8	± *1.1*	14.4	63.0	22.7	0.47	266.9
$CrHY_{SBR}$	72.9	± *1.4*	25.0	65.0	10.0	0.59	255.2
$[Cr\text{-}DPT]HY_{SBR}$	71.6	± *1.3*	22.8	66.8	10.3	0.55	268.7
$Cr(III)\text{-}NaY_2$	34.8	± *1.3*	7,8	37,6	54,6	0.36	199,7
$[Cr(III)\text{-}DPT]NaY_2$	32.7	± *0.8*	7,6	40,9	51,5	0.38	177,5

The blank reaction assays run without catalyst or in the presence of parent NaY or HY zeolite revealed an interesting feature: while NaY remains inactive for this reaction, HY zeolite presents slight catalytic activity, with a conversion near 30 %. However, the selectivity is the same as for the non-catalyzed reaction, showing only Ch-TBHP product. This indicates that HY zeolite only assists the formation of the intermediary product.

Comparing the performance of the recovered biotreatment supports, it can be seen that CrNaY, CrNaY EXT and $CrHY_{SBR}$ present comparable conversion results, despite their varying chromium contents. Contrarily to the observations for the oxidation of cyclohexanol, $CrHY_{SBR}$ is more active than the CrNaY support for this reaction. This indicates that the intrinsic activity of HY zeolite is also contributing to the overall reaction

and the $CrHY_{SBR}$ can be considered a bifunctional catalyst for the oxidation of cyclohexene. The CrNaY-based catalyst series follows an increasing trend of conversion *vs*. chromium loading of catalysts, as it is presented in Figure 6.11, without reaching an apparent saturation of the catalytic active centres with the increase in metal loading.

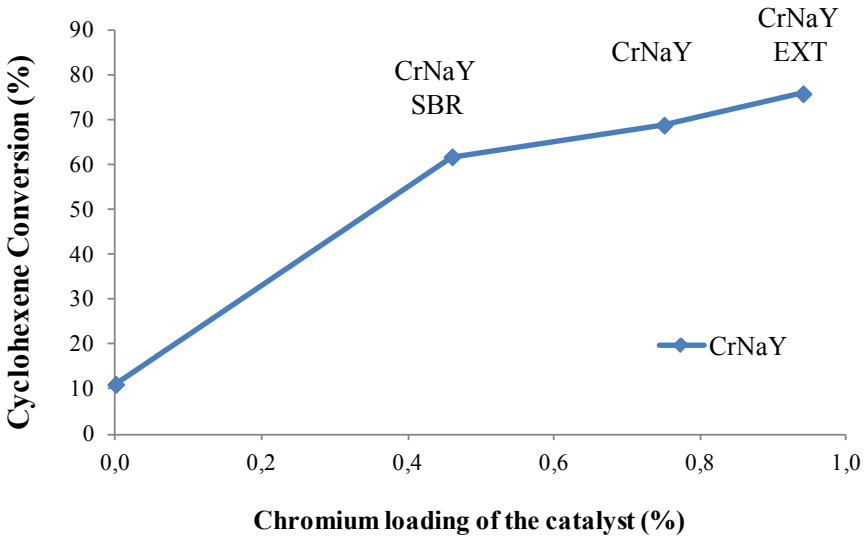

Figure 6.11: Plotting of the cyclohexene conversion *vs*. chromium loading of the catalyst, for the CrNaY series of biotreatment supports.

Comparing the selectivity of the biotreatment supports, the ketone, ChOne, remains the main reaction product. An increase in ChOl selectivity is observed compared with the supports used in the previous section (presented in Table 6.2). A residual amount of Ch-TBHP intermediary remains in all solutions, maybe due to the high conversion of cyclohexene, resulting directly in a high formation of the intermediary, that would not be decomposed into ChOl or ChOne at the same rate as cyclohexene would be transformed into Ch-THBP.

Cr(III)-NaY_2 showed less activity on the conversion of cyclohexene than the Cr(VI)-containing counterparts. Additionally, this support evidenced less ability to decompose the intermediary peroxide product, Ch-TBHP, into ChOl and ChOne. Nevertheless, the ratio between ChOl and ChOne appears to be of the same magnitude as for the other catalysts. This supports the conclusion that Cr(VI) species are more active towards the disproportionation of the cyclohexenyl peroxides than Cr(III) species. However, this finding turns the catalytic behaviour of $CrHY_{SBR}$ and its encapsulated complex even more

intriguing, as this is a Cr(III)-rich catalyst that achieves comparable selectivity as the CrNaY-based catalyst, whose XPS spectra showed higher availability of Cr(VI) species on the surface. The explanation for this fact could be given by a synergetic effect between the activity of the HY framework and the presence of the Cr(III) ions.

The catalytic activity of the encapsulated Cr-diphenyltriazene complexes decreases slightly when compared to the respective parent hosts. This is again explained by the leaching of chromium from the catalysts, which in turn minimizes the contribution of homogenous catalysis to the overall process. An exception is seen on [Cr-DPT]HY_{SBR} catalyst that presents comparable catalytic activity, selectivity and TON as the $CrHY_{SBR}$ host. Since this support behaves as a bifunctional catalyst, the process of encapsulation of the complex in the host does not promote any interference on the contribution of the HY framework to the overall conversion of cyclohexene. This is of great interest as this catalyst showed to be a truly heterogeneous catalyst on the oxidation of cyclohexanol. From the distinct ligand molecules employed, [Cr-NODPT]NaY showed higher activity than the [Cr-DPT]NaY 100 and [CrMeDPT]NaY counterparts. This might be due to the inefficiency in encapsulating Cr-complexes with this ligand, as well as a possible retardation effect on TBHP decomposition (free radical formation) by the presence of small amounts of free NODPT ligand [25].

An attempt to determine the presence of chromium on liquid samples recovered from the concluded reaction mediums was carried out in a similar way as it was described for the oxidation of cyclohexanol. However, it was not possible to perform the acid digestion of the liquid medium samples, due to the inertness and immiscibility of decane and the eventual digestion samples showed random and irreproducible results when analyzed for total chromium contents. Therefore, the interpretation of the relative leaching proneness of the catalysts is limited to the conclusions of the study on cyclohexanol oxidation.

A catalyst reuse test was performed in a similar procedure as it was conducted for the oxidation of cyclohexanol. It was not possible to perform three reaction cycles with the same initial mass of CrNaY and [Cr-DPT]NaY, as the mass loss between cycles was greater than in the case of the cyclohexanol reaction. Reasons for this fact are not clear, being most likely due to solvent effects on the zeolite crystal sizes, which given the repulsion between the non-polar moiety and the hydrophilic nature of the zeolite could limit the aggregation of zeolite crystals into greater size particles that could be retained by the 10-16 μm pore glass filter upon recovery. Hence, only two cycles were possible for each

catalyst, with the mass in cycle 2 being roughly half of the initial. Figure 6.12 presents the conversion of cyclohexene for each catalyst on each cycle, whereas the product selectivity is shown in Table 6.4.

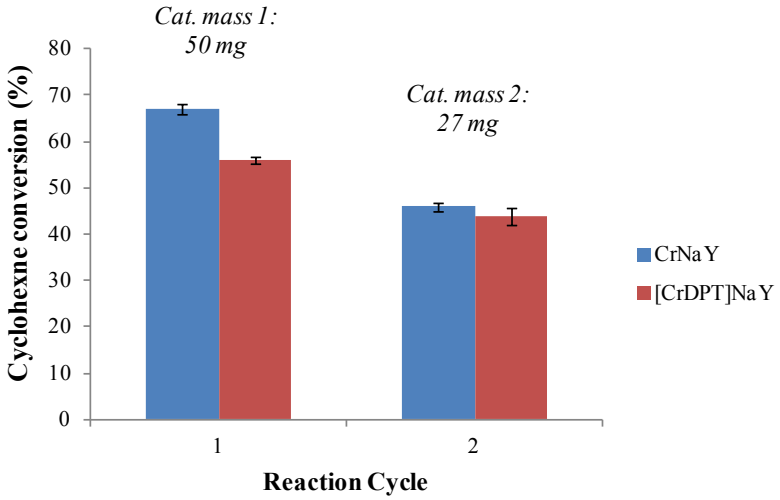

Figure 6.12: Conversion of cyclohexene with CrNaY and [CrDPT]NaY, for the different reaction cycles. Average catalyst masses on each cycle are indicated on the graph.

Table 6.4: Product selectivity from the oxidation of cyclohexene with CrNaY and [Cr-DPT]NaY catalysts, for the different cycles.

Catalyst	Reaction cycle	Product Selectivity (%)		
		ChOl	ChOne	Ch-TBHP
CrNaY	1	23.2	63.6	13.3
	2	13.4	50.0	36.6
[Cr-DPT]NaY	1	12.4	59.8	27.9
	2	13.1	45.6	41.3

The decrease in cyclohexene conversion for both catalysts was observed, from cycle 1 to 2. Although this can be attributed to the lower catalyst mass employed in cycle 2, the decrease in conversion is less pronounced on the encapsulated catalyst than on the CrNaY host, indicating that the [Cr-DPT]NaY catalyst is more stable. Product selectivity showed a reduced capacity for the decomposition of Cr-TBHP intermediary, which is related to the lower catalytic activity of the catalysts on cycle 2 (in parallel to the results presented in Table 6.2).

6.3 Conclusions

The recovered Cr(VI) biotreatment supports and related catalysts prepared by *in-situ* synthesis revealed activity for the liquid-phase oxidation of cyclohexanol and cyclohexene using TBHP oxidant.

The oxidation of cyclohexanol was useful to evaluate the activity and stability of biosorption supports and encapsulated catalysts. The experimental results showed that CrNaY-based catalysts were more active than the CrHY-based counterparts. Comparing the activity of a Cr(III)-containing zeolite, the results supported the conclusions from previous chapters on the complex chemistry of the chromium species present on the zeolites, where CrHY had a more distinct Cr(III)-like performance and CrNaY catalysts evidenced the presence of Cr(VI) on the surface. The immobilized complexes showed efficiency in the limitation of chromium leaching from the respective hosts. However, leaching is still possible from CrNaY-based encapsulated complexes. Nevertheless, although still suffering lesser leaching than its host, [Cr-DPT]NaY proved to be more stable than CrNaY when recycled 3 times. [Cr-DPT]HY_{SBR} is the least leaching-prone catalyst, being the loss of chromium ions negligible.

The catalysts also presented activity for the oxidation of cyclohexene. For NaY-based catalysts, the activity is related to the chromium contents on the support, while HY zeolite revealed minor activity for this reaction, still observeable on the CrHY-based catalysts. $CrHY_{SBR}$ showed comparable catalytic activity to CrNaY and CrNaY EXT, which possess a higher amount of chromium. This is due to a synergetic effect of the HY framework with the Cr(III) ions present, being considered a bifunctional catalyst.

The study on product selectivity indicates that the first product to be formed is the intermediary *tert*-butyl-cyclohexenylperoxide, being the sole product when chromium is absent from the catalyst. With the increase in metal loading of the catalyst, the decomposition of the intermediary Ch-TBHP into ChOne is observed and for the higher Cr-containing catalyst, ChOl is also detected. Cr(VI)-containing catalysts showed good activity for the decomposition of Ch-TBHP into alcohol and ketone, whereas Cr(III)-catalysts are less active on this aspect and the selectivity towards Ch-TBHP is higher on these supports.

The encapsulation of Cr-complexes resulted in a decrease of catalytic activity of the respective hosts. This indicates that part of the observed cyclohexene conversion by the hosts is due to the contribution of homogeneous chromium, or the decrease of substrate conversion for cyclohexanol and cyclohexene can also be explained by blocking effect of Cr-complexes that could limit the accessibility of the molecules in the zeolite channels. However, [Cr-DPT]HY_{SBR} was able to maintain the activity compared to the respective $CrHY_{SBR}$ host, being the bifunctional character of this catalyst deemed responsible for that fact. A recycling study was carried out again with CrNaY and [Cr-DPT]NaY and the results showed that the encapsulation of Cr-DPT complex limited the loss of activity from reaction cycle 1 to cycle 2, due to the limitation of Cr leaching.

6.4 References

[1] H. Figueiredo, I.C. Neves, C. Quintelas, T. Tavares, M. Taralunga, J. Mijoin, P. Magnoux, Oxidation Catalysts Prepared From Biosorbents Supported on Zeolites, Applied Catalysis B: Environmental. 66 (2006) 274-280.

[2] S. Laha, R. Glaser, Characterization and Catalytic Performance of [Cr]MCM-41 and [Cr]MCM-48 Prepared by Either Classical or Microwave Heating, Microporous nd Mesoporous Materials. 99 (2007) 159-166.

[3] A. Sakthivel, S.E. Dapurkar, P. Selvam, Allylic Oxidation of Cyclohexene Over Chromium Containing Mesoporous Molecular Sieves, Applied Catalysis A: General. 246 (2003) 283-293.

[4] Q.N. Zhang, J. Zhang, T.H. Wu, X.P. Zhou, The Oxidation of Olefins by t-butyl Hydrogen Peroxide to Prepare 1,2-diols Over Metal Oxide Catalysts, Catalysis Communications. 10 (2009) 1279-1283.

[5] M.M. Heravi, D. Ajami, K. Tabar-Heydar, Oxidation of Alcohols by Montmorillonite K-10 Supported Bis(trimethylsilyl)chromate, Monatshefte Fuer Chemie/Chemical Monthly. 129 (1998) 1305-1308.

[6] J. Muzart, Chromium-catalyzed Oxidations in Organic Synthesis, Chemical Reviews. 92 (1992) 113-140.

[7] C.T. Dalton, K.M. Ryan, I.J. Langan, É.J. Coyne, D.G. Gilheany, Asymmetric Alkene Epoxidation With Chromium Oxo Salen Complexes: Effect of π-rich and

Other Types of Additives, Journal of Molecular Catalysis A: Chemical. 187 (2002) 179-187.

[8] M. Álvaro, B. Ferrer, H. García, A. Sanjuán, Heterogeneous Gif Pxidation of Cyclohexane Esing Fe^{3+}-picolinate Complex Encapsulated Within Zeolites, Tetrahedron. 55 (1999) 11895-11902.

[9] M.R. Maurya, S.J.J. Titinchi, S. Chand, Oxidation of Phenol With H_2O_2 Catalysed by Cr(III), Fe(III) or Bi(III) N,N'-bis (salicylidene) Diethylenetriamine (H_2saldien) Complexes Encapsulated in Zeolite-Y, Journal of Molecular Catalysis A: Chemical. 193 (2003) 165–176.

[10] M. Salavati-Niasari, S. Abdolmohammadi, Host (nanocavity of zeolite-Y)/guest (12- and 14-membered azamacrocyclic Ni(II) complexes) Nanocatalyst: Synthesis, Characterization and Catalytic Oxidation of Cyclohexene With Molecular Oxygen, Journal of Inclusion Phenomena and Macrocyclic Chemistry. 60 (2007) 145-152.

[11] R.A. Sheldon, M. Wallau, I.W.C.E. Arends, U. Schuchardt, Heterogeneous Catalysts for Liquid-Phase Oxidations: Philosophers' Stones or Trojan Horses?, Accounts of Chemical Research. 31 (1998) 485-493.

[12] I.W.C.E. Arends, R.A. Sheldon, Activities and Stabilities of Heterogeneous Catalysts in Selective Liquid Phase Oxidations: Recent Developments, Applied Catalysis A: General. 212 (2001) 175-187.

[13] J.D. Chen, H.E.B. Lempers, R.A. Sheldon, Ti-Al-β and CrAPO-5 as Heterogeneous Catalysts for Selective Oxidations in the Liquid Phase, Colloids and Surfaces A: Physicochemical and Engineering Aspects. 101 (1995) 137-146.

[14] G. Olason, D.C. Sherrington, Oxidation of cyclohexene by t-butylhydroperoxide and Dioxygen Catalysed by Polybenzimidazole-supported Cu, Mn, Fe, Ru and Ti Complexes, Reactive and Functional Polymers. 42 (1999) 163-172.

[15] M.R. Maurya, A.K. Chandrakar, S. Chand, Oxovanadium(IV) and copper(II) Complexes of 1,2-diaminocyclohexane Based Ligand Encapsulated in Zeolite-Y for the Catalytic Oxidation of Styrene, Cyclohexene and Cyclohexane, Journal of Molecular Catalysis A: Chemical. 270 (2007) 225-235.

[16] N. Nunes, R. Amaro, F. Costa, E. Rombi, M.A. Carvalho, I.C. Neves, A.M. Fonseca, Copper(II)–Purine Complexes Encapsulated in NaY Zeolite, European Journal of Inorganic Chemistry. 2007 (2007) 1682-1689.

[17] H.S. Abbo, S.J.J. Titinchi, Metallo Salicylidenetriazol Complexes Encapsulated in Zeolite-Y: Synthesis, Physicochemical Properties and Catalytic Studies, Topics in Catalysis. 53 (2010) 1401-1410.

[18] I. Kuźniarska-Biernacka, K. Biernacki, A.L. Magalhães, A.M. Fonseca, I.C. Neves, Catalytic Behaviour of 1-(2-pyridylazo)-2-naphthol Transition Metal Complexes Encapsulated in Y Zeolite, Journal of Catalysis. 278 (2011) 102-110.

[19] H. Figueiredo, B. Silva, C. Quintelas, M.M.M. Raposo, P. Parpot, A.M. Fonseca, A.E. Lewandowska, M.A. Bañares, I.C. Neves, T. Tavares, Immobilization of Chromium Complexes in Zeolite Y Obtained From Biosorbents: Synthesis, Characterization and Catalytic Behaviour, Applied Catalysis B: Environmental. 94 (2010) 1-7.

[20] M. Salavati-Niasari, Host (nanopores of zeolite-Y)/guest [manganese(II) with 12-membered tetradentate N_2O_2, N_2S_2 and N_4 Donor Macrocyclic Ligands] Nanocatalysts: Flexible Ligand Synthesis, Characterization and Catalytic Activity, Transition Metal Chemistry. 33 (2008) 443-452.

[21] W. Buijs, R. Raja, J.M. Thomas, H. Wolters, On the Similarity in Catalytic Activity of Homogeneous and Heterogeneous Cr(VI) Catalysts in the Decomposition of Cyclohexyl Hydroperoxide, Catalysis Letters. 91 (2003) 253-259.

[22] F. Adam, C.L. Fook, Chromium Modified Silica From Rice Husk as an Oxidative Catalyst, Journal of Porous Materials. 16 (2008) 291-298.

[23] S.-N. Masoud, Host (nanocage of zeolite–Y)/guest (manganese(II), cobalt(II), nickel(II) and copper(II) Complexes of 12-membered Macrocyclic Schiff-base Ligand Derived from Thiosemicarbazide and Glyoxal) Nanocomposite Materials: Synthesis, Characterization and Catalytic Activity, Journal of Molecular Catalysis A: Chemical. 283 (2008) 120-128.

[24] A.S. Kanmani, S. Vancheesan, Selective Oxidation of Alkenes Catalysed by Ruthenium(II) Complexes Containing Coordinated Perchlorate, Journal of Molecular Catalysis A: Chemical. 150 (1999) 95-104.

[25] G. Rothenberg, H. Wiener, Y. Sasson, Pyridines as Bifunctional Co-catalysts in the CrO_3-catalyzed Oxygenation of Olefins by t-butyl Hydroperoxide, Journal of Molecular Catalysis A: Chemical. 136 (1998) 253-262.

(this page is intentionally left blank)

CHAPTER 7

FINAL REMARKS AND PERSPECTIVES

CHAPTER 7 – FINAL REMARKS AND PERSPECTIVES

This chapter presents a global overview of the conclusions of this work, interlinking the different experimental fields that were individually discussed on the previous chapters. This will be developed in section 7.1. Perspectives for future work will be presented in section 7.2.

7.1 Conclusion summary

The motivation for the development of a biosorption based process for the treatment of Cr(VI) liquid solutions which endowed recovery and reuse of the metal led to the successful application of a system consisting of an *Arthrobacter viscosus* biofilm supported on zeolites.

The initial application of this system showed that the biofilm was able to reduce the Cr(VI) species to Cr(III) ions, that were exchanged by the zeolite support, turning the zeolite into an *active* support. This reduction was found to be limited and efforts towards the improvement of biosorption conditions were conducted. The control of pH plays an active role on the performance of the system; however, although very acid pH favours the reduction of Cr(VI), the retention by the biomass-zeolite system was found to be greater at pH 4.0. Also, the extent of Cr(VI) reduction is dependent on the biomass availability, hence reactors with 5.0 $g_{biomass}$/L under a fix pH of 4.0 were used in the optimization studies.

Initial assays with Cr(VI) concentrations up to 100 mg_{Cr}/L showed that the reactors were able to remove 50 % of Cr(VI) during the first 24 hours if FAU-type zeolites were employed. MOR-type zeolites were also used on these experiments and the combination of MOR supports and biomass resulted in a less efficient system than the FAU-supported biomass.

The chemistry of the support was found to be of importance in assisting the bioreduction of Cr(VI), as well as the subsequent retention of the Cr(III) ions. Na^+-containing zeolites were found to be less efficient than H^+-containing FAU or MOR supports, due to the removal of H^+ ions from the reactor medium that are required for the acid reduction of chromate.

However, while the biofilm supported on H^+-zeolites performs better in the first 24 hours of the assay, the subsequent Cr(VI) reduction and removal performance by the system decreases drastically. Conversely, the NaY-based system was able to maintain the performance during the experimental time of 27 days, ultimately achieving the highest uptake of chromium, from the four zeolites in study: HY, NaY, HMOR and NaMOR. The respective uptake values were 10.8, 11.7, 9.9 and 9.5 $mg_{Cr}/g_{zeolite}$.

The bioreduction of Cr(VI) after the initial 24 hours was found to be a slow process: a study demonstrated that an *A. viscosus* -NaY system on a single batch experiment required 98 days to fully reduce the hexavalent chromium from a 100 mg_{Cr}/L solution. In order to take advantage of the fast initial Cr(VI) reduction promoted by the system, this was operated on a sequencing-batch process (SBR) using an initial 100 mg_{Cr}/L solution that passed through 3 reactors with fresh biomass-zeolite (residence time of 4 days). Results showed that HY zeolite was the best support in terms of overall Cr(VI) reduction and chromium retention in SBR operation, being the only system that achieved a final Cr(VI) and total chromium concentration within the legal limits for environmental discharge (achieved at the third SBR cycle). Furthermore, the operation on SBR highlighted the different dynamics promoted by the several zeolites on study: HY zeolite-based systems performed the bioreduction and ion-exchange by the zeolite in the first 4 days of experimental time, whereas the NaY-based system required the subsequent secondary reduction stage to achieve higher chromium removal.

In terms of chromium loading into the zeolitic support, HY zeolite achieved comparable results whether on a single-batch study or SBR (first cycle), a 0.5-0.6 % loading. NaY zeolite requires the additional experimental time of a single-batch assay, however, ultimately achieving higher chromium loadings of 0.74 % (27 days) or almost 1.0 % (98 days).

After the biotreatment experiments, the calcination of the collected solid reactor contents allowed the recovery of Cr-containing zeolites. The several characterization techniques permitted a thorough analysis of the solid content, confirming that the zeolite structure was kept unchanged while chromium species were successfully retained. Raman and XPS analyses demonstrated the complexity of chromium distribution on the zeolite surface, with co-existing Cr(III) and Cr(VI) species. The presence of Cr(VI) species was related to a re-

oxidation of Cr(III) ions during calcination, which was conducted in the presence of oxygen.

The immobilization of chromium species in the biosorption supports was conducted by *in-situ* synthesis of coordination compounds. Different heterocyclic ligands containing nitrogen atoms for coordination in different chemical structures (pyridazine, azo and triazenido groups) were successfully used. The extent of complex formation was estimated by TGA analysis and crossing data with several other analytical techniques (BET area, FTIR and Raman spectroscopy) it was possible to confirm that Cr-complexes were immobilized within the FAU-type recovered samples.

The catalytic tests allowed a double purpose: the evaluation of catalytic activity of the supports and prepared catalysts in liquid-phase reactions, and a further insight into the characterization of Cr(VI) biotreatment-recovered supports. The oxidation of cyclohexanol, being a simple Cr-specific reaction, was used for the catalytic tests with the high Cr-content supports with diphenyltriazene ligands. CrNaY-based catalysts were found to be the most active, with TON values up to 372 ($CrNaY_{SBR}$ host). However, it was found that chromium leaches from CrNaY catalysts into the reaction medium, being some of the overall cyclohexanol conversion attributed to the homogenous contribution. The immobilization of complexes decreased the leaching proneness of the corresponding hosts, achieving negligible leaching for [Cr-DPT]HY_{SBR} catalyst. The comparison with a Cr(III) catalyst indicated two distinct activity tendencies: a Cr(III)-alike series, which included CrHY hosts, and a Cr(VI)-alike counterpart series, correspondent to CrNaY series. This information corroborates the XPS data for CrNaY and CrHY, showing the dual presence of Cr(III) and Cr(VI) species in the first, while the second showed predominance of Cr(III) species on its surface.

The oxidation of cyclohexene is more interesting in terms of the assessment of the activity and selectivity of the catalysts. The previous conclusions on Cr(VI) or Cr(III) active centres for CrNaY and CrHY could not be confirmed by this reaction as parent HY zeolite presents slight catalytic activity. Coupled with the intrinsic activity of chromium, $CrHY_{SBR}$-based catalysts are bifunctional, which explains the higher activity of these supports, compared to the CrNaY-based catalysts, more active for the oxidation of cyclohexanol.

The oxidation of cyclohexene has three reaction products, being *tert*-butyl-cyclohexenylperoxide an intermediary product that transforms into 2-cyclohexene-1-ol and

2-cyclohexene-1-one. The ketone product was found to be the main oxidation product when Cr-containing catalysts were used, depending on the metal loading of the support. For higher Cr-loading of the catalyst, the selectivity towards the alcohol product increases. The Cr-loading is also related to the decomposition of the intermediary peroxide product.

The decrease of substrate conversion (cyclohexanol and cyclohexene) observed for all encapsulated Cr-complexes with different ligands in FAU zeolite hosts can be explained by ´blocking´ effect of the formed Cr-complex.

A recycling test was conducted for both reactions and confirmed that the immobilization of Cr complexes in the Cr(VI) biotreatment supports allows the reuse of the catalysts, since the loss of catalytic activity in each reaction cycle is lower for the immobilized samples than for the corresponding host.

7.2 Perspectives for future work

The experimental work conducted in the scope of this thesis was integrated on a multi-disciplinary project. Therefore, several experimental aspects on the application of zeolite-supported bacteria have also been considered by the research team, leading to an interesting array of options already covered. Some of these issues have been developed and are listed as example of the complexity and/or feasibility of application of the zeolite-supported biomass as a Cr(VI) treatment system:

- the use of different bacterial strains was reported previously, with the performance of *A. viscosus* being compared to *E. coli* and using NaY zeolite as support, with the uptake and removal values similar between the two species;
- the scale-up of the biotreatment system has been performed, using a pilot-scale experimental setup (reactor volume: 150 L). *A. viscosus* was supported on 13X molecular sieve;
- the comparison of Cr(VI) reduction and retention performance by living or dry *A. viscosus* has also been carried out. The reduction rate of hexavalent to trivalent chromium is somewhat faster with dry biomass, although achieving comparable end-of-time reduction and retention of the metal;

- application of the calcined biotreatment supports as catalyst for gas-phase oxidation reactions has also been studied.

Concerning future work on the application of the *A. viscosus*-zeolite treatment system and the catalysts prepared from the respective supports, some additional studies could be pointed out.

Firstly, the choice of zeolitic support could be further explored, although this work demonstrated that high-Al containing zeolites are quite adequate supports, favouring FAU-type structures. Also, application of specific natural zeolites could be considered in order to decrease the overall cost of the system. Another feature worth exploring is the enhancement of the interaction between biomass and the zeolitic support. If the zeolite could hold a significant mass of biofilm, operation with open systems or with flow reactors could be considered in detriment of batch operation.

Still considering the *A. viscosus*-zeolite system, another aspect worth testing is the reutilization of the calcined biotreatment supports in further Cr(VI) treatment cycles, in order to evaluate whether the zeolitic support suffers from depletion of the chromium exchange sites. Also of interest when H^+-containing zeolites are concerned, the influence of the depletion of H^+ ions from the support during the first cycle on its capacity of pH mediation by the system on further cycles. Ultimately, this could lead to a decrease on the overall operational cost of the system, while possibly increasing chromium loading of the zeolite for future catalytic applications. The latest could be an interesting way to compensate the reduced chromium loading of HY zeolites, for example.

To close the perspectives on the biotreatment capacities of the system, another aspect needing evaluation is the test with multi-metal solutions. Although this aspect was already covered for binary mixtures of Cr(VI) with Fe(III) or Cr(III), some metal ions are prone to the formation of chemical sludge when in the presence of dichromate anions and it would be interesting to evaluate the reduction of the formed metal-chromate and -dichromate anions. Another interesting application of the system would be on the treatment of effluents with organic compounds/solvents and ultimately on solvent and metal contaminated effluents. Additionally, a test using a Cr(VI) effluent in the presence of organic matter

would be required to evaluate the possible interference on the reduction capacity of the *A. viscosus* bacterium.

In terms of the reutilization of the spent Cr-containing zeolites as catalysts, the additional work would be directed towards the use of different ligand structures with specific requirements for a target reaction. In terms of future applications of the Cr-zeolite catalysts in environmental liquid-phase oxidation reaction, the oxidation of phenol-containing effluents could be a possible target reaction, as the prepared catalysts demonstrated activity for the reduction of secondary alcohols.